ISSN print: 1224-5984
ISSN online: 2248-3942

Rom Biotechnol Lett. 2022; 27(5): 3669-3681
doi: 10.25083/rbl/27.5/3669.3681

Received for publication, January, 12, 2023
Accepted, January, 21, 2023

Original article

Synthesis of l-DOPA catalyzed by recombinant *Escherichia coli* expressing tyrosine phenol lyase gene from *Desulfitobacterium hafniense*

YI FENG[1], LIJUAN YU[1], DAYONG JIN[1], SUXIANG ZHENG[1], JIE LI[1], YONGHUI JIANG[1]

[1]School of Life Sciences, Nantong University, Nantong 226019, China

Abstract

L-DOPA (L-dihydroxyphenylalanine) is a potential drug for the treatment of Parkinson's disease, and the demand is increasing every year. Tyrosine phenol-lyase (TPL) is a valuable biocatalyst for the biosynthesis of L-tyrosine and its derivatives, which are valuable intermediates in the pharmaceutical industry. In this study, a new TPL gene (*Dh-TPL*) was cloned from *Desulfitobacterium hafniense*, ligated into pJJDuet30 vector, and successfully expressed in *Escherichia coli*. To increase the yield and stability of L-DOPA, as well as decrease the by-product formation, the enzyme production conditions and the catalytic reaction conditions were studied. The optimal TPL production conditions were as follows: the concentration of IPTG was 0.2 mmol/L and the induction temperature was controlled at 18°C. The optimum medium composition for recombinant bacteria includes yeast extract 64 g/L, tryptone 36 g/L, glycerol 4 g/L, KH_2PO_4 2.31 g/L and K_2HPO_4 9.4 g/L. The best biosynthesis of L-DOPA was performed in a reaction mixture containing 10.0 g/L catechol, 20 g/L sodium pyruvate and 20 g/L recombinant *E. coli* resting cells. The optimal reaction temperature and pH were determined to be 18°C and pH 8.5, respectively. Under these conditions, the yield of L-DOPA was 0.21 mol/L (41.7 g/L) after 3 hours reaction.

Keywords Tyrosine phenol lyase, l-DOPA, Biotransformation, *Desulfitobacterium hafniense*, catechol

To cite this article: YI FENG. Synthesis of l-DOPA catalyzed by recombinant *Escherichia coli* expressing tyrosine phenol lyase gene from *Desulfitobacterium hafniense*. *Rom Biotechnol Lett.* 2022; 27(5): 3669-3681 DOI: 10.25083/rbl/27.5/3669.3681

*Corresponding author: Lijuan Yu; email: ylj200908@ntu.edu.cn

Introduction

L-DOPA (3,4-dihydroxyphenyl-L-alanine), an amino acid produced by the oxidation of L-tyrosine, is a precursor of the neurotransmitter dopamine. L-DOPA has been an essential commodity for the pharmaceutical companies since the 1960s as it is used as a therapeutic agent for dopamine-responsive dystonia and Parkinson's Disease.

The traditional method to obtain L-DOPA is direct extraction from plants, which is usually restricted by the limitation of raw material sources and the complexity of extraction steps. Monsanto [1] developed a method for the production of L-DOPA by asymmetric hydrogenation. However, the chemical synthesis of L-DOPA has many problems, such as poor conversion, low optical selectivity, high catalysts cost (e.g., Rb-complex), and harsh operational conditions [2, 3]. The main enzymes used for L-DOPA synthesis include tyrosinase, p-hydroxyphenylacetate 3-hydroxylase (PHAH), aminoacylases, and tyrosine phenol lyase (TPL).

L-DOPA can be synthesized from L-tyrosine by tyrosinase, and at the same time, a large number of by-products (mainly dopaquinone) are produced. To reduce L-DOPA to dopaquinone, chemical reducing agents are usually employed [3]. Lee and Xun [4] reported another process for L-DOPA production from L-tyrosine based on PHAH. However, the reaction requires NADH as the cofactor. The high cost of NADH limits the industrial applications of this method. Pragati Agarwal *et al*. [5] used aminoacylases to produce L-DOPA. Aminoacylases are a class of enzymes that specifically hydrolyze the amide bonds in N-acetyl-L-amino acids, and have high enantioselectivity. However, the reaction conversion is low, and the final replacement step of hydrogen bromide will generate a large amount of methyl bromide, which can destroy ozone and causes serious environmental pollution.

TPL can degrade L-tyrosine to pyruvate, ammonia, and phenol. This reaction is reversible. Therefore, L-DOPA can be produced if phenol is substituted by catechol as shown in Scheme 1. Hitoshi Enei *et al*. [6] used *Erwinia herbicola* ATCC 21434 whole cells with high TPL activity to synthesize L-DOPA. However, the yield of L-DOPA was limited (only 11.5 g/L after 24 hours of reaction).

The microbial transformation based on TPL activity usually shows higher productivity than that based on tyrosinase activity [7-10]. Consequently, we use TPL to produce L-DOPA from catechol, sodium pyruvate, and ammonia. In this study, we cloned and expressed TPL gene from *Desulfitobacterium hafniense* DP7 (DSM 13498) in *E. coli*, and investigated the enzyme production conditions and the catalytic reaction conditions in order to synthesize L-DOPA more efficiently.

Materials and methods

Strains, plasmids, and reagents

E. coli DH5α, pJJDuet30, and *E. coli* BL21 (DE3) were purchased from Addgene. Luria-Bertani (LB) medium (10 g/L tryptone, 5 g/L yeast extract, 10 g/L NaCl) was used for the cultivation of *E. coli* strains. L-DOPA, sodium pyruvate, catechol, ammonium acetate, sodium sulfite, EDTA were purchased from Sigma-Aldrich. Plasmid Mini Preparation Kit, DNA Gel Extraction Kit, SDS-PAGE Gel Quick Preparation Kit, and restriction endonucleases were purchased from Beyotime Biotechnology.

Analytical methods

The conversion reaction solutions were filtered with 0.22 μm polytetrafluoroethylene membrane and analyzed by Agilent 1200 HPLC. The samples were separated on an Agilent Eclipse XDB-C18 column. The mobile phase consisted of 0.1% formic acid and methanol (6:4, v/v). The column temperature was maintained at 35°C and the detection wavelength was 280 nm. The injection volume of the samples was set at 20 μL and the flow rate was 0.8 mL/min.

Construction of plasmid pJJ-dhtpl

Standard operating measures were adopted for PCR, DNA purifications, enzyme digestions, ligations, and plasmid extractions. The *Dh*-TPL (GenBank: EHL08374.1) was chemically synthesized and inserted into a pJJDuet30 plasmid between *Sac* II site and BamH I site. The ligation product was transformed into *E. coli* DH5α and verified by colony PCR and DNA sequencing. The plasmid with the correct sequence was named pJJ-dhtpl.

Transformation and screening of transformants

The recombinant plasmid pJJ-dhtpl was transformed into *E. coli* BL21 (DE3) to obtain the genetically engineered strain BL21/pJJ-dhtpl. The heat shock method [11] was used to transfer the plasmid pJJ-dhtpl into *E. coli* competent cells. Single colonies on kanamycin-resistant plates were verified by colony PCR, restriction enzyme digestion (QuickCut *Sac* II/ QuickCut BamH I), and sequencing.

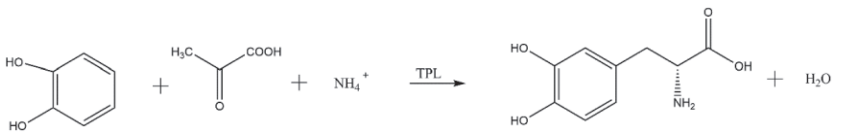

Scheme 1. Schematic diagram of l-DOPA synthesis catalyzed by TPL from pyruvate, ammonia and catechol.

Expression of Dh-TPL and SDS-PAGE analysis

The recombinant strains were routinely cultivated in LB medium and 50 μg/mL of antibiotics (kanamycin) were added. For *Dh-TPL* expression, a single colony was inoculated in 50 mL of LB medium and cultured at 37°C in a rotary shaker at 200 r/min. The overnight seed culture was inoculated in 2 L LB medium. When the optical density of the culture at 600 nm (OD_{600}) reached 0.6, IPTG was added to a final concentration of 0.1 mmol/L to induce the gene expression at 18°C for 12 h. The cells were then collected by centrifugation at 4,000 r/min for 10 min and washed twice with double-distilled water. The harvested cells were suspended in 5 mL double distilled water and disrupted by ultrasonication at 200 W for 10 min (ultrasonicated for 2 sec/gap 2 seconds). Supernatants and sediments were collected by centrifugation at 12,000 r/min for 5 minutes at 4°C and analyzed by 4-20% BeyoGel™ SDS-PAGE Precast Gel.

Determination of the *Dh*-TPL activity

One unit (U) of *Dh*-TPL activity was defined as the amount of enzyme that catalyzed the formation of 1 μmol L-DOPA per minute under the described assay conditions.

$$Dh\text{-TPL activity (U/g)} = \frac{\rho V \times 10^6}{mtM_r}$$

ρ, the mass concentration of L-DOPA, g/L. V, the reaction volume, L. M_r, the molecular weight of L-DOPA (197.19), g/mol. t, the reaction time, min. m, the wet weight of the injected bacteria, g.

Synthesis of L-DOPA catalyzed by recombinant *E. coli* cells

The recombinant *E. coli* cells expressing *Dh-TPL* were used for L-DOPA biosynthesis with catechol, sodium pyruvate, and ammonium acetate as substrates. The cells were collected by centrifugation at 4,000 r/min for 10 min and washed twice with double-distilled water. The harvested cells (20 g/L) were suspended in the L-DOPA transformation system. The L-DOPA transformation system (Ammonia adjustment pH 8) was composed of 5 g/L sodium pyruvate, 8 g/L catechol, 50 g/L ammonium acetate, 2 g/L sodium sulfite, and 1 g/L EDTA. The synthesis reaction were conducted at 16°C for 3 h at 150 r/min. After centrifugation (12000 r/min, 4°C, 2 min), the supernatant was analyzed using HPLC.

Optimization of *Dh*-TPL production conditions

Effects of medium type on Dh-TPL activity

Using LB medium as the initial fermentation medium, six nutritive sources were added at 2.5 g/L (glucose, lactose, sucrose, glycerol, sodium acetate and ammonium sulphate). Terrific Broth TB medium (24g/L yeast extract, 20g/L tryptone, 4ml/L glycerol, 0.017 M KH_2PO_4, 0.072 M K_2HPO_4)as well as LB medium were used as controls. After the induction, the *Dh*-TPL activity was determined. All experiments were carried out in triplicates and L-DOPA was detected and quantified by HPLC.

Effects of medium composition on Dh-TPL activity

By comparing these eight media, TB medium was determined to be the optimum medium. Further, the yeast extract concentrations were set to 4, 24, 44, 64 and 84 g/L. After the induction, the *Dh*-TPL activity was determined. All experiments were carried out in triplicates and L-DOPA was detected and quantified by HPLC.

At the optimum yeast extract concentration, the tryptone concentration was further set to 6, 12, 24, 36, 48 g/L. After the induction, the *Dh*-TPL activity was determined. All experiments were carried out in triplicates and L-DOPA was detected and quantified by HPLC.

At the optimum yeast extract and tryptone concentration, the glycerol addition was set to 2, 4, 8, 10, 12, 14, 16, 18 and 20 g/L. After the induction, the *Dh*-TPL activity was determined. All experiments were carried out in triplicates and L-DOPA was detected and quantified by HPLC.

Effects of IPTG concentration on Dh-TPL activity

IPTG as an inducer can influence the *Dh-TPL* expression. The cells were cultured at 37°C until the OD_{600} was 0.6, then IPTG was added until the final IPTG concentrations in the medium were 0.05, 0.1, 0.2, 0.4, and 0.6 mmol/L, respectively. The induction was carried out at 18°C for 12 h. After the induction, the *Dh*-TPL activity was determined. All experiments were carried out in triplicates and L-DOPA was detected and quantified by HPLC.

Effects of induction temperature on Dh-TPL activity

The cells were cultured at 37°C until the OD_{600} was 0.6, then IPTG (0.2 mmol/L) was added. The induction was carried out at different temperatures ranging from 12 to 36°C for 12 h. After the induction, the *Dh*-TPL activity was determined. All experiments were carried out in triplicates and L-DOPA was detected and quantified by HPLC.

Optimization of the synthesis conditions of L-DOPA

Effects of initial catechol concentration on l-DOPA synthesis

To optimize the initial catechol concentration, the reaction was performed in a shake flask (pH 8.0, 16°C, 150 r/min) based on the fixed sodium pyruvate concentration of 5 g/L, including different concentrations of catechol, 50 g/L ammonium acetate, 2 g/L sodium sulfite, 1 g/L EDTA, and 20 g/L recombinant *E. coli* resting cells. All experiments

were carried out in triplicates and the concentration of L-DOPA, residual catechol and the by-product were detected and quantified by HPLC.

Effects of initial main substrates ratio on l-DOPA synthesis

To optimize the initial main substrates ratio, the reaction was performed in a shake flask (pH 8.0, 16°C, 150 r/min) based on the fixed catechol concentration of 10 g/L, including different concentrations of sodium pyruvate, 50 g/L ammonium acetate, 2 g/L sodium sulfite, 1 g/L EDTA, and 20 g/L recombinant *E. coli* resting cells. All experiments were carried out in triplicates and the concentration of L-DOPA, residual catechol and the by-product were detected and quantified by HPLC.

Effects of reaction pH on L-DOPA synthesis

The optimal pH for L-DOPA biosynthesis was analyzed. The reaction system containing 20 g/L sodium pyruvate, 10 g/L catechol, 50 g/L ammonium acetate, 2 g/L sodium sulfite, 1 g/L EDTA sodium, and 20 g/L resting recombinant *E. coli* cells was mixed evenly. The synthesis was performed at pH ranging from 7.0 to 9.0 (adjusted by ammonia) at 16°C for 3 h. All experiments were carried out in triplicates and the concentration of L-DOPA, residual catechol and the by-product were detected and quantified by HPLC.

Effects of reaction temperature on L-DOPA synthesis

The product L-DOPA is easily oxidized and degraded at high temperature. Therefore, in this study, the synthesis of L-DOPA was conducted at lower temperatures (11°C-36°C), and the yields of L-DOPA at different temperatures were measured. The reaction system (pH 8.5) contained 20 g/L sodium pyruvate, 10 g/L catechol, 50 g/L ammonium acetate, 2 g/L sodium sulfite, 1 g/L EDTA sodium, and 20 g/L resting recombinant *E. coli* cells. All experiments were carried out in triplicates and the concentration of L-DOPA, residual catechol and the by-product were detected and quantified by HPLC.

Results and discussion

Construction of plasmid pJJ-dhtpl

To obtain active TPL, the target gene was cloned to the *Sac* II/BamH I site of pJJDuet30. The construction of the pJJ-dhtpl plasmid was shown in Fig. 1. The pJJ-dhtpl

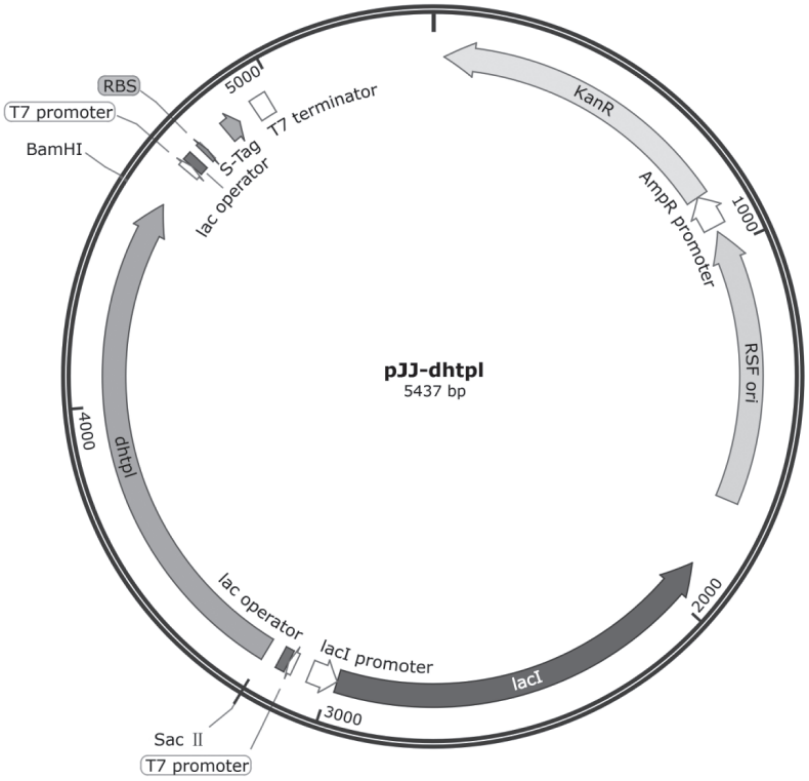

Figure 1. Construction of the pJJ-dhtpl plasmid.

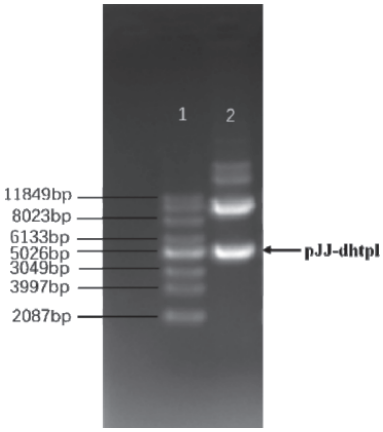

Figure 2. The electrophoresis of recombinant pJJ-dhtpl. Lane 1: the supercoiled DNA ladder; Lane 2: pJJ-dhtpl plasmid.

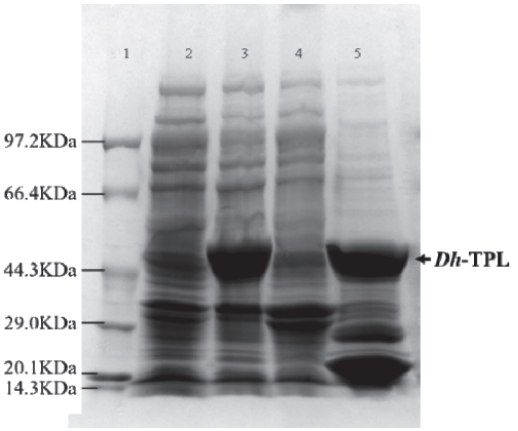

Figure 3. SDS-PAGE analysis of supernatants and sediments after ultrasonication and centrifugation. Lane 1: the Premixed Protein Marker (Low) standard; Lane 2 and Lane 4: the supernatant and sediment of BL21; Lane 3 and Lane 5: the supernatant and sediment of BL21/pJJ-dhtpl

plasmid was transformed into *E. coli* DH5α and the transformants selection was made on LB plates containing kanamycin. The plasmid size (Fig. 2) was consistent with the theoretical 5437 bp. The pJJ-dhtpl plasmid with correct sequence was used to transform *E. coli* BL21 (DE3) competent cells.

Expression of Dh-TPL and SDS-PAGE analysis

To achieve a large amount of TPL, the expression of TPL encoding gene was induced by 0.1 mmol/L IPTG for 12 h. The induction need to be carried out at 18°C to reduce the production of other proteins. The expression products were analyzed by SDS-PAGE. As shown in Fig. 3, *Dh-TPL* was expressed within the host cell with soluble and insoluble forms. Due to the large amount of insoluble TPL, the expression conditions need to further optimize to increase the TPL activity. The molecular weight of target band was about 50 KDa, which was in accordance with the molecular mass calculated by its primary amino acid sequence.

The rest cells expressing *TPL* were used in the synthesis of L-DOPA. The HPLC chromatogram of the conversion reaction solution was shown in Fig. 4. The retention time of the product L-DOPA was 2.900 min, the retention time of the by-product was 3.536 min and the retention time of the substrate catechol was 5.425 min.

Effects of medium type on Dh-TPL activity

The nutritive sources are the essential energy supply for the vital activity of bacteria and is the basis for bacterial cell formation and target protein synthesis. The initial medium

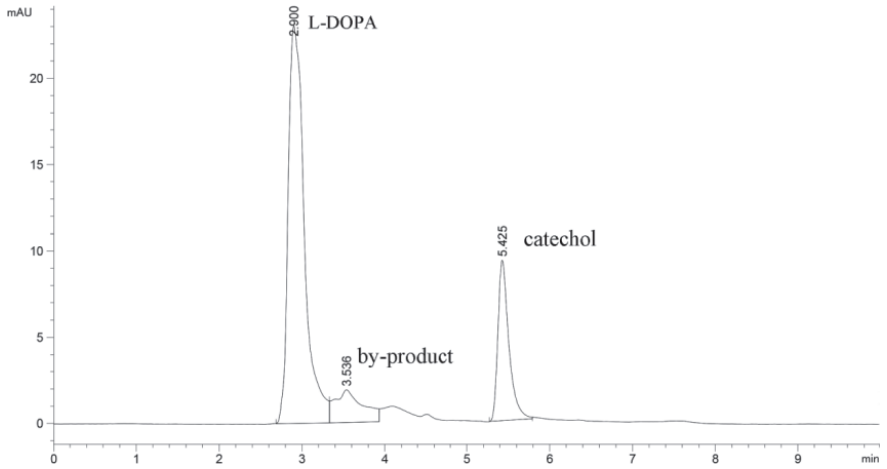

Figure 4. The HPLC chromatogram of the conversion reaction solution catalyzed by recombinant *E. coli* cells.

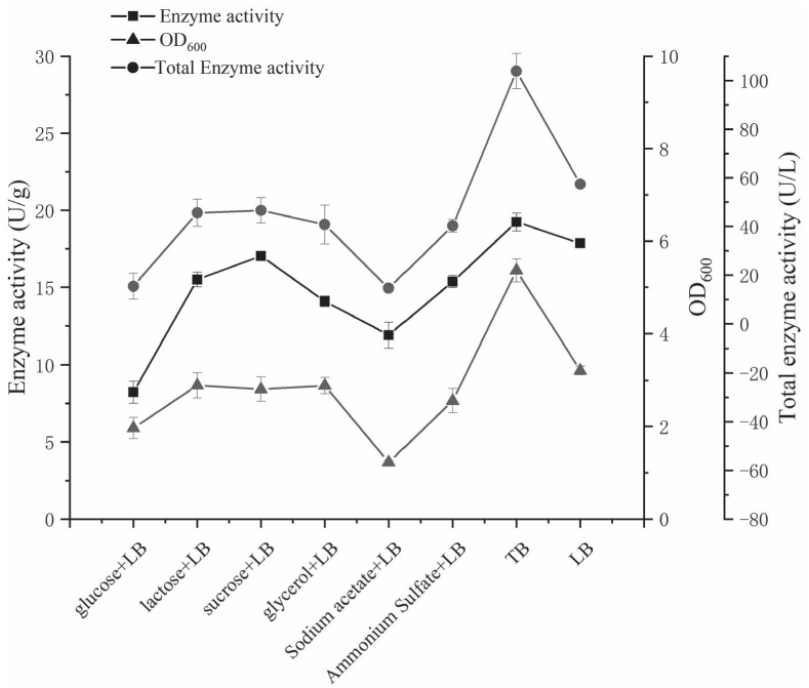

Figure 5. The effects of medium type on *Dh*-TPL activity.

LB was enriched with peptone and yeast extract. Based on the initial medium LB, six different types of nutritive sources were added and the results are shown in Fig. 5. It can be seen that the type of nutritive source has a great influence on the growth of recombinant bacteria and the enzyme activity, and the amount of bacteria in the medium with various nutritive sources added on top of LB medium was less than that of the original LB medium. The enzyme activity of TB medium was much higher than that of the other mediums, which indicated that TB medium was not only beneficial to

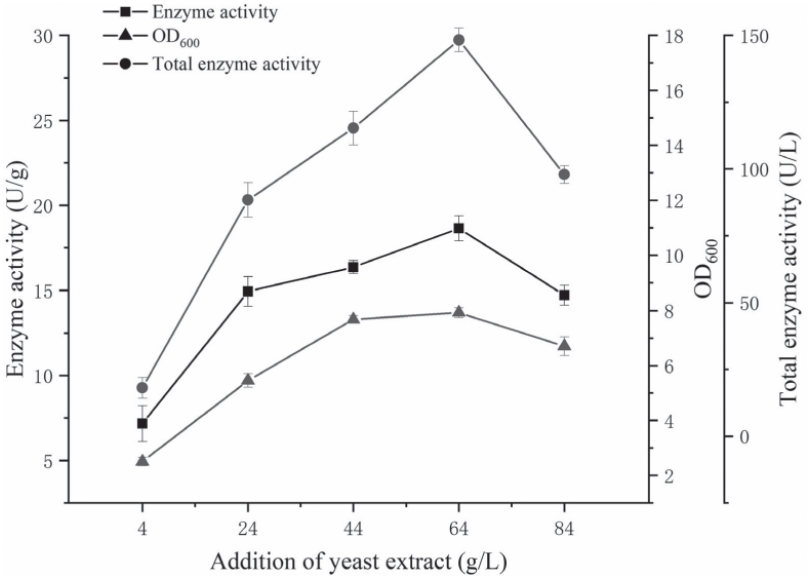

Figure 6. The effects of yeast extract addition on *Dh*-TPL activity.

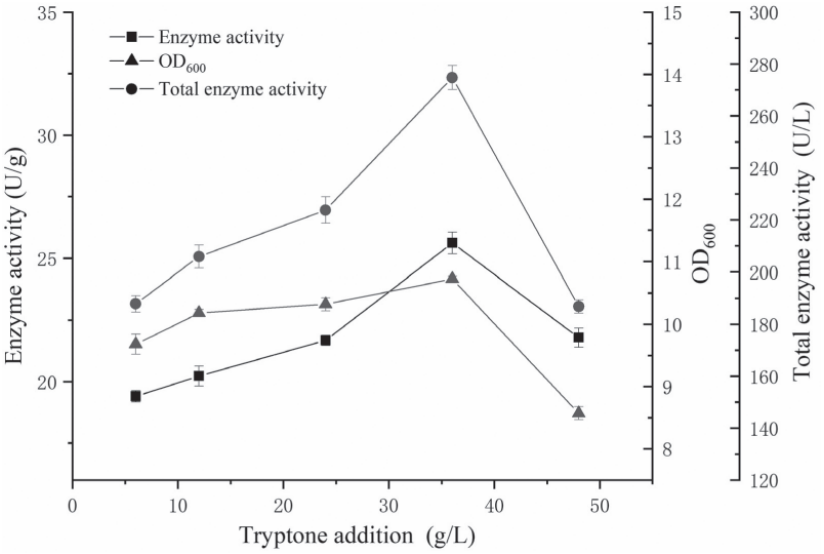

Figure 7. The effects of tryptone addition on *Dh*-TPL activity.

the growth of the bacteria but also to the enzyme production of the bacteria, which led to a significant increase in L-DOPA production.

Effects of medium composition on Dh-TPL activity

On the basis of TB medium, the addition of yeast extract was further optimized, and it can be seen from Fig. 6 that when the concentration of yeast extract was only 4 g/L, the enzyme activity per unit TPL was much lower than other concentrations, and with the increase of yeast extract, the enzyme activity per unit TPL gradually increased, but the bacterial volume showed a rapid increase, and when the addition of yeast extract reached 64 g/L, at which time the amount of bacteria, unit enzyme activity and total enzyme activity all reached the peak. When the addition of yeast extract increased to 84 g/L, the amount of bacteria, unit enzyme activity and total enzyme activity all decreased, indicating that excessive yeast extract inhibited the growth and metabolism of bacteria.

As can be seen from Fig. 7, the amount of bacteria increased slowly with the addition of tryptone, but decreased rapidly when the addition amount exceeded 36 g/L. This indicates that the excessive amount of tryptone was not conducive to the massive expansion of the recombinant bacteria, which in turn led to a decrease in the total enzyme activity. At the stage of addition of 24-36 g/L, the unit enzyme activity increased rapidly and the total enzyme activity reached the peak at this time, indicating that the right amount of tryptone was conducive to the massive expression of the target protein by the recombinant bacteria.

As shown in Fig. 8, when glycerol was added at 4-20 g/L, there was no significant increasing trend in unit enzyme activity, OD_{600} and total enzyme activity, which remained in a relatively stable range, but the total enzyme activity reached the highest when glycerol was added at 4 g/L. The recombinant *E. coli* in this study showed the highest enzyme activity when only a small amount of glycerol was added, which greatly reduced the production costs for the subsequent industrial production of L-DOPA.

Effects of IPTG concentration on Dh-TPL activity

IPTG as an important and toxic inducer, regulates the expression of cloned *Dh-TPL*. The influences of IPTG concentration on TPL activity were shown in Fig. 9. The values of OD_{600} decreased with the increase of IPTG concentration. The enzyme activity of unit cells and the total enzyme activity reached the maximums when the IPTG concentration was 0.2 mmol/L. However, excessive addition of IPTG did not increase enzyme activity and total enzyme activity, a significant decline was observed when IPTG concentration exceeded 0.4 mmol/L. This due to the fact that high concentration of IPTG delayed the growth of cells and caused the metabolic burden to the host cells [12].

Effects of IPTG induction temperature on Dh-TPL activity

As shown in Fig. 10, when the temperature was 12°C, the OD_{600} value was only 10.3808. At 18°C, the OD_{600} value raised to 11.44703. Then, with the increase of temperature, OD_{600} value raised very slowly. The values of OD_{600} improved with the increase of temperature, which indicated

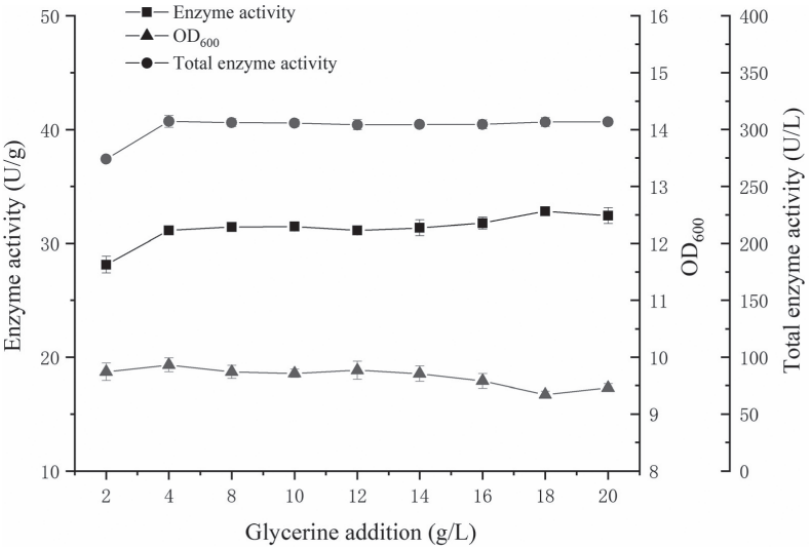

Figure 8. The effects of glycerol addition on *Dh*-TPL activity.

that high temperature was beneficial to the growth of bacteria to a certain degree. The enzyme activity of unit cells and the total enzyme activity increased significantly from 12°C to 18°C, then decreased above 18°C. Too low induction temperature (12°C) slowed down bacterial growth and affected the expression of foreign gene, while higher induction temperature would cause a large number of insoluble inclusion body to form in the cell, resulting in excessive accumulation of insoluble TPL and reducing enzyme activity. Therefore, the optimal induction temperature was fixed at 18°C.

Effects of initial catechol concentration on* l*-DOPA synthesis

Proper initial substrate concentration is not only conducive to the synthesis of L-DOPA, but also can reduce the formation of by-products. Under the condition of sufficient enzymes (cells), increasing the concentration of catechol can accelerate the initial reaction rate. However, the high concentration of catechol in the system has toxic and inhibitory effects on cells and enzyme activity [13, 14]. It has been reported that high concentration of catechol can destroy cell

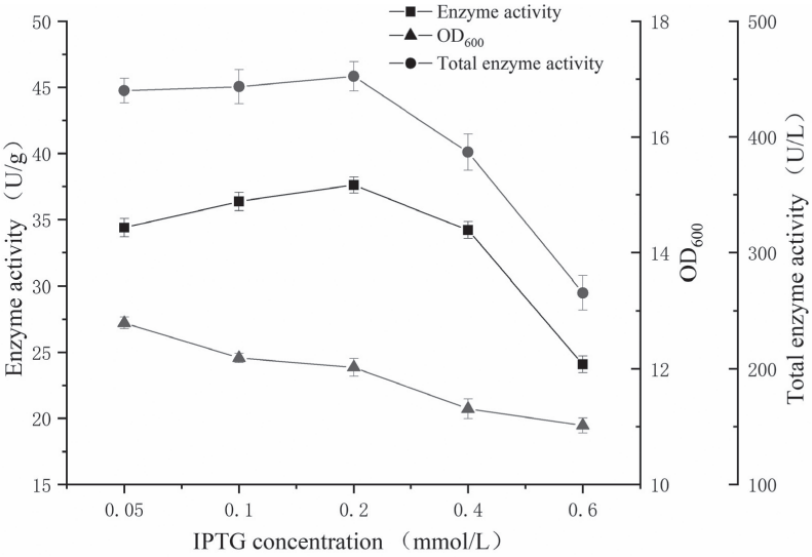

Figure 9. The effects of IPTG concentration on *Dh*-TPL activity.

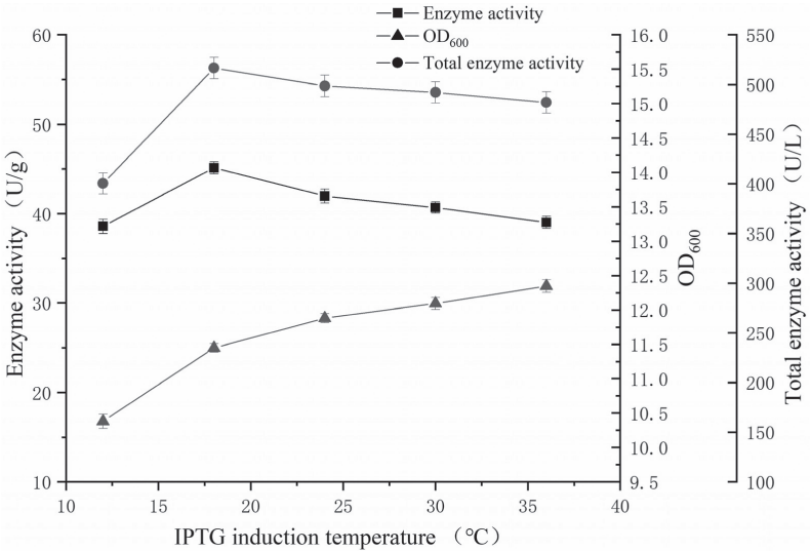

Figure 10. The effects of induction temperature on *Dh*-TPL activity and cell growth.

membrane components and accelerate cell lysis [15]. In order to improve the yield of L-DOPA and decrease the toxicity of catechol to cells, the appropriate catechol concentration in the synthesis system was investigated. As shown in Fig. 11, when the catechol concentration increased, the yield of L-DOPA raised too, and when initial catechol concentration was 10 g/L, the greatest L-DOPA yield could be obtained. Subsequently, an excessive addition of catechol was obviously unfavorable to the production of L-DOPA, which indicated that high concentrations of catechol can irreversibly inhibit the activity of *Dh*-TPL. Meanwhile, when the concentrations of catechol were lower than 8 g/L, due to the relative shortage of catechol, the spontaneous reaction between newly formed L-DOPA and residual sodium pyruvate leads to a large amount of by-product. When the initial concentration of catechol was 10 g/L, the minimum amount of by-product was achieved. After 10 g/L, the activity of *Dh*-TPL was inhibited by catechol, the quantity of residual sodium pyruvate increased, and the amount of by-product also began to raise. Therefore, the initial con-

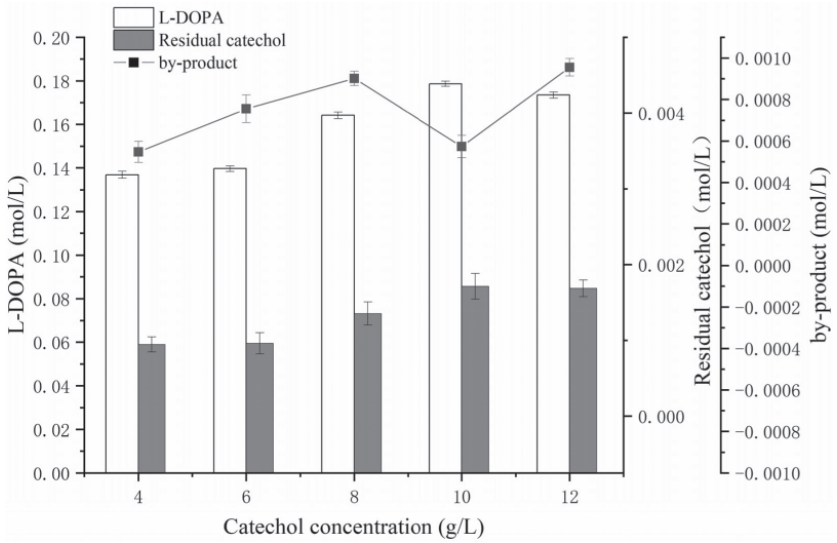

Figure 11. The effects of initial catechol concentration on L-DOPA synthesis.

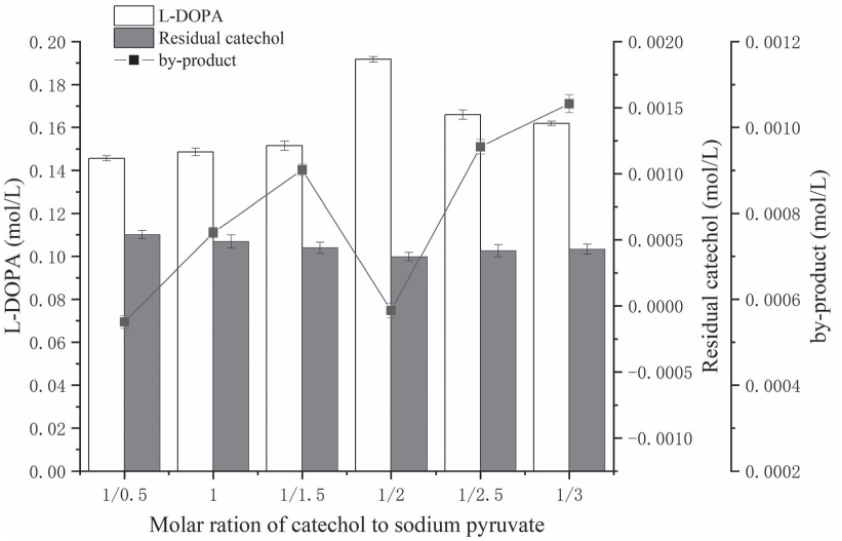

Figure 12. The effects of initial molar ratio of catechol to sodium pyruvate on L-DOPA synthesis.

centration of catechol was fixed at 10 g/L in the subsequent reaction, which is consistent with E313W and E313M TPL (from *Citrobacter freundii*) [16] and *Eh*-TPL (from *Erwinia herbicola*) [17]. This value is much higher than that of *Fn*-TPL (from *Fusobacterium nucleatum*, 5 g/L) [10]. Wei Yuan *et al.* [18] adopted 12.5 g/L of initial catechol concentration in 10 L fermenter, which was the highest level currently reported. Compared with them, the catechol tolerance of *Dh*-TPL is slightly lower, however, the synthesis reactions in this study were carried out in shake flasks. According to experience, there may be a large upside in the subsequent scale-up reactions.

Effects of initial main substrates ratio on* l*-DOPA synthesis

During the synthesis of L-DOPA catalyzed by *Dh*-TPL, the excessive sodium pyruvate can react with L-DOPA spontaneously without enzyme catalysis. Therefore, the proper initial ratio of catechol to sodium pyruvate is very important for the reaction. The effects of catechol/ sodium pyruvate ratios on L-DOPA synthesis were shown in Fig. 12. With the increase of sodium pyruvate, the conversion of catechol increased obviously. When the molar ratio of catechol to sodium pyruvate was set at 1:0.5, the yield of L-DOPA only reached 0.146 mol/L after 3 h. Further increas-

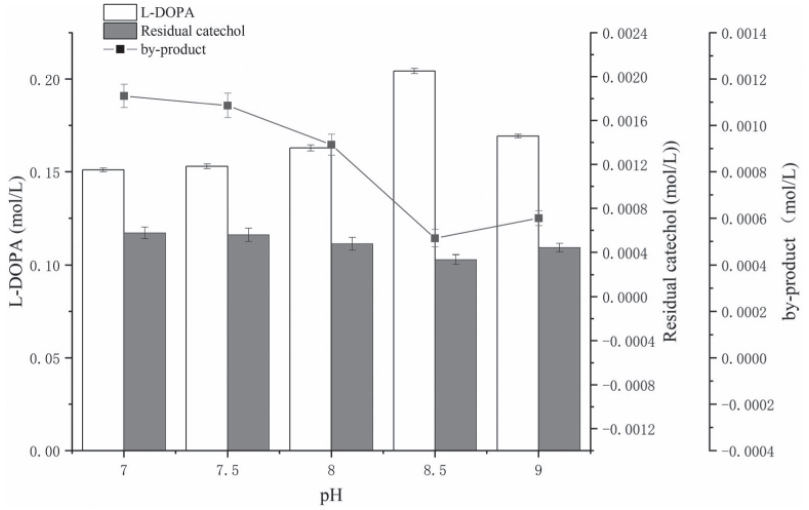

Figure 13. The effects of reaction pH on L-DOPA synthesis.

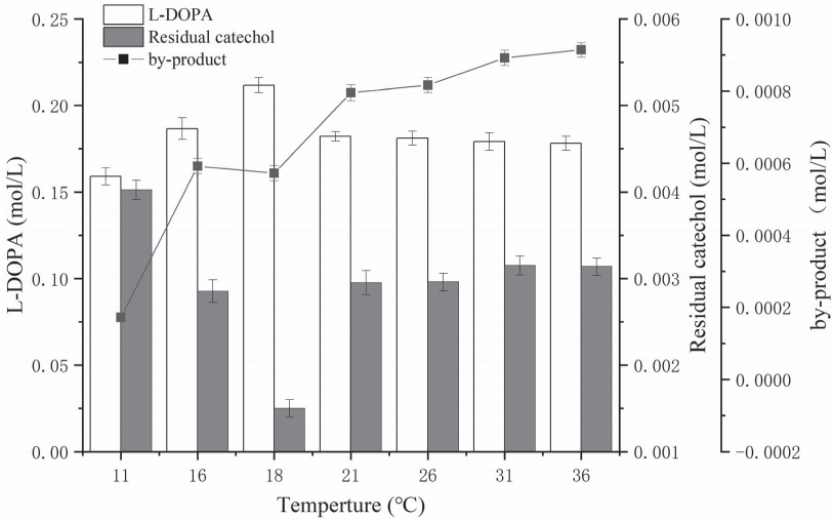

Figure 14. The effects of reaction temperature on L-DOPA synthesis.

ing the ratio of catechol to sodium pyruvate leads to an increase in sodium pyruvate consumption and an increase in L-DOPA production; when the ratio of catechol to sodium pyruvate reached 1:2, the yield of L-DOPA in the reaction solution was the largest, moreover the amount of by-products was the smallest. Further increasing the amount of sodium pyruvate, more by-products were produced by a spontaneous non-enzymatic reaction between excessive sodium pyruvate and L-DOPA, which resulted the rapid decrease of L-DOPA. So, the mole ratio of 1:2 between catechol and sodium pyruvate was determined as the best initial substrate proportion. Tang *et al.* [19] adopted 5 g/L catechol and 1:1.6 catechol to sodium pyruvate to produce L-DOPA, which was much lower than those in our studies. Thus the *Dh*-TPL constructed by us was more favorable for the synthesis of L-DOPA.

Effects of reaction pH on* l*-DOPA synthesis

The effects of pH on L-DOPA synthesis were investigated over a pH range from 7.0 to 9.0. As shown in Fig. 13, the maximum production of L-DOPA was observed at pH 8.5. When pH was lower than 8.5, the production of L-DOPA decreased significantly. It has been reported that the optimum pH of *Ki*-TPL (from *Kluyvera intermedia*), *Eh*-TPL (from *Erwinia herbicola*) and *Fn*-TPL (from *Fusobacterium nucleatum*) was 8.0 [6, 18, 19]. Meenakshi Chandel *et al*. [13] ever proposed that the optimal pH of *Cf*-TPL from *Citrobacter freundii* was 8.5. All the results indicated that weak alkaline environment was favorable for the synthesis of L-DOPA. However, too strong alkalinity can affect the activity of *Dh*-TPL, the production of L-DOPA was cut down. At the same time, the concentration of by-product was the lowest at pH 8.5. When the pH was increased from 8.5 to 9.0, or decreased from 8.5 to 7.0, the by-product concentration raised clearly. Hitoshi Enei *et al* [6] reported that the pH of the minimum by-products was 9, and Xiao-Ling Tang *et al*. [19] proposed that the pH of the minimum by-products was 8, respectively. Our results were essentially in agreement with the previous studies. From all above, it was recommended to perform the biosynthesis of L-DOPA at pH 8.5.

Effects of reaction temperature on* l*-DOPA synthesis

The substrate catechol and product L-DOPA were unstable at high temperatures. The influences of temperature during L-DOPA synthesis were investigated. The production of L-DOPA increased with the increase of temperature (Fig. 14). The maximum L-DOPA yield was obtained at 18°C and decreased at higher temperatures. In the process of L-DOPA biosynthesis catalyzed by *Dh*-TPL, it is proved that L-DOPA and pyruvate can form by-product through Pictet-Spengler reaction, which proved to be tetrahydroisoquinoline derivatives [6]. The formation of the by-product was affected by both temperature and pH [19]. As shown in Fig. 14, with the increase of temperature, the production of by-product was raised similarly. After 3 hours reaction, the amount of by-product at 36°C was the highest. In consideration of L-DOPA and by-product, the biosynthesis of L-DOPA should be carried out at 18°C. It has been recommended to perform the biosynthesis of L-DOPA at a temperature of 15 to 20°C [6], because high temperature promotes the formation of by-product. Wei Yuan *et al*. [18] employed 25°C to syn-

thetise L-DOPA with *Ki*-TPL (from *Kluyvera intermedia*), while Meenakshi Chandel *et al*. [13] prepare L-DOPA using *Cf*-TPL (from *Citrobacter freundii*) at 45°C. Compared with *Dh*-TPL, their reaction temperature was much higher and likely to produce more by-product. The synthesis of L-DOPA by *Dh*-TPL at the lower temperature (18°C) is very beneficial as low temperature greatly improves the stability of L-DOPA, reduces the generation of by-product and simplifies the subsequent purification process.

Under the optimal conditions (10.0 g/L catechol, 1:2 catechol to sodium pyruvate, pH 8.5 and 18°C), the yield of L-DOPA was 0.21 mol/L (41.7 g/L) after 3 hours reaction. Wei Yuan *et al.* [18] obtained 5.74 g/L/h L-DOPA by the wild-type YW000 (from *Kluyvera intermedia*, 25°C, fed batch process) and 7.52 g/L/h L-DOPA by mutant YW021 in 10 L fermenter (25°C, fed batch process), which was the highest level reported at present. In this study, the yield of L-DOPA obtained in the shake flask system was increased by 84.8% compared to the highest level reported so far, up to 13.9 g/L/h. In addition, the *TPL* gene is wild type. There may be a large space of improvement after amplifying the reaction scale and using the fed-batch mode or by genetic modification. These works are currently being studied in our lab. So, *Dh*-TPL may be a promising biocatalyst for the large-scale production of L-DOPA.

Conclusion

In summary, a new TPL from *D. hafniense* was constructed and its potential application for L-DOPA synthesis was explored. Types and composition of enzyme-producing media, the IPTG concentration and induction temperature both had an obviously influences on the enzyme activity, which provided important information for further study of *Dh*-TPL. The most suitable medium for the growth and expression of target proteins in recombinant *E. coli* was explored. The biosynthesis conditions of L-DOPA were discussed. The optimised enzyme-producing medium consists of yeast extract 64 g/L, tryptone 36 g/L, glycerol 4 g/L, KH_2PO_4 2.31 g/L and K_2HPO_4 9.4 g/L. The optimal reaction pH and temperature were 8.5 and 18°C, respectively. The best catechol concentration was 10.0 g/L and the mole ratio of catechol to sodium pyruvate was 1:2. Under these conditions, the yield of L-DOPA was 0.21 mol/L after 3 hours reaction, which was much higher than the highest level reported so far. However, the reactions were conducted in shaking flask reaction system, which may have a large space of improvement. Furthermore, the whole-cell catalysis exhibits many advantages including ease of operation, convenient downstream separation and low cost of industrialization. Consequently, the expression of *Dh-TPL* in *E. coli* provides another cheap and efficient biocatalyst for large-scale production of L-DOPA.

Conflict of Interest The authors declare that they have no conflict of interest.

References

1. Knowles William S. in Asymmetric Catalysis on Industrial Scale. (ed. W.S. Knowles) 21-38 (Wiley-VCH Verlag GmbH & Co. KGaA, Weinheim, FRG; 2003).
2. Sayyed Iliyas Ali,Sudalai Arumugam. Asymmetric synthesis of l-DOPA and (R)-selegiline via, OsO4-catalyzed asymmetric dihydroxylation. *Tetrahedron: Asymmetry*. 2004; 15 (19):3111-3116. doi: 10.1016/j.tetasy.2004.08.007
3. Valdés Ricardo Hernández, Puzer Luciano, Gomes Marlito, Marques Carlos E. S. J., Aranda Donato A. G., Bastos Marcelo L., Gemal André L.,Antunes O. A. C. Production of L-DOPA under heterogeneous asymmetric catalysis. *Catalysis Communications*. 2004; 5 (10):631-634. doi: 10.1016/j.catcom.2004.07.018
4. Lee Jang-Young,Xun Luying. Novel biological process for L-DOPA production from L-tyrosine by p-hydroxyphenylacetate 3-hydroxylase. *Biotechnology Letters*. 1998; 20 (5):479-482. doi: 10.1023/a:1005440229420
5. Agarwal Pragati, Pareek Nidhi, Dubey Swati, Singh Jyoti,Singh R. P. Aspergillus Niger PA2: A novel strain for extracellular biotransformation of l-tyrosine into l-DOPA. *Amino Acids*. 2016; 48 (5):1253-1262. doi: 10.1007/s00726-016-2174-7
6. Enei Hitoshi, Nakazawa Hidetsugu, Okumura Shinji,Yamada Hideaki. Synthesis of L-Tyrosine or 3, 4-Dihydroxyphenyl-L-alanine from pyruvic acid, ammonia and phenol or pyrocatechol. *Agricultural and Biological Chemistry*. 1973; 37 (4):725-735. doi: 10.1271/bbb1961.37.725
7. Li Tao,Li Xuan. Comprehensive mass analysis for chemical processes, a case study on L-Dopa manufacture. *Green Chemistry*. 2014; 16 (9):4241-4256. doi: 10.1039/c4gc00565a
8. Li Weiping, Wang Shuying, Yan Qun,Li Huazhong. Construction of tyrosine phenol lyase over-expression recombinant E. coli for the biosynthesis of levodopa. *Zhongguo Yiyao Gongye Zazhi*. 2005; 36 (12):743-746.
9. Min K., Park K., Park D. H.,Yoo Y. J. Overview on the biotechnological production of L-DOPA. *Appl Microbiol Biotechnol*. 2015; 99 (2):575-584. doi: 10.1007/s00253-014-6215-4
10. Zheng Ren Chao, Tang Xiao Ling, Suo Hui, Feng Li Lin, Liu Xiao, Yang Jian,Zheng Yu Guo. Biochemical char-

acterization of a novel tyrosine phenol-lyase from Fusobacterium nucleatum for highly efficient biosynthesis of L-DOPA. *Enzyme and Microbial Technology*. 2018; 112:88-93. doi: 10.1016/j.enzmictec.2017.11.004

11. Panja Subrata, Aich Pulakesh, Jana Bimal,Basu Tarakdas. How does plasmid DNA penetrate cell membranes in artificial transformation process of Escherichia coli? *Molecular Membrane Biology*. 2008; 25 (5):411-422. doi: 10.1080/09687680802187765
12. Malakar Pushkar,Venkatesh K. V. Effect of substrate and IPTG concentrations on the burden to growth of Escherichia coli on glycerol due to the expression of Lac proteins. *Applied Microbiology and Biotechnology*. 2012; 93 (6):2543-2549. doi: 10.1007/s00253-011-3642-3
13. Chandel M.,Azmi W. Purification and characterization of tyrosine phenol lyase from Citrobacter freundii. *Appl Biochem Biotechnol*. 2013; 171 (8):2040-2052. doi: 10.1007/s12010-013-0491-9
14. Kim D. Y., Rha E., Choi S. L., Song J. J., Hong S. P., Sung M. H.,Lee S. G. Development of bioreactor system for L-tyrosine synthesis using thermostable tyrosine phenol-lyase. *Journal of Microbiology and Biotechnology*. 2007; 17 (1):116-122. doi:
15. De Smet Marie Jose, Kingma Jaap,Witholt Bernard. The effect of toluene on the structure and permeability of the outer and cytoplasmic membranes of escherichia coli. *BBA - Biomembranes*. 1978; 506 (1):64-80. doi: 10.1016/0005-2736(78)90435-2
16. Han Hongmei, Zeng Weizhu, Du Guocheng, Chen Jian,Zhou Jingwen. Site-directed mutagenesis to improve the thermostability of tyrosine phenol-lyase. *Journal of Biotechnology*. 2020; 310:6-12. doi: 10.1016/j.jbiotec.2020.01.005
17. Zeng Weizhu, Xu Bingbing, Du Guocheng, Chen Jian,Zhou Jingwen. Integrating enzyme evolution and high-throughput screening for efficient biosynthesis of l-DOPA. *Journal of Industrial Microbiology and Biotechnology*. 2019; 46 (12):1631-1641. doi: 10.1007/s10295-019-02237-8
18. Yuan Wei, Zhong Shuang, Xiao Yanming, Wang Zhao,Sun Jie. Efficient biocatalyst of L-DOPA with Escherichia coli expressing a tyrosine phenol-lyase mutant from Kluyvera intermedia. *Applied Biochemistry and Biotechnology*. 2020; 190 (4):1187-1200. doi: 10.1007/s12010-019-03164-1
19. Tang Xiao Ling, Liu Xiao, Suo Hui, Wang Zhi Chao, Zheng Ren Chao,Zheng Yu Guo. Process development for efficient biosynthesis of l-DOPA with recombinant Escherichia coli harboring tyrosine phenol lyase from Fusobacterium nucleatum. *Bioprocess and Biosystems Engineering*. 2018; 41 (9):1347-1354. doi: 10.1007/s00449-018-1962-8

ISSN print: 1224-5984
ISSN online: 2248-3942

Rom Biotechnol Lett. 2022; 27(5): 3682-3690
doi: 10.25083/rbl/27.5/3682.3690

Received for publication, December, 29, 2022
Accepted, January, 21, 2023

Original article

Experimental research on the use of innovative phytoextracts in cow with clinical endometritis

IONIȚĂ CARMEN[1], ȚOGOE DORIN[1]*, MICȘA CĂTĂLIN[1], MIHAI A.[1], IGNĂTESCU (ȚÎMPĂU) ROXANA MARIANA[1], MINCĂ NICOLETA[1], IONIȚĂ L.[1]

[1]University of Agronomic Science and Veterinary Medicine of Bucharest, Romania

Abstract

Clinical endometritis is a frequent and important pathology on farms in Romania and not only, so we created and obtained a preparation exclusively from plants in different forms of administration (tablets and intrauterine solution), with which to treat the cows under study. We chose a group of cattle that we divided into 4 batches of cows, a control batch treated with classical medication, a batch treated with intrauterine solution, a batch treated only with tablets, and the fourth batch was treated with tablets and intrauterine solution.

Based on a well-established working protocol and paraclinical investigations performed, it was demonstrated the usefulness of phytoextracts in the prevention and treatment of clinical endometritis, but also the way of stimulating the immune response associated with a shorter healing time.

Keywords endometritis; post-partum; phytoextract, cows; experimental

To cite this article: IONIȚĂ CARMEN. Experimental research on the use of innovative phytoextracts in cow with clinical endometritis. *Rom Biotechnol Lett.* 2022; 27(5): 3682-3690 DOI: 10.25083/rbl/27.5/3682.3690

*Corresponding author: Țogoe Dorin, University of Agronomic Science and Veterinary Medicine of Bucharest, Splaiul Independenței nr 105.
E-mail: dtogoe@yahoo.com

Introduction

Endometritis is known as inflammatory pathology in the endometrium and results in the accumulation of purulent contents or polymorphonuclear cells (PMN). In clinical cases, in cows, it is classified into clinical endometritis or subclinical endometritis, often having a bacterial or infectious substrate. Most often they identify themselves as a result of abortions, the presence of metritis and calving dystocia, as well as in the case of fetal retention. (Fabio Lima, 2022). Opportunistic pathogens at the vaginal level or external environment should be remembered as predisposition factors, although naturally cows with an appropriate immune status can eliminate infections of a temporary nature. Inadequate or poor immunological state may be the basis of endometritis of a chronic and hardly treatable character. In cows, clinical endometritis is manifested by purulent or mucopurulent vaginal discharge 21 days after calving, and the subclinical one is characterized by a lack of secretions at the vaginal level. (Fabio Lima, 2022).

It is known that in cattle farms the management of dairy and reproductive production occupies a major interest in research, that is why we have chosen to study and get involved in the treatment of clinical endometritis. Diagnosis of post-partum diseases at the uterine level is a very important aspect for practicing veterinarians. We conducted this study based on the controversies created by its treatment and effectiveness in clinical endometritis, which has as a principle the stopping and reversal of inflammatory changes that affect fertility, as well as the increase of the immune response (S. J. LeBlanc, 2002).

Known major economic losses due to endometritis include decreased fertility, decrease in the number of products of conception, decrease in the number of parturitions, decrease in milk production, as well as premature depreciation of cattle, thus increasing production costs and decreasing profit (Haben Fesseha, 2020). Clinical endometritis is characterized by the presence of purulent-looking discharge from the uterine level and is complicated with infertility or subfertility. Their impact from an economic point of view is major, some studies recognize the decrease in the number of conception products by up to 20% compared to healthy cows and the increase in the interval from calving to conception by 30 days (Timothy J. Potter, 2010). Infertility is a biological phenomenon that is manifested by the degradation of the reproductive function in females, caused by abnormalities or diseases of the genital system or of other organs and systems, or by abnormal conditions of exploitation (improper nutrition, maintenance, environmental and climate factors) and the non-observance of the biotechnological conditions of reproduction. (M. Umer, 2022). Very often, endometritis is associated with diseases of the genital sphere (retention of fetal coverings, ketosis or specific/nonspecific uterine infections). Even during the normal puerperium in dairy cattle, multi-pathogen bacterial infection of the uterus occur, altering the immunological homeostasis and resumption of ovarian cyclicity (Kiracofe GH, 1980).

Multifactorial causes and post-partum physiology of the cervix to dilate, while the vestibule and vagina relax, make bacterial contamination inevitable and require mobilization of components with an immune role. The presence of leukocyte infiltrate and congestion of the endothelial endothelium, with or without edema, has been shown to involve the start of drug treatment. Cattle that have had such post-partum reactions, are those in which the interval between calving increases by up to 12 days or shows abortion or dystocia. (Haben Fesseha, 2020). In general, acute forms of the disease, untreated or improperly treated, take on subacute or chronic clinical aspects. Always the acute forms of the disease have an obvious character that is very easy to recognize, the subclinical or chronic forms cause subfertility or infertility (Wagener K et al., 2017).

It has been reported that the immune capability of the uterus is influenced by steroid hormones, especially luteal progesterone, which increases the susceptibility of the postpartum endometrium to infection in dairy cattle (Sheldon IM et al., 2009). Bovine endometrium cells presents Toll-like receptors which recognize and respond to bacterial infection (certain components of bacteria like LPS) leading to secretion of cytokines, chemokines and antimicrobial peptides (Davies D et al., 2006, Menzies M et al.,2006). Subclinical endometritis defines endometrial inflammation in the absence of clinical signs (without leakage) or by the presence of over 18% polymorphonuclear (PMN) at the endometrial level between days 22 and 33 post-partum or over 10% polymorphonuclear between days 34 and 47 post-partum. The impact of subclinical endometritis on reproductive performance results from the decrease in the rate of conception and the prolongation of the service-period. Moreover, it has been shown that these types of infections negatively influence the viability and quality of embryos.

In subclinical forms of the disease, microorganisms that determine the inflammatory reaction at the level of the endometrium are most often eliminated by complex humoral mechanisms, but an active imbalance of anti- and pro-inflammatory factors at the uterine level is maintained, which will prevent the resumption of normal reproductive activity and the onset of gestation. (Iain Martin, 2017).

Materials and Methods

Materials

Based on the studies carried out by colleagues from other countries, who used as an adjuvant treatment in endometritis produced from plants (cinnamon oil, oregano,

thyme), we created products containing fennel oil, cumin, sage, fennel, Lychnis, *Achillea millefolium*. The still unknown antibacterial activity of these plant products makes the study a research one. The clinical study was conducted on Holstein dairy cows, at 40-45 days post-partum, with infected uterine secretions, detected by clinical and gynecological examination in order to identify the post-partum status and conduct experimental studies in the therapy of these states with our products. Clinical examination revealed the general condition of the animal in the first post-partum month, by assessing the score of the body condition and digestive, respiratory and urinary function. The gynecological examination was performed through specific tests and investigations aimed at highlighting the specific changes in the genital apparatus, the extension of the lesions and the susceptibility of the uterus to infections with specific or nonspecific pathogenic germs.

In particular, there were appreciated the quality and quantity of the vaginal discharge as well as their appearance. Ultrasound examinations were carried out to highlight the structures on the surface of the ovaries and the appearance of the uterus. there was appreciated the amount of uterine contents, the appearance and thickness of the walls of the uterine horns and cervical canal. Being a septic inflammatory process, the content of the uterus in bacteria fluctuates greatly as a result of contamination, elimination and recontamination, due to imposed defense mechanisms. Pathogenic germs persist at the uterine level and will delay resumption of uterine function and normality. Uterine cytological examination is recommended in this situation to identify the types of pathogenic germs and test their sensitivity.

Method

In our experimental studies, there were used 3 batches, combining the 2 products, experimentally tested separately in cows with clinical endometritis. There were created 3 batches composed of 2 cows with subclinical endometritis.

We collected biological samples in cows before the experiment, 3 days, 7 days, and 14 days after the start of the experiment. The treatment was done for 7 days by combining the two forms, with the mention that the medicinal forms of the tablet type (10 tablets / animals) were administered in the form of a food bowl. Dairy animals are subject to clinical observation.

The experimental model was:

On day 1 clinical and gynecological examination in all animals taken under study. After ultrasound and clinical/gynecological examination, cows without clinical signs of endometritis (clinical endometritis) were selected in the study. On postpartum day 2, biological products (blood, secretions) are collected and medication is administered. Three different batches of cows were made in which the treatment was divided as follows:

1. the first batch was considered a witness and received classical treatment (antibiotherapy and support), which was not our object of research was not included in the monitoring and results tables.
2. the second batch was treated only with intrauterine solution - charge 1.
3. the third batch was treated only with phytoextracts tablets (10 tablets / animal in the form of a food bowl) – charge 2.
4. the fourth batch was treated with both tablets and intrauterine solution – charge 3.

On day 3, biological samples were collected from the 3 batches of cows. On day 7, biological samples were collected from the 3 batches of cows.On day 14, biological samples were collected from the 3 batches of cows.

Discussion

According to the experimental protocol, for the combined batches of product (in the form of tablets and liquid) 2 cows with clinical endometritis were chosen. Vaginal discharge was highlighted only after transrectal examination (see picture) and have a yellowish white appearance with a strong odor (Fig 1).

Figure 1. Vaginal discharge in clinical endometritis.

Experimental results of the use of our combined products from batch 1, 2 and 3

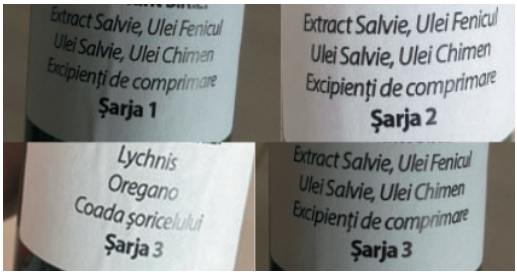

Figure 2. Experimental products.

Table 1 :

Paramet.	U/m	Physiology.	Charge 1		Charge 2		Charge 3	
		limits	1.1	1.2	2.1	2.2	3.1	3.2
WBC	10-9/mm^3	4-12	8,81	10,52	8,75	13,22	8,82	11,4
lym	10-9/mm^3	2,5-7,5	3,28	6,56	3,76	5,61	3,30	4,26
MON	10-9/mm^3	0-1	0,84	0,94	0	0,12	0,13	0,15
NEU	10-9/mm^3	0,6-7,6	4,62	2,65	4,75	7,18	5,19	7,3
EOS	10-9/mm^3	0,1-1	0,07	0,35	0,16	0,30	0,20	0,47
BASS	10-9/mm^3	0-0,5	0	0,01	0,01	0,01	0,01	0,01
lym	%	45-75	**37,2**	**72,3**	**42,9**	**42,4**	**37,4**	54,2
MON	%	2-7	**9,6**	**9,0**	**0,9**	**0,9**	**1,5**	0,8
NEU	%	15-45	**52,4**	**25,2**	54,3	54,3	58,8	53,8
EOS	%	1-8	0,8	3,4	1,9	2,3	2,2	2,2
BASS	%	0-3	0	0,1	0,1	0,1	0,1	0,1
RBC	10-12/mm^3	5-10	5,98	RBC	7,34	8,18	7,29	8,02
hgb	g/dl	8-15	9,3	hgb	11,3	11,9	11,5	11,8
Hct	%	24-46	28,49	28,76	33,51	37,55	34,59	34,65
CVM	fl	40-60	48	52	46	46	48	45
MCH	pg	11-17	15,6	17,3	15,3	14,5	15,7	13,8
MCHC	g/dl	30-36	32,7	33,5	33,6	31,7	33,1	32,4

The results of the hematological examination of blood samples taken on day 3 of the experiment are shown in Table 1. From the table it is noted that the hematological values are inscribed in the physiological parameters. Only in the leukocyte formula is observed in case 1.1. neutrophils with monocytosis. On day 7 of the experiment, the values shown in Table 2 were registered, showing slight changes in hematological parameters. Thus, in case 2.2 where batch 2 preparations were administered, a hyperleukocytosis with monocytosis. The data recorded at 14 days (Table 3) shows again, that the hematological examination is a little conclusive. It turns out that the 2 cows responded positively to the preparations of the batch 1. The results of the blood biochemical examination reveal important changes, recorded at days (Table 4). Changes are observed in the 2 cows throughout the experiment in terms of increased LDH, total bilirubin, alkaline phosphatase. 7 days after the beginning of the experiment (Table 5), the increase in total proteins with hyperglobulinemia is observed, the other biochemical parameters having values similar to those of day 3 of sampling. This also entitles us to perform an electrophoretic examination to elucidate which of the globulins undergoes changes and can explain, in addition to the clinical examination, the therapeutic evolution. And at 14 from the beginning of the experiment it turns out that they are the same changes in biochemical parameters (Table 6). And this time a hyperproteinemia occurs with an increase in globulin fractions.

We conducted the research between 01.05.202 and 19.05.2022.

Table 2 :

Paramet.	U/m	Physiology.	Charge 1		Charge 2		Charge 3	
		limits	1.1	1.2	2.1	2.2	3.1	3.2
WBC	10-9/mm^3	4-12	8,11	8,23	10,52	**13,03**	8,90	9,59
lym	10-9/mm^3	2,5-7,5	4,63	4,47	6,56	5,88	5,89	5,62
MON	10-9/mm^3	0-1	0,04	0,08	0,94	**1,29**	0,05	0,06
NEU	10-9/mm^3	0,6-7,6	3,21	3,10	2,65	5,02	2,63	3,42
EOS	10-9/mm^3	0,1-1	0,22	0,57	0,35	0,75	0,33	0,49
BASS	10-9/mm^3	0-0,5	0,01	0,01	0,01	0,09	0,01	0
lym	%	45-75	57,0	54,3	62,3	45,1	66,1	58,6
MON	%	2-7	**0,5**	**0,9**	**9,0**	**9,9**	**0,5**	**0,6**
NEU	%	15-45	39,6	37,7	25,2	38,5	29,5	35,7
EOS	%	1-8	2,7	6,9	3,4	5,8	3,7	5,1
BASS	%	0-3	0,1	0,1	0,1	0,7	0,1	0
RBC	10-12/mm^3	5-10	5,75	5,94	5,57	5,92	6,07	6,35
hgb	g/dl	8-15	10,4	9,7	9,6	10,0	9,1	10,2
Hct	%	24-46	32,59	30,77	28,76	31,19	30,30	33,82
CVM	fl	40-60	57	52	52	53	50	53
MCH	pg	11-17	**18,1**	16,3	**17,3**	16,9	14,9	16,0
MCHC	g/dl	30-36	32,0	31,5	33,5	32,0	29,9	30,1

A few days before the start of the experiment, I conducted a dosage of protein fractions in 5 control cows.

Serum protein electrophoresis is a technique that consists in the separate migration of protein fractions of serum on a semi-solid gel in the presence of an electric current.

The only individual protein that was distinctly separated from electrophoresis is albumin that showed a clinical correlation only when low values from normal appeared.

The 5 samples after staining to reveal the migration of protein fractions.

Table 3 :

Paramet.	U/m	Physiology.	Charge 1		Charge 2		Charge 3	
		limits	1.1	1.2	2.1	2.2	3.1	3.2
WBC	$^{10-9}$/mm^3	4-12	8,21	10,52	8,68	8,51	8,81	6,45
lym	$^{10-9}$/mm^3	2,5-7,5	3,20	5,64	4,87	4,00	3,26	3,66
MON	$^{10-9}$/mm^3	0-1	0,08	0,09	0,08	0,05	0,84	0,06
NEU	$^{10-9}$/mm^3	0,6-7,6	4,40	4,37	3,31	4,33	4,62	2,58
EOS	$^{10-9}$/mm^3	0,1-1	0,53	0,41	0,40	0,13	0.07	0,14
BASS	$^{10-9}$/mm^3	0-0,5	0,02	0,02	0,02	0	0	0
lym	%	45-75	**38,9**	53,6	56,2	47,0	37,2	56,8
MON	%	2-7	**1,0**	**0,8**	**0,9**	**0,6**	**9,6**	0,9
NEU	%	15-45	**53,6**	41,5	38,1	**50,9**	**52,4**	40,1
EOS	%	1-8	6,3	3,9	4,6	1,5	0,8	2,2
BASS	%	0-3	0,2	0,2	0,2	0	0	0,1
RBC	$^{10-12}$/mm^3	5-10	5,55	5,80	5,47	6,14	5,96	5,68
hgb	g/dl	8-15	9,0	9,5	8,9	9,2	9,3	9,7
Hct	%	24-46	28,04	29,76	28,01	29,15	28,49	31,11
CVM	fl	40-60	51	55	52	47	48	53
MCH	pg	11-17	**16,2**	16,4	16,2	15,0	15,6	16,5
MCHC	g/dl	30-36	32	32	31,7	31,6	32,7	31,0

Table 4 :

Paramet.	U/m	Physiology.	Charge 1		Charge 2		Charge 3	
		limits	1.1.	1.2.	2.1	2.2	3.1	3.2
Protein all	g/dl	5,8-8,5	**11,0**	**11,8**	7,1	6,8	6,3	7,6
Albumin	g/dl	2,5-3,7	3,8	3,8	2,7	3,3	3,5	3,3
Globulin	g/dl	3,3-4,8	7,2	8,2	4,4	3,5	2,8	4,3
GOOD	mg/dl	10-25	13	12	9	11	13	10
UA	mg/dl	1,0-2,1	2,0	2,0	1,0	1,1	0,9	2,3
The Create	mg/dl	0,4-1,0	0,4	0,6	1,0	1,2	1,1	0,5
T-Cho	mg/dl	70-280	152	127	75	85	71	230
GOT	UI/m	78-132	**42**	**27**	68	91	92	46
ldh	UI/m	692	**4000**	**4000**	**1422**	**1654**	**1637**	**3700**
T-Bil	mg/dl	0-0,3	**0,7**	**0,6**	**0,4**	**0,7**	**0,5**	**0,4**
GPT	UI/m	0-82	17	12	9	12	7	17
ALP	UI/m	0-80	118	113	110	135	69	**89**

Table 5:

Paramet.	U/m	Physiology.	Charge 1		Charge 2		Charge 3	
		limits	1.1.	1.2.	2.1	2.2	3.1	3.2
Protein all	g/dl	5,8-8,5	**11,0**	**11,2**	**12,4**	**10,5**	**10,4**	**9,6**
Albumin	g/dl	2,5-3,7	3,8	3,8	3,8	3,5	3,4	3,6
Globulin	g/dl	3,3-4,8	**7,2**	**7,4**	**9,6**	**7,0**	**7,0**	**6,0**
GOOD	mg/dl	10-25	12	13	12	13	10	11
UA	mg/dl	1,0-2,1	2,0	2,0	2,4	2,2	2,0	2,1
The Create	mg/dl	0,4-1,0	0,5	0,6	0,6	0,4	0,5	0,7
T-Cho	mg/dl	70-280	154	178	244	212	123	122
GOT	UI/m	78-132	**41**	**63**	**27**	**42**	**41**	39
ldh	UI/m	692	**4.000**	**3789**	**3560**	**3980**	**3800**	**3980**
T-Bil	mg/dl	0-0,3	0,4	0,4	0,3	0,3	0,3	0,4
GPT	UI/m	0-82	23	20	12	17	21	18
ALP	UI/m	0-80	**99**	**132**	**122**	**121**	**132**	**125**

Table 6:

Paramet.	U/m	Physiology. limits	Charge 1		Charge 2		Charge 3	
			1.1.	1.2.	2.1	2.2	3.1	3.2
Protein all	g/dl	5,8-8,5	**11,0**	**9,6**	**12,2**	**11,3**	**10,4**	**9,8**
Albumin	g/dl	2,5-3,7	3,7	3,6	**4,0**	**3,8**	3,7	3,5
Globulin	g/dl	3,3-4,8	**7,3**	**6,0**	**8,2**	**7,5**	**6,7**	**6,3**
GOOD	mg/dl	10-25	15	13	13	13	11	12
UA	mg/dl	1,0-2,1	2,8	2,0	2,2	2,3	2,1	2,1
The Create	mg/dl	0,4-1,0	0,6	0,6	0,6	0,5	0,5	0,6
T-Cho	mg/dl	70-280	160	162	142	123	133	154
GOT	UI/m	78-132	**44**	**41**	**31**	50	**46**	58
ldh	UI/m	692	**3800**	**3650**	**3880**	**3900**	**4000**	**3800**
T-Bil	mg/dl	0-0,3	0,4	0,2	0,3	0,4	0,3	0,3
GPT	UI/m	0-82	8	15	12	13	36	10
ALP	UI/m	0-80	**134**	**122**	**133**	**138**	**143**	**149**

Table 7:

Parameter	U/m	Physiology. limits	Case 1	Case 2	Case 3	Case 4	Case 5
Protein all	g/dl	5,8-8,5	8,60	9,40	7,10	6,80	6,30
Albumin	g/dl	2,5-3,7	3,80	3,80	2,70	3,30	3,50
Globulin	g/dl	3,3-4,8	4,80	5,60	4,40	3,50	2,80

Table 8:

Fraction	U/m	Physiology. limits	Case 1	Case 2	Case 3	Case 4	Case 5
Total Protein	g/dl	5,8-8,5	6,40	7,10	6,70	6,90	6,30
Albumin	g/dl	1,3-2,47	1,83	2,08	2,20	**2,62**	**2,76**
α1	g/dl	0,19-0,78	0,42	0,35	**0,10**	0,41	0,30
α2	g/dl	0,19-0,78	0,60	0,79	0,78	0,49	0,40
β1	g/dl	0,32-0,84	**1,00**	0,75	0,97	0,69	0,64
β2	gd/m	0,32-0,84	0,44	0,57	0,76	0,52	0.35
γ	g/dl	1,75-2,72	2,21	2,57	2,09	2,17	1,86
White/Globe Ratio	/	0,45-1,31	**1,83: 4,57**	**2,08: 5,02**	0,48	0,61	0,78

The value of protein parameters, by biochemical examinations, using kits (Table 7).

Determination of protein fractions by electrophoresis revealed the following situation (Table 8).

The most important observations on the therapeutic efficacy of the tested preparation were found in the clinical and gynecological examinations, for which we present the appearance of the vaginal discharge certifying endometrial infection: on the first day of the experiment, after performing the transrectal examination, a purulent discharge appears; 10 days after the beginning of the experiment the secretion disappeared, and at the control on the 14th day, samples were collected for cytological and bacteriological examination.

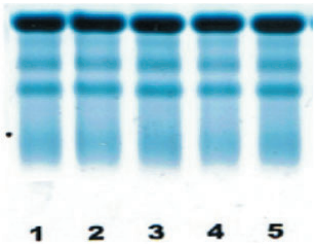

Figure 3. Migration of protein fractions.

Conclusions

1. Depending on the severity of endometritis may be used different pharmaceutical forms created for preventive, curative purposes or with the aim of supporting classical treatment, with antibiotic.
2. For a better management of clinical endometritis we recommend the association of the created phytoextracts with the treatment used at the classical case.
3. Following the analyzes and researches carried out, it was identified the stimulation of the cellular immune response in the studied cows, a faster healing time being

Case 1

FACULTY OF VETERINARY MEDICINE BUCHAREST
28.04.2022

Pacient:

Varsta: Sex: ID:

Rezultate analiza:

Total Proteine = 6,40 g/dl Raport A/G = 2,19

Parametru	*Rezultate (%)*	*Rezultate (g/dl)*	*Referinte (%)*
[H] Alb	68,63	4,39	27...38
Alfa1	5,30	0,34	4...8
Alfa2	5,64	0,36	4...8
[H] Beta	18,57	1,19	5...10
[L] Gama	1,86	0,12	12...22

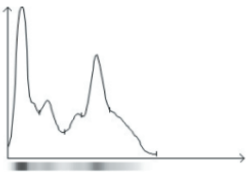

Case 2

FACULTY OF VETERINARY MEDICINE BUCHAREST
28.04.2022

Pacient:

Varsta: Sex: ID:

Rezultate analiza:

Total Proteine = 7,10 g/dl Raport A/G = 0,64

Parametru	*Rezultate (%)*	*Rezultate (g/dl)*	*Referinte (%)*
[H] Alb	38,96	2,77	27...38
Alfa1	5,79	0,41	4...8
[H] Alfa2	8,48	0,60	4...8
[H] Beta	13,88	0,99	5...10
[H] Gama	32,88	2,33	12...22

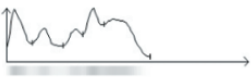

Case 3

FACULTY OF VETERINARY MEDICINE BUCHAREST
28.04.2022

Pacient:

Varsta: Sex: ID:

Rezultate analiza:

Total Proteine = 6,70 g/dl Raport A/G = 1,04

Parametru	*Rezultate (%)*	*Rezultate (g/dl)*	*Referinte (%)*
[H] Alb	51,01	3,42	27...38
Alfa1	5,54	0,37	4...8
[H] Alfa2	8,18	0,55	4...8
[H] Beta	18,20	1,22	5...10
Gama	17,06	1,14	12...22

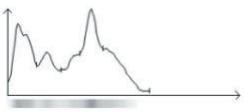

Case 4

FACULTY OF VETERINARY MEDICINE BUCHAREST
28.04.2022

Pacient:

Varsta: Sex: ID:

Rezultate analiza:

Total Proteine = 6,90 g/dl Raport A/G = 1,24

Parametru	*Rezultate (%)*	*Rezultate (g/dl)*	*Referinte (%)*
[H] Alb	55,34	3,82	27...38
Alfa1	5,44	0,38	4...8
[H] Alfa2	8,32	0,57	4...8
[H] Beta	14,43	1,00	5...10
Gama	16,47	1,14	12...22

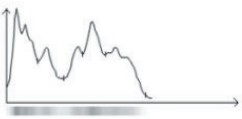

Case 5

FACULTY OF VETERINARY MEDICINE BUCHAREST

28.04.2022

Pacient:

Varsta: Sex: ID:

Rezultate analiza:

Total Proteine = 6,30 g/dl Raport A/G = 2,19

Parametru	*Rezultate (%)*	*Rezultate (g/dl)*	*Referinte (%)*
[H] Alb	68,60	4,32	27...38
Alfa1	4,98	0,31	4...8
[H] Alfa2	8,58	0,54	4...8
[H] Beta	14,67	0,92	5...10
[L] Gama	3,16	0,20	12...22

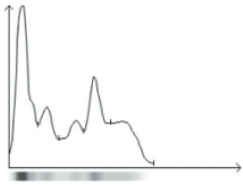

Figure 4. Vaginal discharge in first day.

Figure 5. Secretion disappeared in 10th day.

established in the animals of group 3 in which the two products (tablets and intrauterine solution) were associated in the treatment.

4. It has been found that the product has a local antiseptic effect.

References

5. Fabio Lima, University of California, Davis (2022). Endometritis in Production Animals
6. Kassahun A. Negasee (2020). Clinical Metritis and Endometritis in Diary Cattle: A Review,
7. Iain Martin Sheldon, Sian E Owens (2017). Postpartum uterine infection and endometritis in dairy cattle.
8. Meng-Ling Wang, Ming-Chao Liu, Jin Xu, Li-Gang An, Jiu-Feng Wang, and Yao-Hong Zhu (2018). Uterine Microbiota of Dairy Cows With Clinical and Subclinical Endometritis.
9. Cows S. J. LeBlanc, T. F. Duffield, K. E. Leslie,K. G. Bateman,G. P. Keefe, J. S. Walton, and W. H. Johnson (2002). The Effect of Treatment of Clinical Endometritis on Reproductive Performance in Dairy.
10. Haben Fesseha (2020). Clinical and Sub-Clinical Endometritis and its Impact in Reproductive Performance of Cattle: A Review.
11. Timothy J. Potter, Javier Guitian, John Fishwick , Patrick J. Gordon, I. Martin Sheldon , March (2010). Risk factors for clinical endometritis in postpartum dairy cattle.
12. M. Umer, S. F. Syed, Bunesh, Q. A. Shah and I. U. Kakar, (2022). Pathogenesis, treatment and control of bovine clinical endometritis: a review.
13. Renan Braga Paiano, Ricardo Luiz Moro de Sousa, Jeannine Bonilla, Andrea Micke Moreno (2022). In vitro effects of cinnamon, oregano, and thyme essential oils against Escherichia coli and Trueperella pyogenes isolated from dairy cows with clinical endometritis.
14. Kiracofe GH (1980). Uterine involution: its role in regulating postpartum intervals. Journal of animal science 51 Suppl 2: 16–28.
15. Wagener K, Gabler C, Drillich M (2017). A review of the ongoing discussion about definition, diagno-

sis and pathomechanism of subclinical endometritis in dairy cows. Theriogenology 94: 21–30. 10.1016/j.theriogenology.2017.02.005

16. Sheldon IM, Price SB, Cronin J, Gilbert RO, Gadsby JE (2009). Mechanisms of infertility associated with clinical and subclinical endometritis in high producing dairy cattle. Reproduction in domestic animals = Zuchthygiene 44 Suppl 3: 1–9
17. Davies D, Meade KG, Herath S, Eckersall PD, Gonzalez D, et al. (2008). Toll-like receptor and antimicrobial peptide expression in the bovine endometrium. Reprod Biol Endocrinol 6: 53 10.1186/1477-7827-6-53
18. Herath S, Fischer DP, Werling D, Williams EJ, Lilly ST, et al. (2006). Expression and function of Toll-like receptor 4 in the endometrial cells of the uterus. Endocrinology 147: 562–570. 10.1210/en.2005-1113
19. Menzies M, Ingham A (2006). Identification and expression of Toll-like receptors 1–10 in selected bovine and ovine tissues. Veterinary immunology and immunopathology 109: 23–30. 10.1016/j.vetimm.2005.06.014.

ISSN print: 1224-5984
ISSN online: 2248-3942

Rom Biotechnol Lett. 2022; 27(5): 3691-3698
doi: 10.25083/rbl/27.5/3691.3698

Received for publication, August 27, 2020
Accepted, October, 20, 2020

Original article

Biphasic response of epidermoid adenocarcinoma cells to curcumin and EGCG co-treatment

OANA-ALINA HAZAPARU[1#], ALEXANDRU FILIPPI[1,2#], OANA-CEZARA VLAD[1], CARMEN-MARIANA CHIFIRIUC[3,4], CONSTANȚA GANEA[1], MARIA-MAGDALENA MOCANU[1*]

[1] Department of Biophysics, "Carol Davila" University of Medicine and Pharmacy, 050474, Bucharest, Romania

[2] Department of Pathophysiology and Pharmacology, "Nicolae Simionescu" Institute of Cellular Biology and Pathology, 030167 Bucharest, Romania

[3] Microbiology Immunology Department Faculty of Biology University of Bucharest 1-3 Portocalelor Lane, 77206 Bucharest, Romania

[4] Research Institute of University of Bucharest – ICUB, Bucharest, Romania

[#] These two authors equally contributed to this work

Abstract

We investigated the combinatorial treatment of curcumin and epigallocatechin-gallate (EGCG) in human epidermoid carcinoma cell line A-431. When combined, concentrations of EGCG and curcumin lower than 25 μM increased proliferation, but 50 μM curcumin led to near complete proliferation/viability inhibition. As reference, the compounds were also tested on normal fibroblast cells, CCD-1070Sk, where they did not show any toxicity, except in the highest concentration sample. In A-431 cell line, curcumin and EGCG combinations induced cell death by apoptosis, collapse of the mitochondrial membrane depolarization (ΔΨm) and increase the cell number in S phase of cell cycle. Nevertheless, the most powerful compound in inducing the above effects was curcumin. Next, we have shown that EGCG scavenged ROS produced by 25 μM curcumin with an EC50 of 44.34 μM EGCG. In conclusion, curcumin and EGCG combinations exert ΔΨm collapse, cell death and cell cycle arrest in A-431 cells at concentrations not affecting the viability of normal skin fibroblasts.

Keywords curcumin, EGCG, epidermoid adenocarcinoma, biphasic response, cytotoxicity

To cite this article: OANA-ALINA HAZAPARU. Biphasic response of epidermoid adenocarcinoma cells to curcumin and EGCG co-treatment. *Rom Biotechnol Lett.* 2022; 27(5): 3691-3698
DOI: 10.25083/rbl/27.5/3691.3698

*Corresponding author: Maria-Magdalena Mocanu; e-mail: magda.mocanu@umfcd.ro;
Cell phone: +40745084184

Introduction

The polyphenols are known for their ability to interfere with tumor formation, which may also reduce the risk of developing different types of cancer (LAUBACH et al. [10]). A better understanding of the mechanisms of actions of phytochemicals can help us adopt the best strategy in cancer prevention. One of the most well-known polyphenols are the catechins found in green tea, especially epigallocatechin-3-gallate (EGCG) and it has been used frequently as an anti-carcinogenic agent *in vivo* and *in vitro* studies (HU et al. [5]). Curcumin is the natural polyphenol from turmeric, found in the roots of the herbaceous perennial plant, *Curcuma longa*, which is naturally found in Asian countries (HEWLINGS et al. [4]). Recent studies revealed the useful properties of curcumin in cancer progression by inducing apoptosis and oxidative stress in tumour formation, in cooperation with modulator activity of inflammatory signaling pathways (SHABANINEJAD et al. [13]). In previous studies, our research group studied the effects of curcumin or EGCG in A-431 epidermoid cancer cell line, but as individual exposure (CIOLAC et al. [2], MOCANU et al. [12], FILIPPI et al. [3]). New studies demonstrated that EGCG may also have synergistic activity with curcumin and other drugs, in different cancer cell lines (JIN et al. [6]).

The aim of the study was to investigate the combinatorial effect of curcumin and EGCG in the hypertriploid human epidermoid carcinoma cell line, A-431. Several concentrations of curcumin and EGCG are used to study the effect of curcumin and EGCG on colony formation, viability, mitochondrial membrane depolarization and formation of reactive oxygen species (ROS). We also demonstrated that curcumin and EGCG induce apoptosis in a dose-dependent manner and this is correlated with the increase of curcumin concentration. To investigate whether EGCG and curcumin have harmful effects onto normal human cells, these two compounds were tested in experiments with CCD-1070Sk, a normal fibroblast skin cell line.

Materials and Methods

Cell cultures and treatments

Experiments were performed using epidermoid carcinoma cell line A-431 and normal skin fibroblast CCD-1070Sk cells from American Type Culture Collection. The cells were grown in DMEM (Sigma, Saint Louis, MO) supplemented with 10% heat inactivated FBS (Sigma, Saint Louis, MO), 2 mM L-glutamine (Thermo Fisher Scientific/ Gibco, Carlsbad, CA) and 1% Penicillin/Streptomycin (Thermo Fisher Scientific/ Gibco, Carlsbad, CA), in a humidified incubator at 37°C, 5% CO2. Curcumin (Sigma, Saint Louis, MO) and EGCG (Sigma, Saint Louis, MO) were used from 50 mM solutions prepared in DMSO (Sigma, Saint Louis, MO) in the day of the experiment. In all control samples, DMSO was added at the same volume as in the treated samples.

Cytotoxicity assay

A-431 and CCD-1070Sk cells were seeded in 96-well flat-bottom microplates at a density of 10^4 and 2 x 10^4 cells/well, respectively 24 h prior to the experiments and incubated for 48 h with either 25 μM curcumin plus 0, 5, 10, 25, 50 μM EGCG or 25 μM EGCG plus 0, 5, 10, 25, 50, 100 μM curcumin or DMSO control. The viability assay was carried out with water soluble tetrazolium salt (Roche Diagnostics GmbH, Mannheim, Germany) to evaluate the influence of number of the cells on the viability experiments. The assay is based on the reduction of water soluble tetrazolium salt (WST-1) to formazan in viable cells due to mitochondrial dehydrogenase activity. The absorbance of formazan was measured at 450 nm and corrected at 620 nm using a 96-well spectrophotometer (Infinite 200 PRO plate reader, Tecan Life Sciences).

ROS production and viability assay

Cells plated in 6 well plates at 2 x 10^5 cells/well were let to adhere for 24 h and then treated with 25 μM curcumin plus 0, 5, 10, 25, 50,100 μM EGCG or 25 μM EGCG plus 0, 5, 10, 25, 50, 100 μM curcumin or DMSO control for 48 h. Trypsinized cells and those found in the supernatant were stained for 30 min with 5-(and-6)-carboxy-2',7'- dichlorodihydro-fluorescein diacetate (caboxy-

H_2DCFDA, Molecular Probes) and propidium iodide for 15 min and washed in PBS; the samples were measured with Gallios (Beckman Coulter, Brea, CA) flow cytometer (excitation: 488 nm, emission: 525 ± 40 nm for carboxy-H_2DCFDA and emission: 620 ± 30 nm for propidium iodide). Curcumin fluorescence was subtracted from treated, non-stained samples. EC50 was calculated by the best nonlinear fit using Equation (1):

$$Y = \frac{Top - Bottom}{1 + 10^{(LogIC50 - X) \times HillSlope}} \quad (1)$$

where, X is logarithm with base 10 of the concentration of EGCG, LogEC50 is the logarithm with base 10 of the half-maximal effective concentration, Y is carboxy-H_2DCFDA fluorescence intensity, and "top" and "bottom" are plateau values.

Mitochondrial membrane potential

A-431 cells were grown in 6 well plates, incubated for 48 h with 25 μM curcumin plus 0, 5, 10, 25, 50, 100

μM EGCG or 25 μM EGCG plus 0, 5, 10, 25, 50, 100 μM curcumin or DMSO control, stained 15 minutes with 5 μg/ml JC-1 (Thermo Fisher, Carlsbad, CA) at 37°C, trypsinized, washed in PBS and measured with Gallios (Beckman Coulter, Brea, CA) flow cytometer (excitation: 488 nm, JC1 monomer emission: 525 ± 40 nm, JC1 aggregates emission: 575 ± 30 nm). Curcumin fluorescence was subtracted from treated, non-stained samples. EC50 values were calculated from inhibition curves fitted in Prism 5 (GraphPad Software Inc., USA).

Cell cycle evaluation

A number of 2 x 10^5 A-431 cells were seeded in 6 well plates and, after being left to adhere for 24 h, the cells were synchronized in the G_0/G_1 phase of the cell cycle by 24 h incubation in serum free media. At this point, the cells were treated for 48 h with 25 μM curcumin plus 0, 5, 10, 25, 50 μM EGCG or 25 μM EGCG plus 0, 5, 10, 50, 100 μM curcumin or DMSO control, fixed for 3 h in 70% ethanol at -20°C, stained with propidium iodide in RNase staining buffer (BD Bioscience, San Jose, CA). Measurements are carried out with Gallios (Beckman Coulter, Brea, CA) flow cytometer (excitation: 488 nm, emission: 620 ± 30 nm). Deconvolution and gating of the populations in different cell cycle phases was done automatically in Flowing Software 2.5.1 (University of Turku, Finland).

Apoptosis assay

A-431 cells plated in 6 well plates at 2 x 10^5 cells/well were let to adhere for 24 h and then treated with 25 μM curcumin plus 0, 5, 10, 25, 50, 100 μM EGCG or 25 μM EGCG plus 0, 5, 10, 25, 50, 100 μM curcumin or DMSO control for 48 h. The supernatant was collected, added to the trypsinized cells, washed in PBS and stained with propidium iodide and Annexin V-APC. The samples were measured with Gallios (Beckman Coulter, Brea, CA) flow cytometer (excitation: 488 nm, emission: 620 ± 30 nm for propidium iodide and excitation: 635 nm, emission: 660 BP for Annexin V-APC). Curcumin fluorescence was subtracted from treated, non-stained samples.

Data analysis

Data are represented as mean ± standard error of the mean (s.e.m.). Significance was assayed ANOVA with Dunnett post-test for multiple column analysis. A value of $p < 0.05$ was set as level of significance. Raw data were analyzed using Flowing Software 2.5.1 (University of Turku, Finland) and ImageJ v.1.48 (NIH, USA) and for the statistical analysis Microsoft Excel 2010 (Microsoft Inc., USA) and Prism 5 (GraphPad Software Inc., USA) were used.

Results and Discussions

Small EGCG and curcumin concentrations increase cell proliferation, high curcumin concentrations lead to cytotoxicity in the A-431 cell line. Normal fibroblasts are unaffected

In our experiments (Fig. 1A, 1B) with A-431 cell line, small concentrations of EGCG and curcumin led to a moderate increase in proliferation (a maximum of 167.8 ± 26.22 % for the 25 μM EGCG, 10 μM curcumin sample compared to the 100 ± 35.4 % in the control), while the higher curcumin concentrations of 50 and 100 μM highly reduced the number of metabolically active cells (21.6 ± 5.2% and 14.26 ± 4.2%, respectively). In normal fibroblasts cell line, CCD-1070Sk small compound concentrations also led to an increase in proliferation (160.2 ± 30.3% in the 25 μM curcumin plus 5 μM EGCG sample), while the highest concentrations tested, 25 μM plus 100 μM curcumin led to a moderate drop in viable cells (60.2 ± 21.7%).

EGCG and curcumin combinations induce cell death in the A-431 cell line

To confirm the results obtained in WST-1 tests, we assayed cell death by flow cytometric measurement of propidium iodide stained A-431 cells (Fig. 1C, 1D). The viability of 25 μM EGCG plus up to 10 μM curcumin treated samples was not affected while higher curcumin concentrations were highly cytotoxic. 25 μM EGCG plus 25 μM curcumin reduced viability to 42.7 ± 12.7% (**$p<0.01$, one way ANOVA, Dunnett post-test), 25 μM EGCG plus 50 μM curcumin to 36.0 ± 4.6% (***$p<0.001$) and 25 μM EGCG plus 100 μM curcumin to 7.0 ± 0.9% (***$p<0.001$). This effect is caused mainly by curcumin as 25 μM curcumin alone reduced viability to 47.0 ± 4.3% and the addition of increasing EGCG concentrations up to 100 μM did not substantially change this proportion.

Curcumin induces reactive oxygen species formation, EGCG scavenges ROS

The concentration of 25 μM curcumin, found to induce cell death in about 50% of cells, induced massive ROS production (MFIR of 7.7). EGCG alone did not generate ROS as it does when used alone (FILIPPI et al. [3]) and increasing concentrations of EGCG scavenged ROS efficiently (with a MFIR of 5.03 in the 25 μM curcumin and 50 μM EGCG sample, **$p<0.01$, and a MFIR of 3.81 in the 25 μM curcumin and 100 μM EGCG sample, ***$p<0.001$, one way ANOVA, Dunnett post-test) (Fig. 2). EGCG mediated the reduction of curcumin-induced ROS production with an EC50 of 43.3 μM. Increasing curcumin concentrations could not be tested as carboxy-H_2DCFDA bleached curcumin fluores-

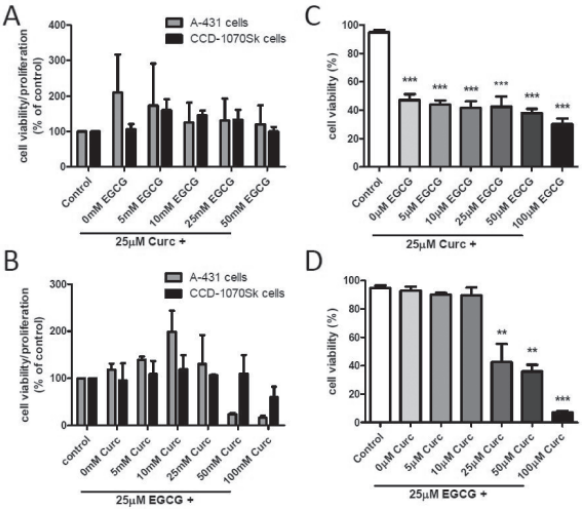

Figure 1. EGCG – curcumin co-treatment induces tumor cell death. (A) The total number of viable cells as influenced by cell death and cell proliferation is mainly unaffected by 25 μM curcumin plus varying EGCG concentrations in both cancer and normal cells. (B) 25 μM EGCG plus higher than 50 μM curcumin drastically reduces the viability/proliferation of cancer cells, with no or little effect on normal, not transformed, cells. (C) 25 μM curcumin reduces by itself the viability to about 50% and the addition of up to 100 μM EGCG contributes to an additional drop in viability to about 30% in A-431 cells. (D) By itself, 25 μM EGCG does not influence tumor cell viability and the addition of curcumin reduces the viability in a dose-dependent manner, with 100 μM curcumin being toxic to almost all A-431 cells. Each column represents mean and s.e.m. from three repetitions and significance was assessed with ANOVA / Dunnett post-test *p<0.05, **p<0.01, ***p<0.001.

cence possibly by FRET and curcumin only treated cells had higher fluorescence than the corresponding curcumin plus carboxy-H_2DCFDA samples.

Mitochondrial membrane potential collapse after exposure to treatment

When cells were treated with a fixed 25 μM EGCG concentration and increasing curcumin concentrations, curcumin showed an EC50 value 23.5 μM in mitochondrial membrane depolarization, with 50 and 100 μM curcumin inducing $\Delta\Psi m$ collapse in most of the cells (85.1 ± 8.3% cells and 83.6 ± 15.7, respectively, **p<0.01, way ANOVA, Dunnett post-test) (Fig. 3B). This effect was almost entirely caused by curcumin and not EGCG as 25 μM curcumin alone induced mitochondrial potential collapse in about half the cells (48.9 ± 18.7%) (Fig. 3E). The lower $\Delta\Psi m$ reduction action of EGCG was also shown in experiments where the curcumin concentration was fixed at 25 μM and no substantial added drop in $\Delta\Psi m$ was observed

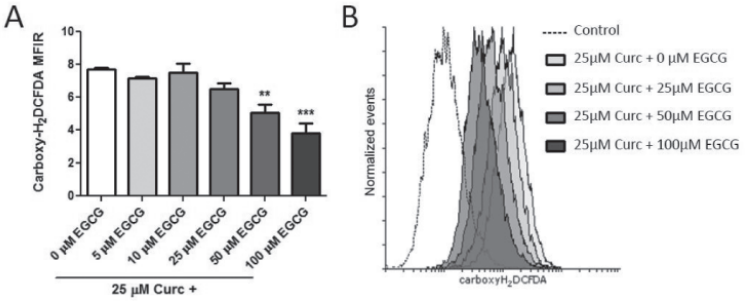

Figure 2. EGCG scavenges the Reactive Oxygen Species (ROS) produced by curcumin. (A) EGCG shows a dose dependent decrease in the ROS generated after 25 μM curcumin treatment, the highest concentration tested, 100 μM EGCG, halving the fluorescence associated with the ROS intracellular concentration. (B) Also shown are representative histograms for 25 μM curcumin plus varying EGCG concentrations treated samples versus control. **p<0.01, ***p<0.001 by ANOVA with the Dunnett post-test.

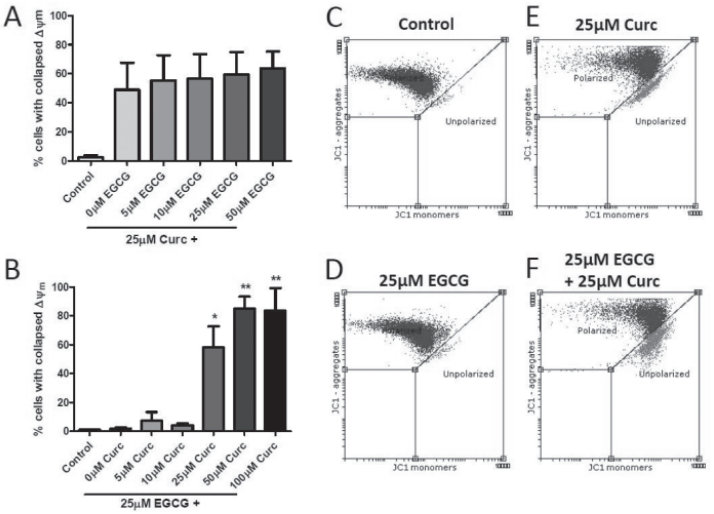

Figure 3. Curcumin leads to mitochondrial membrane depolarization. (A) 25 μM curcumin treatment results in $\Delta\Psi m$ collapse in more than half the cancer cells, while the co-administered EGCG adds little to this effect. (B) 25 μM EGCG alone does not alter the $\Delta\Psi m$, but the co-administered curcumin shows a dose dependent collapse of the $\Delta\Psi m$. The dot plots show in blue cells with normal $\Delta\Psi m$, as indicated by the predominance of JC-1 aggregates fluorescence and in red cells with collapsed $\Delta\Psi m$ having more JC-1 in monomeric form for the (C) control cells, (D) 25 μM EGCG, (E) 25 μM curcumin and co-treatment with (F) 25 μM EGCG and 25 μM curcumin. *p<0.05, **p<0.01 by ANOVA with the Dunnett post-test.

with an increase in EGCG concentration of up to 50 μM (Fig. 3A).

Flow cytometric measurement of cell cycle phase after exposure to treatment

Incubation with 25 μM curcumin (9.6 ± 2.5 compared to 5.8 ± 3.5% in control) nearly doubled the number of A-431 cells in the S phase of the cell cycle and this level maintained in plateau with the addition of up to 100 μM EGCG (with the sole exception of an even higher increase to 13.7 ± 3.5% in the case of 50 μM EGCG) (Fig. 4). The percent of cells in the G_2/M phase also rose moderately (41.1 ± 9.0 compared with 31.8 ± 2.7% in control) and these changes were associated with lower cell numbers in the G_0/G_1 phase. EGCG treatment does not influence the cell cycle progression of A-431 cells.

Effect of the treatment on apoptosis

To test whether the induced cell death was by means of apoptosis, we assessed the Annexin V-APC/ propidium iodide staining of EGCG/curcumin co-treated cells (Fig. 5). In these experiments, 25 μM curcumin alone induced early apoptosis in 11.1 ± 1.8 % cells (compared with the 1.1 ± 0.4% in the control cells, ***p<0.001) and late apoptosis in 23.2 ± 2.5 % (compared with the 0.8 ± 0.6% in the control cells, ***p<0.001). Addition of up to 100 μM EGCG did not significantly change the apoptosis inducement profile of 25 μM curcumin alone. However, when cells were treated with a fixed 25 μM EGCG concentration plus varying amounts of curcumin, a dose-dependent response was obtained for both early and late apoptosis inducement.

The main results of this study are related to biphasic effect of EGCG and curcumin, the lack of toxicity or reduced toxicity in non-transformed cells and the ability of EGCG to scavenge ROS after their induction by curcumin. The anti-proliferative effect of EGCG-curcumin or curcumin-EGCG was associated with mitochondrial membrane collapse and apoptosis. Nevertheless, CCD-1070Sk non-transformed fibroblasts are not sensitive to concentration of EGCG or curcumin used in this study, with only one exception in case of the highest dose of combined treatment, respectively 100 μM curcumin and 25 μM EGCG.

Interestingly, the biphasic effect of EGCG and curcumin was identified in both transformed and non-transformed cell lines. Lower concentrations of EGCG and curcumin increased cell proliferation, while higher concentrations induced cytotoxic effects. These data are in line with previous reported results, since EGCG and curcumin have been shown to display both anti-oxidative effect due the phenol rings (TIPOE et al. [15], ABRAHAMS et al. [1]), and pro-oxidative function through increased production of ROS (LI et al. [11], KOCYIGIT et al. [9]). For instance, the anti-oxidant effect of EGCG has further applications in cardio-vascular protection, where catechin demonstrated the ability to decrease lipid peroxidation or to scavenge free radicals

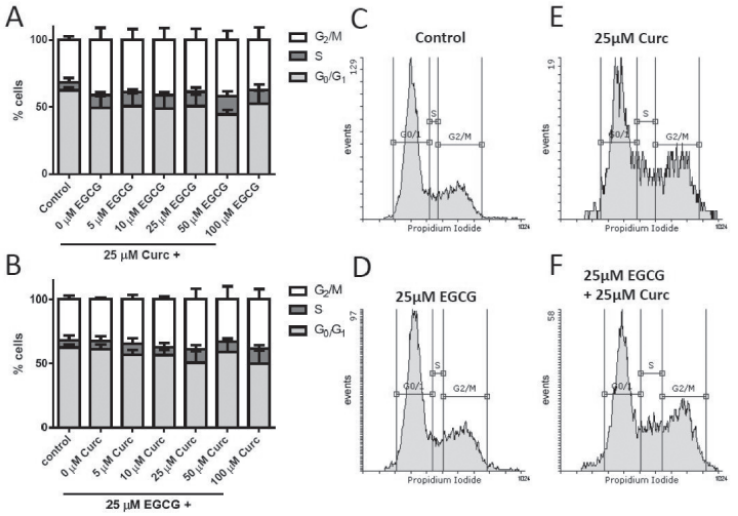

Figure 4. Curcumin alters the cell cycle progression. (A, B) 25 µM curcumin reduces the number of cells found in the G_0/G_1 phase of the cell cycle with a concomitant doubling of the cell numbers in the S phase and a slight increase in the number of cells in the G_2/M phase. Increasing EGCG concentrations of up to 100 µM do not seem to alter the cell cycle progression. Also shown are representative histograms showing gated cells in each cell cycle phase for (C) control cells, (D) 25 µM EGCG treated cells, (E) 25 µM curcumin treated cells and (F) co-treatment with 25 µM EGCG and 25 µM curcumin. Gates were automatically set in Flowing Software 2.5.1 using the built in deconvolution for cell cycle analysis function.

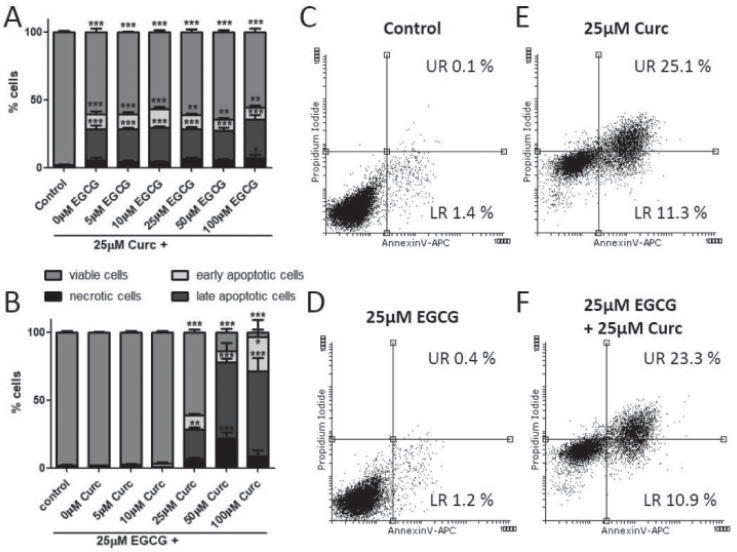

Figure 5. Curcumin induces tumor cell death by apoptosis. (A) 25 µM curcumin led to apoptosis as shown by the Annexin V-APC binding to one third of the cells. Adding EGCG to this concentration did not significantly change the viability or percent late (UR) versus early (LR) apoptotic cells. (B) Also, 25 µM EGCG by itself does not influence apoptosis induction but the addition of curcumin induces apoptosis in a dose-dependent manner for concentration larger than 10 µM curcumin, with 100 µM curcumin killing almost all cells through apoptosis. The dot plots show Annexin V-APC and Propidium Iodide binding in (C) control cells, (D) 25 µM EGCG, (E) 25 µM curcumin and (F) co-treatment with 25 µM EGCG and 25 µM curcumin. At the tested time of 72 h most apoptotic cells were late apoptotic cells. *p<0.05, **p<0.01, ***p<0.001 by ANOVA with the Dunnett post-test.

(TIPOE et al. [15]). At the same time, the anti-oxidant activity of curcumin was investigated in relationship of its ability to protect nervous system (ABRAHAMS et al. [1]). On the other hand, the pro-oxidative activity of both natural compounds, EGCG and curcumin, was frequently associated with inhibition of highly proliferative cancer cells (LI et al. [11], KOCYIGIT et al. [9]).

Combined treatment of curcumin and EGCG resulted in induction of cell death, demonstrated by spectrophotometric and flow cytometric measurements, collapse of mitochondrial membrane potential, cell cycle arrest and apoptosis in A-431 epidermoid carcinoma cells. Nevertheless, most of the effects have been due to curcumin administration and to a lower extent due to EGCG. Curcumin is known to have anti-cancer effects such as autophagy, apoptosis and cell cycle arrest (ZHU et al. [17]), increased expression of death receptor 5 (JUNG et al. [7]), and altered expression of a large number of kinases, enzymes and anti-apoptotic proteins such as Bcl-2 (SHANMUGAM et al. [14]).

Moreover, curcumin is a potent inducer of ROS production in cancer cells is known from studies that use a fixed curcumin concentration and follow the kinetics of ROS production (KHAN et al. [8]). Interestingly, our results indicated a reduction in ROS induced by curcumin after combined treatment with EGCG. This might be seen as a caution when discussing pro-oxidative effect, in case of combined administration of higher doses of curcumin and low doses of EGCG. Nevertheless, this effect might represent an asset in case of EGCG, since this compound might display protective effect in normal cells after exposure to cancer therapy, such as ionizing radiation (ZHU et al. [16]).

Conclusions

In conclusion, our experiments showing the effect of EGCG and curcumin co-treatments, indicate both anti- and pro-oxdative effects, the later ones demonstrating induction of cell death, cell cycle arrest and $\Delta\Psi m$ collapse in A-431 epidermoid cancer cells. These treatment combinations induced a greater drop in viability/proliferation of the cancer cells compared to normal skin fibroblasts. However, caution should be taken in case of utilizing higher concentrations of curcumin as pro-oxidative agent in combination with EGCG, since the later one might be responsible for ROS scavenging.

References

1. ABRAHAMS, S., HAYLETT, W. L., JOHNSON, G., CARR, J. A. & BARDIEN, S. Antioxidant effects of curcumin in models of neurodegeneration, aging, oxidative and nitrosative stress: A review. *Neuroscience* 2019; 406(-): 1-21, doi: 10.1016/j.neuroscience.2019.02.020.
2. CIOLAC, O. A., FILIPPI, A., MARU, N., POPA, M., CHIFIRIUC, C., GANEA, C. & MOCANU, M. M. Reduction of the clonogenic potential and collapse of the mitocondrial membrane potential in A-431 epidermoid carcinoma cell line induced by curcumin *Rom Biotech Lett* 2017; 22(6): 13068-13077, doi: 10.26327/RBL2017.18.
3. FILIPPI, A., PICOT, T., AANEI, C. M., NAGY, P., SZOLLOSI, J., CAMPOS, L., GANEA, C. & MOCANU, M. M. Epigallocatechin-3-O-gallate alleviates the malignant phenotype in A-431 epidermoid and SK-BR-3 breast cancer cell lines. *Int J Food Sci Nutr* 2018; 69(5): 584-597, doi: 10.1080/09637486.2017.1401980.
4. HEWLINGS, S. J. & KALMAN, D. S. Curcumin: A Review of Its' Effects on Human Health. *Foods* 2017; 6(10): 92, doi: 10.3390/foods6100092.
5. HU, G., ZHANG, L., RONG, Y., NI, X. & SUN, Y. Downstream carcinogenesis signaling pathways by green tea polyphenols: a translational perspective of chemoprevention and treatment for cancers. *Curr Drug Metab* 2014; 15(1): 14-22, doi: 10.2174/1389200214666131211155613.
6. JIN, G., YANG, Y., LIU, K., ZHAO, J., CHEN, X., LIU, H., BAI, R., LI, X., JIANG, Y., ZHANG, X., LU, J. & DONG, Z. Combination curcumin and (-)-epigallocatechin-3-gallate inhibits colorectal carcinoma microenvironment-induced angiogenesis by JAK/STAT3/IL-8 pathway. *Oncogenesis* 2017; 6(10): e384, doi: 10.1038/oncsis.2017.84.
7. JUNG, E. M., LIM, J. H., LEE, T. J., PARK, J. W., CHOI, K. S. & KWON, T. K. Curcumin sensitizes tumor necrosis factor-related apoptosis-inducing ligand (TRAIL)-induced apoptosis through reactive oxygen species-mediated upregulation of death receptor 5 (DR5). *Carcinogenesis* 2005; 26(11): 1905-13, doi: 10.1093/carcin/bgi167.
8. KHAN, M. A., GAHLOT, S. & MAJUMDAR, S. Oxidative stress induced by curcumin promotes the death of cutaneous T-cell lymphoma (HuT-78) by disrupting the function of several molecular targets. *Mol Cancer Ther* 2012; 11(9): 1873-83, doi: 10.1158/1535-7163.MCT-12-0141.
9. KOCYIGIT, A. & GULER, E. M. Curcumin induce DNA damage and apoptosis through generation of reactive oxygen species and reducing mitochondrial membrane potential in melanoma cancer cells. *Cell Mol Biol (Noisy-le-grand)* 2017; 63(11): 97-105, doi: 10.14715/cmb/2017.63.11.17.
10. LAUBACH, V., KAUFMANN, R., BERND, A., KIPPENBERGER, S. & ZOLLER, N. Extrinsic or

Intrinsic Apoptosis by Curcumin and Light: Still a Mystery. *Int J Mol Sci* 2019; 20(4): 905, doi: 10.3390/ijms20040905.

11. LI, G. X., CHEN, Y. K., HOU, Z., XIAO, H., JIN, H., LU, G., LEE, M. J., LIU, B., GUAN, F., YANG, Z., YU, A. & YANG, C. S. Pro-oxidative activities and dose-response relationship of (-)-epigallocatechin-3-gallate in the inhibition of lung cancer cell growth: a comparative study in vivo and in vitro. *Carcinogenesis* 2010; 31(5): 902-10, doi: 10.1093/carcin/bgq039.
12. MOCANU, M. M., NAGY, P. & SZOLLOSI, J. Chemoprevention of Breast Cancer by Dietary Polyphenols. *Molecules* 2015; 20(12): 22578-620, doi: 10.3390/molecules201219864.
13. SHABANINEJAD, Z., POURHANIFEH, M. H., MOVAHEDPOUR, A., MOTTAGHI, R., NICKDASTI, A., MORTEZAPOUR, E., SHAFIEE, A., HAJIGHADIMI, S., MORADIZARMEHRI, S., SADEGHIAN, M., MOUSAVI, S. M. & MIRZAEI, H. Therapeutic potentials of curcumin in the treatment of glioblstoma. *Eur J Med Chem* 2020; 188(Article ID: 112040): 1-13, doi: 10.1016/j.ejmech.2020.112040.
14. SHANMUGAM, M. K., RANE, G., KANCHI, M. M., ARFUSO, F., CHINNATHAMBI, A., ZAYED, M. E., ALHARBI, S. A., TAN, B. K., KUMAR, A. P. & SETHI, G. The multifaceted role of curcumin in cancer prevention and treatment. *Molecules* 2015; 20(2): 2728-69, doi: 10.3390/molecules20022728.
15. TIPOE, G. L., LEUNG, T. M., HUNG, M. W. & FUNG, M. L. Green tea polyphenols as an anti-oxidant and anti-inflammatory agent for cardiovascular protection. *Cardiovasc Hematol Disord Drug Targets* 2007; 7(2): 135-44, doi: 10.2174/187152907780830905.
16. ZHU, W., XU, J., GE, Y., CAO, H., GE, X., LUO, J., XUE, J., YANG, H., ZHANG, S. & CAO, J. Epigallocatechin-3-gallate (EGCG) protects skin cells from ionizing radiation via heme oxygenase-1 (HO-1) overexpression. *J Radiat Res* 2014; 55(6): 1056-65, doi: 10.1093/jrr/rru047.
17. ZHU, Y. & BU, S. Curcumin Induces Autophagy, Apoptosis, and Cell Cycle Arrest in Human Pancreatic Cancer Cells. *Evid Based Complement Alternat Med* 2017; 2017(Article ID: 5787218): 1-13, doi: 10.1155/2017/5787218.

ISSN print: 1224-5984
ISSN online: 2248-3942

Rom Biotechnol Lett. 2022; 27(5): 3699-3712
doi: 10.25083/rbl/27.5/3699.3712

Received for publication, January 26, 2023
Accepted, January 31, 2023

Review

Epidemiology, diagnosis, symptoms and TNM classification of head and neck cancers

MARIAN CONSTANTIN[1,2]

[1]Institute of Biology Bucharest of Romanian Academy, 296 Splaiul Independenţei, 060031 Bucharest, Romania

[2]Fellow of the Research Institute of the University of Bucharest, ICUB, Bucharest, Romania

Abstract

Head and neck cancers occur predominantly by transformation of squamous cells lining the mucous membranes of the upper aerodigestive tract and affect one of the most complex regions of the human body. Head and neck cancers are very common, with more than half a million new cases annually, and have a mortality rate of around 50%, and early diagnosis can improve treatment outcomes and increase the life expectancy of those affected. In this paper, we review the epidemiology, the main symptoms, the diagnostic methods, highlighting the few genetic markers identified so far, and the TNM classification of each type of upper aerodigestive cancer.

Keywords head and neck cancer, epidemiology, diagnosis, symptoms, TNM classification

To cite this article: MARIAN CONSTANTIN. Epidemiology, diagnosis, symptoms and TNM classification of head and neck cancers. *Rom Biotechnol Lett.* 2022; 27(5): 3699-3712 DOI: 10.25083/rbl/27.5/3699.3712

*Corresponding author: Marian Constantin, Institute of Biology Bucharest of Romanian Academy, 296 Splaiul Independenţei, 060031 Bucharest, Romania; Fellow of the Research Institute of the University of Bucharest, ICUB, Bucharest, Romania. E-mail: cvgmarian@gmail.com

Introduction

The head and neck region is very complex and comprises the organs and all the tissue structures of the upper airways (nasal cavity; oral cavity and its appendages, including the lips, oral floor, hard palate, palatine veil, tongue, gums and salivary glands; pharynx, with its three sectors: nasopharynx, oropharynx and laryngopharynx, or hypopharynx, with the tonsils and Eustachian tube communicating with the middle ear; larynx, with the vocal cords), where the cancers of the head and neck, cranial cavity, eyes, ears, their appendages, endocrine glands, cervical spine, all cranial and cervical musculature, and the blood vessels, nerves and integument covering them occur (*fig. 1*). In this context, head and neck cancers (ICD-10 code) define only tumours of the upper aerodigestive tract and include a wide variety of malignancies of epithelial origin (*Table 1*).

More than 90% of head and neck cancers originate in the squamous cells lining the mucous membranes of the upper aerodigestive tract and are some of the most common cancers, with more than half a million new cases annually. They also have a high mortality despite cytoreductive surgery, radiotherapy and chemotherapy (when necessary), as diagnosis occurs at advanced stages with involvement of regional lymph nodes. Early diagnosis of head and neck cancers can replace the need to combine surgical resection with radiotherapy with radiotherapy treatment alone, with reduced recovery time and fewer complications after surgery. Distant metastasis is rare and occurs in less than 10% of cases. Survivors of head and neck cancers carry the risk of death for the rest of their lives due to heart and respiratory problems and the development of second primary tumours, especially in smokers. Secondary primary tumours can affect any part of the aerodigestive tract and are developed by 3-5% of cases each year. Head and neck cancers are multistep processes, frequently triggered by mutations in a single gene produced by carcinogens and leading to significant dysregulation of metabolic processes.

Table 1. Major types of neoplasms of the head and neck region according to the 10th revision (ICD-10) of the International Statistical Classification of Diseases and Related Health Problems, 2019 [1,2].

ICD-10 code	Main site of neoplasy
C00	Malignant neoplasms of lip
C01	Malignant neoplasm of base of tongue
C02	Malignant neoplasm of other and unspecified part of tongue
C03	Malignant neoplasm of gum
C04	Malignant neoplasm of floor of mouth
C05	Malignant neoplasm of palate
C06	Malignant neoplasm of other and unspecified parts of mouth
C07	Malignant neoplasm of parotid gland
C08	Malignant neoplasm of other and unspecified major salivary glands
C09	Malignant neoplasm of tonsil
C10	Malignant neoplasm of oropharynx
C11	Malignant neoplasm of nasopharynx
C12	Malignant neoplasm of piriform sinus
C13	Malignant neoplasm of hypopharynx
C14	Malignant neoplasm of other and ill-defined sites in the lip, oral cavity and pharynx
C30	Malignant neoplasm of nasal cavity and middle ear
C31	Malignant neoplasm of accessory sinuses
C32	Malignant neoplasm of larynx
C76	Malignant neoplasm of other and ill-defined sites

The main factor causing head and neck tumours is smoking (active and passive), followed by alcohol consumption, alone or in combination with smoking, viral infections such as HPV (human papillomavirus) and EBV (Epstein-Barr virus), chewing Areca nuts in the form of betel quid, other eating habits which can also introduce carcinogens into the

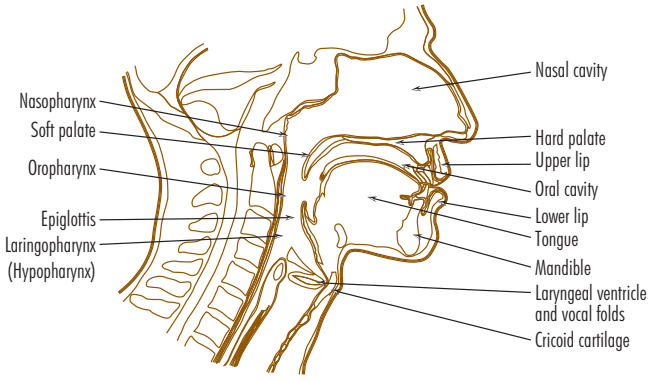

Figure. 1. Sagittal section through the head and neck region, showing the main anatomical landmarks used to define head and neck cancers.

body, as well as oral hygiene and the compounds with which people in various occupations come into contact [3–6]. From a molecular point of view, head and neck cancers are poorly known and characterized, although there are references on: (1) the positive correlation of N6-adenosine methylation and tumorigenesis of head and neck cancers [7]; (2) the relationship between increased expression of programmed death receptor 1 (PD1) and its ligand (PDL1) and increased size of head and neck tumors, suggesting the inclusion of these two molecules among tumor markers of laryngeal cancers and monoclonal antibodies in therapeutic regimens targeting laryngeal tumors [8]; (3) the possibility of using mi-RNAs (microRNAs - non-coding RNAs of about 22 nucleotides, involved in the post-translational regulation of gene expression) as biomarkers for head and neck cancers [9].

Epidemiology of head and neck cancers

Globally, the incidence of head and neck cancers ranks sixth, accounting for about 6% of all cancers (estimated 650,000 new cases annually) [3]. Thus, in 2020, the incidence of head and neck cancers was 699,840 cases in men (264,211 cases of lip and oral cavity cancers, 29,694 cases of salivary gland cancers, 79,045 cases of oropharyngeal cancers, 96,371 cases of nasopharyngeal cancers, 70,254 cases of laryngopharyngeal or hypopharyngeal cancers and 160, 265 cases of laryngeal cancers) and 232,091 cases in women (113,502 cases of lip and oral cavity cancers, 23,889 cases of salivary gland cancers, 19,367 cases of oropharyngeal cancers, 36,983 cases of nasopharyngeal cancers, 14,000 cases of laryngopharyngeal or hypopharyngeal cancers and 24,350 cases of laryngeal cancers). The mortality rate in people who develop head and neck cancers is very high, at around 350,000 annually. Thus, the total number of deaths in people with head and neck cancers in 2020 was 353,713 in men (125,022 cases of lip and oral cavity cancers, 13,353 cases of salivary gland cancers, 39,590 cases of oropharyngeal cancers, 58,094 cases of nasopharyngeal cancers, 32,303 cases of laryngopharyngeal or hypopharyngeal cancers and 85, 351 cases of laryngeal cancers) and 113,412, in women (52,735 cases of lip and oral cavity cancers, 9,425 cases of salivary gland cancers, 8,553 cases of oropharyngeal cancers, 21,914 cases of nasopharyngeal cancers, 6,296 cases of laryngopharyngeal or hypopharyngeal cancers and 14,489 cases of laryngeal cancers) [10]. The overall incidence of head and neck cancers shows an increasing trend in both developed and developing countries, with the Southeast Asia and Asia-Pacific regions showing an increasing number of oral cancers due to the habit of chewing Areca nuts (betel quid, a highly potent drug), whether or not associated with smoking, while in Europe and the USA, HPV infection (*fig. 2*). By 2030, the number of cases may increase by 30% annually [2]. The incidence of head and neck cancers is at least twice as high in men as in women, with the proportions varying by country. For example, according to https://gco.iarc.fr/today/, in Romania, where the incidence of head and neck cancers in both sexes is 19.0/100,000 inhabitants (ranking third in the world after Papua New Guinea with 26.7/100,000 and Bangladesh with 22.2/100,000), the incidence in men is 35.8/100,000 (the second highest after Papua New Guinea with 37.6/100,000), while in women it is much lower at 4.1/100,000. The gender gap tends to become smaller in some countries, such as Papua New Guinea, with a total incidence of 26.7/100,000 population (37.6/100,000 for men and 17.1/100,000 for women), India, with a total incidence of 17.0/100,000 population (26.3/100,000 for men and 7.0/100,000 for women) and the United Republic of Tanzania, with a total incidence of 4.4/100,000 for men and 4.4/100,000 for women. 6/100,000), France, with a total incidence of 16.2/100,000 (men 24.8/100,000 and women 8.5/100,000), United Kingdom, with a total incidence of 11.4/100,000 (men 16.2/100,000 and women 6.8/100,000), USA, with a total incidence of 10. 4/100,000 inhabitants (in men 15.8/100,000 and in women 5.4/100,000), Germany, with a total incidence of 10.3/100,000 inhabitants (in men 14.9/100,000 and in women 5.9/100,000), or Israel, with a total incidence of 5.1/100,000 inhabitants (in men 7.1/100,000 and in women 3. 4/100,000), or even close to balance in other countries, including Saudi Arabia, with a total incidence of 4.4/100,000 (in men, 5.1/100,000, and in women, 3.3/100,000), or the United Mexican States, with a total incidence of 2.7/100,000 (in men, 3.5/100,000, and in women, 2.0/100,000).

Main symptoms

Depending on location, head and neck cancers produce a plethora of symptoms. Thus, cancers occurring in the nasal cavity and nasopharynx may unilaterally obstruct the airways, reduce olfactory sensitivity, produce mucus, with or without the presence of blood, which may flow outwards or inwards towards the throat. Oral or oropharyngeal cancers may initially appear as single or multiple precancerous lesions or as persistent ulcerations due to viral or fungal infections (e.g. candida leukoplakia), repeated consumption of betel quid or other causes. They may progress to oral or oropharyngeal cancers synchronous (occurring simultaneously or up to 6 months after lesion formation) or metachronous (occurring more than 6 months after lesion formation), which may occupy less or more space in the oral cavity or oropharynx, affecting the digestive function of these organs. Laryngopharyngeal (hypopharyngeal) cancers can cause persistent sore throat, earache, painful swallowing and hoarseness. On the

other hand, pharyngeal cancers (of the nasopharynx, oropharynx and laryngopharynx) cause obstruction of the pharynx and frequently dysphagia and sore throat much delayed after onset, as well as painless damage to a cervical lymph node. Due to impaired vocal cord functionality, laryngeal cancers frequently produce hoarseness, while cancers of the epiglottis area cause difficulty swallowing. Head and neck cancers also produce many non-specific symptoms, such as enlargement of cervical lymph nodes, unilateral otalgia (ear pain) or wheezing, which can be mistaken for other conditions, delaying correct diagnosis. Persistent enlargement of cervical lymph nodes in people aged 30-50 years, non-smokers and non-smokers who do not consume excessive alcohol or betel quid, may be caused by the presence of small tonsillar tumours of viral (HPV) origin, which may be mistaken for benign conditions, delaying their correct diagnosis. Unilateral pain occurring in people over 30 years of age without signs of otitis may be caused by neoplasms of the pharynx. In people over 40 years of age who smoke heavily or drink alcohol excessively, the occurrence of wheezing may be caused by slow-growing laryngeal neoplasms, although these can be diagnosed as bronchial asthma [11,4].

Diagnosis of head and neck cancers

The appearance of one or more of the symptoms listed may be just one indication of the likelihood of developing head and neck cancer and a good reason to visit the doctor. Most of the time, these are not sufficient for an accurate diagnosis of head and neck cancer, but are the start of more detailed investigations, including direct visual assessment or endoscopy, biopsy, imaging explorations and detection of specific biomarkers. To begin with, the doctor will perform

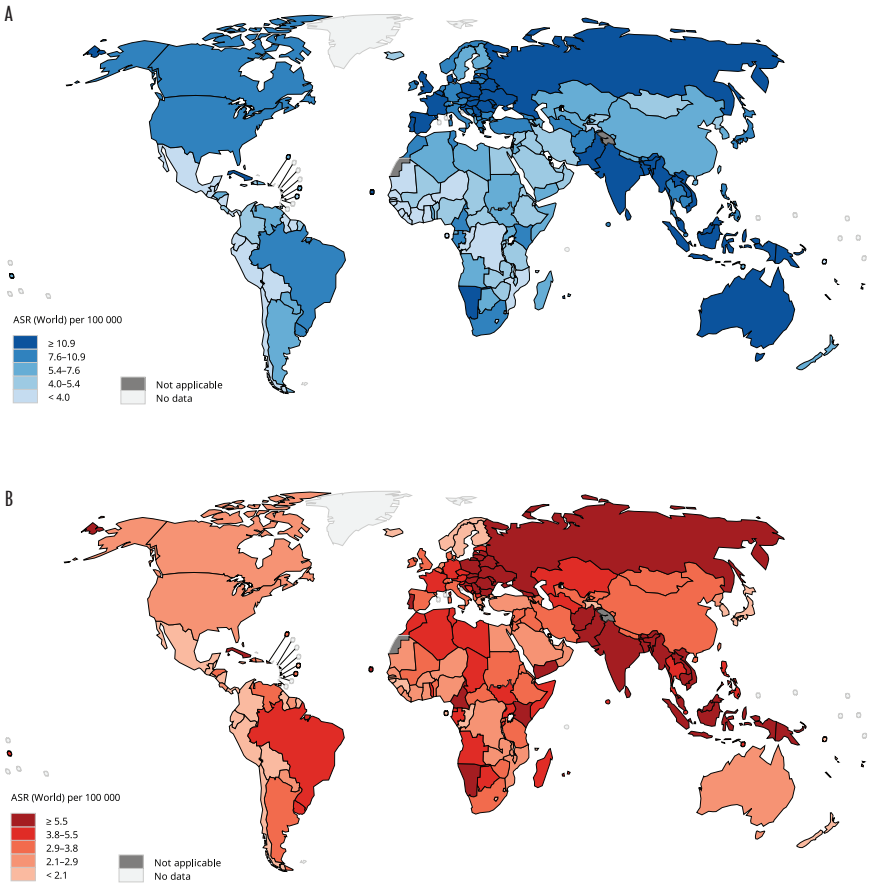

Figure. 2. World estimated age-standardized incidence rates in 2020, for head and neck (lip, oral cavity, larynx, hypopharynx, nasopharynx, salivary glands, and oropharynx) cancers, for both sexes of all ages. Maps are reprinted from International Agency for Research on Cancer, Cancer today – Data visualization tools for exploring the global cancer burden in 2020, Copyright 2022, available at http://gco.iarc.fr/today, and accessed in December 2022.

a visual assessment of accessible tissues to identify areas of macroscopically altered appearance. When these are not directly accessible, endoscopic examination of the suspicious area may be recommended. In endoscopy, an endoscope (a tube with a camera and a light at the tip) is used, which, in the case of upper aerodigestive tract explorations, is inserted through the nose or mouth. In the upper aerodigestive sphere, three common types of endoscopy are possible, nasopharyngoscopy, pharyngoscopy or laryngoscopy, which require local anesthesia, and the fourth type, panendoscopy, which requires general anesthesia [12].

After identifying the suspicious area, the physician will extract a tissue sample, necessary for microscopic or molecular examination (biopsy), which will allow him to correctly diagnose the altered area [13]. The biopsy is minimally invasive, surgical or aspiration. Thus, minimally invasive biopsy usually requires very small incisions (2-5 mm) and consists of sampling using a needle, directed by duplication with radiology imaging, ultrasound or CT. Recovery from the minimally invasive biopsy procedure occurs within 48 hours and results are released after two working days. Surgical biopsy is invasive, consists of making an incision to remove a tissue sample or tumour nodule, and may require local or general anesthesia. Because some tumours, such as appendiceal tumours, are discovered during or after appendectomies, by pathological examination, the incision is larger, deeper and leads to removal of the entire affected organ. In head and neck squamous cell carcinomas, surgical biopsies are much less extensive. Fine needle aspiration biopsy is the insertion of a very fine needle into areas of altered tissue, from which a small sample is taken to check for neoplastic cells. Generally, biopsy specimens are sent for pathological examination. This may be limited to staining of the sample, microscope slide staining and microscopic visualization for identification of transformed cells, or may include paraffin embedding for immunohistochemical examination [14].

After receiving results confirming the presence of transformed cells in the suspicious area, detailed imaging exploration of the area of interest may be performed by computed tomography (CT) scan, MRI scan, PET scan or ultrasound. Computed tomography is the acquisition of a suite of images of the area of interest using a source of X-rays that passes through living tissue and capture the signals via a computer-connected device, where they appear as image files. By viewing the image sequences, doctors observe the three-dimensional extent of the tumour and its relationship to neighbouring structures. Nuclear magnetic resonance MRI scans use magnetic fields and radio waves to capture detailed image sequences of the head and neck region, which are then stored in a computer and provide information on the extent of the tumour and its relationship to neighbouring tissues. Both CT and MRI scans can use contrast agents, through which tissue structures are better highlighted. PET (positron emission tomography) scans use a radioactive tracer (dye) administered intravenously, which provides very detailed detail about the health and function of organs and tissues at the microscopic level, generating images that provide clues to the presence of tumour transformation before it becomes visible on other types of images [15,14]. In head and neck squamous cell carcinomas, a very useful tool for diagnosis, staging and assessment of response to treatment is positron emission tomography using 18F-fluorodeoxyglucose (FDG-PET). Applied to patients with cervical lymph node metastases and unidentified origin, this method can identify the primary tumour in 25-38.5% of cases [15,16].

Earlier studies of head and neck cancers in the early third millennium identified several chromosomal aberrations, such as amplification of the 11q13 region, and genetic aberrations, including in *TP53* (Tumor Protein 53/Tumor Suppressor P53), *EGFR* (Epidermal Growth Factor Receptor), *STAT3* (Signal Transducer And Activator Of Transcription 3), *VEGFR* (Vascular Endothelial Growth Factor Receptor), *RB*, including *RB1* (RB Transcriptional Corepressor 1), *RBL1* (RB Transcriptional Corepressor Like 1) and *RBL2* (RB Transcriptional Corepressor Like 2), *p16/INK4A/CDKN2AI* (Cyclin Dependent Kinase Inhibitor 2A), *CCND1* (Cyclin D1), *XRCC1* (X-Ray Repair Cross Complementing 1) and *XPD/ERCC2* (ERCC Excision Repair 2, TFIIH Core Complex Helicase Subunit), affecting the functionality of the proteins encoded by them and signal transduction through the signaling pathways in which they are included [17–21]. Since the introduction of modern sequencing techniques (next-generation sequencing, NGS), knowledge of genetic alterations in some subtypes of these tumours has been continuously enriched, with the signaling of mutations in *PIK3CA* (Phosphatidylinositol-4, 5-Bisphosphate 3-Kinase Catalytic Subunit Alpha), *HRAS* (HRas Proto-Oncogene, GTPase), *PTEN* (Phosphatase And Tensin Homolog), *NOTCH1* (Notch Receptor 1) [22], *OGG1* (Human 8-oxoguanine glycosylase 1, the enzyme responsible for excision 7, 8-dihydro-8-oxoguanine, a mutagenic by-product resulting from exposure to reactive oxygen species) [23], *CHECK2* (Checkpoint Kinase 2), *ATR* (ATR Serine/Threonine Kinase), involved in the TP53 signaling pathway, which determines the fate of cells whose genetic material is altered, in HPV-negative smokers) [24], *RAD51C* (RAD51 Paralog C) [25], *FAT1* (FAT Atypical Cadherin 1), *AJUBA* (Ajuba LIM Protein), both involved in the WNT signaling pathway; in addition, *AJUBA* undergoes EGFR–RAS–RAF–MEK–ERK-dependent phosphorylation and participates in the HIPPO signaling pathway and in the ATR-mediated response

to DNA damage), *NSD1* (histone methyltransferase H3K36), *TRAF3* (TNF Receptor Associated Factor 3), *NFE2L2* (NFE2 Like BZIP Transcription Factor 2), *CASP8* (Caspase 8, whose product is involved in the caspase pathway of apoptosis), *KMT2D/MLL2* (Lysine Methyltransferase 2D, involved in chromatin remodeling), *HLA-A/CMH-IA* (Major Histocompatibility Complex, Class I, A, involved in immune surveillance, which becomes deficient when mutated), *SCN9A* (Sodium Voltage-Gated Channel Alpha Subunit 9), *PTCH1* (Patched 1), *MYC* (MYC Proto-Oncogene, BHLH Transcription Factor) and *PIK3R1* (Phosphoinositide-3-Kinase Regulatory Subunit 1). In addition to these, whole exome sequencing of oral squamous cell carcinomas from Taiwanese men also identified mutations in *RASA1* (RAS P21 Protein Activator 1), *CHUK* (Component of Inhibitor of Nuclear Factor Kappa B Kinase Complex) and *ELAVL1* (ELAV Like RNA Binding Protein 1) genes, the latter two affecting the function of tumor suppressor and oncogene suppressor genes [26]. Rarely, the genes *ASXL1* (ASXL Transcriptional Regulator 1), encoding a transcription factor, and *RPTN* (Repetin), encoding an epithelial differentiation factor, are affected [27]. Of these, *TP53*, *HRAS*, *EGFR* and *PIK3CA* genes have important functions in cell survival and proliferation (wild-type *TP53* controlling them negatively and the other three positively), *CDKN2A* and *CCND1* in cell cycle control, *NOTCH1* in cell differentiation, and *FAT1* in cell invasiveness and adhesion. The most frequent somatic mutations occur in the *TP53* gene, with 50-80% of cases (predominantly in introns 4 and 6), in the early stages of carcinogenesis, and in *CDKN2A*, with important roles in the development of head and neck tumours (inactivation of p53 protein, encoded by *TP53*, being of major importance in preventing apoptotic guidance of genetically defective cells, and inactivation of p16 protein, encoded by *CDKN2A*, blocks cell cycle progression from G1 to S phase by inhibiting cyclin D1), followed by *FAT1*, *PIK3CA*, *NOTCH1*, *KMT2D/MLL2*, *NSD1*, *CASP8*, *AJUBA* and *NFE2L2* [27–29]. Early studies on genetic alterations in head and neck tumors showed that mutations in the TP53 gene are frequently reported in HPV-negative tumors and rarely in HPV-positive tumors, amid its inactivation by the viral protein E6 via ubiquitination [18–20,27].

Currently, there are a small number of biomarkers used for the diagnosis of head and neck squamous cell carcinomas, including HPV infection and specific molecular targets. Since HPV infection is present in approximately 90% of oral squamous cell carcinomas, the association between symptoms and HPV infection may lead to the diagnosis of these and oropharyngeal cancers [16]. For the assessment of the risk of malignancy of oral pre-malignant lesions, loss of heterozygosity for the 9p and 13p regions can be used as a molecular biomarker [30]. Candidate genes for use as biomarkers for head and neck cancers include *CDKN2A*, *ARF* (ADP Ribosylation Factor) (located in 9p21), *TP53* (located in 17p13), *PTEN* [31], *PD1* and *PDL1* [8], but these need to be validated. A 2019 study indicates the serum presence of three miRNAs (hsa-mir-383, hsa-mir-615 and hsa-mir-877) as an effective biomarker for the diagnosis of head and neck squamous cell carcinomas [32].

TNM classification of head and neck cancers

The TNM classification of head and neck cancers includes the same parameters considered in the general staging of tumours, T (presence of primary tumour), N (lymph node metastasis) and M (presence of metastases in distant regions).

Oral cancers

For the definition of the T-parameter, in oral cancers the largest size of these tumours and the depth of invasion (DOI) are taken into account, as deeper tumours increase the risk of ganglion metastasis and reduced survival, with an increase of 5 mm each advancing the category by one T stage. Assessment of primary tumour thickness is a criterion used in clinical staging and is performed by manual palpation by experienced surgeons, with primary tumours <5 mm considered thin, 5-10 mm thick and >10 mm very thick [33–35] (*Table 2*).

Table 2. T staging of oral cancers, according to AJCC Staging Manual [38]

T Category	T Criteria
TX	Primary tumor cannot be assessed
Tis	Carcinoma in situ
T1	Primary tumor ≤ 2 cm, DOI ≤ 5 mm
T2	Primary tumor ≤ 2 cm, DOI > 5 mm and ≤ 10 mm or tumor > 2 cm and ≤ 4 cm, DOI ≤ 10 mm
T3	Primary tumor > 2 cm and ≤ 4 cm, DOI > 10 mm or tumor > 4 cm, DOI ≤ 10 mm
T4	Moderately/very advanced local disease
T4a	Moderately advanced local disease, with primary tumor > 4 cm, DOI > 10 mm or tumor invading adjacent structures only
T4b	Very advanced local disease, with primary tumor invading masticator space, pterygoid plates, or skull base and/or encasing the internal carotid artery

In addition to lymph node involvement, the definition of N-parameter categories also includes extra-nodal extension of lymph node metastases (ENE), as this greatly influences the prognosis of head and neck cancers, with the exception of HPV-positive tumours. Thus, correct identification, supported with radiological evidence, of the presence of extra-nodal ex-

enteration (ENE+), advances the N category to N3b, and inconclusive cases are categorized ENE– [35–37] (*Table 3*).

Table 3. N staging of oral cancers, according to AJCC Staging Manual [38]

N Category	N Criteria
NX	Regional lymph nodes cannot be assessed
N0	No regional lymph node metastasis
N1	Metastasis in a single ipsilateral lymph node, ≤ 3 cm, ENE(−)
N2	Metastasis in a single ipsilateral node > 3 cm and ≤ 6 cm, ENE(−); or metastases in multiple ipsilateral lymph nodes, ≤ 6 cm, ENE(−); or in bilateral or contralateral lymph nodes, ≤ 6 cm, ENE(−)
N2a	Metastasis in a single ipsilateral node > 3 cm and ≤ 6 cm, ENE(−)
N2b	Metastases in multiple ipsilateral nodes ≤ 6 cm, ENE(−)
N2c	Metastases in bilateral or contralateral lymph nodes ≤ 6 cm, ENE(−)
N3	Metastasis in a lymph node > 6 cm, ENE(−); or metastasis in any node(s) and clinically overt ENE(+)
N3a	Metastasis in a lymph node > 6 cm, ENE(−)
N3b	Metastasis in any node(s) and clinically overt ENE(+)

Oropharyngeal and laryngopharyngeal/hypopharyngeal cancers

In the TNM classification of oropharyngeal cancers, the presence or absence of HPV infection is taken into account due to the different biological behavior of the two types of cancers, with HPV-positive tumours offering better diagnosis and survival rates compared to HPV-negative ones [39]. For this reason, the T classification system has some peculiarities for each of the two tumour types, with the same categories maintained overall. Thus, for HPV-positive tumours the Tis category has been excluded, the T0 category is used only for HPV-positive metastatic lymph nodes, where the primary lymph node is considered the primary tumour, and the T4b category is eliminated (*Table 4*). For HPV-negative tumours, the T-system comprises a wider range of categories (*Table 4*), also found in laryngopharyngeal/hypopharyngeal carcinomas, with some particularities regarding the criteria (*Table 5*). The N classification of oropharyngeal cancers also takes into account the presence or absence of HPV. Thus, for HPV-positive oropharyngeal cancers, the transformation of at least one ipsilateral lymph node less than 6 cm in size is considered N1, contralateral or bilateral lymph nodes less than 6 cm in size are considered N2, and nodes larger than 6 cm are included in the N3 category [40,35] (*Table 6*). The N system for laryngopharyngeal/hypopharyngeal carcinomas is complex and includes the same categories as for oral carcinomas, similarly, the presence of extra-nodal extension (ENE+), advancing the N category to clinically N3b (*Table 7*).

Table 4. T staging of oropharyngeal cancers, according to AJCC Staging Manual [38]

HPV-positive oropharyngeal tumors	
T Category	**T Criteria**
T0	No primary identified
T1	Primary tumor ≤ 2 cm
T2	Primary tumor > 2 cm and ≤ 4 cm
T3	Primary tumor > 4 cm *or* extended to lingual surface of epiglottis
T4	Moderately advanced local disease, with primary tumor invading the larynx, extrinsic muscle of tongue, medial pterygoid, hard palate, or mandible or beyond
HPV-negative oropharyngeal tumors	
T Category	**T Criteria**
TX	Primary tumor cannot be assessed
Tis	Carcinoma *in situ*
T1	Primary tumor ≤ 2 cm
T2	Primary tumor > 2 cm and ≤ 4 cm
T3	Primary tumor > 4 cm *or* extended to lingual surface of epiglottis
T4	Moderately advanced and very advanced local disease
T4a	Moderately advanced local disease, with primary tumor invading the larynx, extrinsic muscle of tongue, medial pterygoid, hard palate, or mandible
T4b	Very advanced local disease, with primary tumor invading lateral pterygoid muscle, pterygoid plates, lateral nasopharynx, or skull base or encasing carotid artery

Table 5. T staging of laringopharyngeal/hypopharyngeal cancers, according to AJCC Staging Manual [38]

T Category	T Criteria
TX	Primary tumor cannot be assessed
Tis	Carcinoma in situ
T1	Primary tumor limited to one subsite of hypopharynx and/or ≤ 2 cm
T2	Primary tumor invades more than one subsite of hypopharynx or an adjacent site, or > 2 cm and ≤ 4 cm without fixation of hemilarynx
T3	Primary tumor > 4 cm or with fixation of hemilarynx or extension to esophageal mucosa
T4	Moderately advanced and very advanced local disease
T4a	Moderately advanced local disease, primary tumor invading thyroid/cricoid cartilage, hyoid bone, thyroid gland, esophageal muscle or central compartment soft tissue
T4b	Very advanced local disease, primary tumor invading prevertebral fascia, encasing carotid artery, or involving mediastinal structures

Table 6. N staging of oropharyngeal cancers, according to AJCC Staging Manual [38]

N Category	N Criteria
NX	Regional lymph nodes cannot be assessed
N0	No regional lymph node metastasis
N1	One or more ipsilateral lymph nodes, none > 6 cm
N2	Contralateral or bilateral lymph nodes, none > 6 cm
N3	Lymph node(s) > 6 cm

Table 7. N staging of laringopharyngeal/hypopharyngeal cancers, according to AJCC Staging Manual [38]

N Category	N Criteria
NX	Regional lymph nodes cannot be assessed
N0	No regional lymph node metastasis
N1	Metastasis in a single ipsilateral lymph node ≤ 3 cm, ENE(−)
N2	Metastasis in a single ipsilateral node > 3 cm and ≤ 6 cm, and ENE(−); or metastases in multiple ipsilateral lymph nodes ≤6 cm, and ENE(−); or in bilateral or contralateral lymph nodes ≤ 6 cm, and ENE(−)
N2a	Metastasis in a single ipsilateral node > 3 cm ≤ 6 cm, and ENE(−)
N2b	Metastases in multiple ipsilateral nodes ≤ 6 cm, and ENE(−)
N2c	Metastases in bilateral or contralateral lymph nodes, ≤ 6 cm, and ENE(−)
N3	Metastasis in a lymph node > 6 cm, and ENE(−); or metastasis in any node(s) and clinically overt ENE(+)
N3a	Metastasis in a lymph node > 6 cm, and ENE(−)
N3b	Metastasis in any node(s) and clinically overt ENE(+)

Table 8. T staging of nasopharyngeal cancers, according to AJCC Staging Manual [38]

T Category	T Criteria
TX	Primary tumor cannot be assessed
T0	No tumor identified, but EBV-positive cervical node(s) involvement
Tis	Tumor in situ
T1	Tumor confined to nasopharynx, or extension to oropharynx and/or nasal cavity with no parapharyngeal involvement
T2	Tumor extended to parapharyngeal space, and/or to adjacent soft tissue (including medial pterygoid, lateral pterygoid, prevertebral muscles)
T3	Tumor with infiltration of bony structures at skull base, cervical vertebra, pterygoid structures, and/or paranasal sinuses
T4	Tumor with intracranial extension, involvement of cranial nerves, hypopharynx, orbit, parotid gland, and/or extensive soft tissue infiltration beyond the lateral surface of the lateral pterygoid muscle

Table 9. N staging of nasopharyngeal cancers, according to AJCC Staging Manual [38]

N Category	N Criteria
NX	Regional lymph nodes cannot be assessed
N0	No regional lymph node metastasis
N1	Unilateral metastasis in cervical lymph node(s) and/or unilateral or bilateral metastasis in retropharyngeal lymph node(s) ≤6 cm, above the caudal border of cricoid cartilage
N2	Bilateral metastasis in cervical lymph node(s) ≤ 6 cm, above the caudal border of cricoid cartilage
N3	Unilateral or bilateral metastasis in cervical lymph node(s) > 6 cm, and/or extension below the caudal border of cricoid cartilage

Nasopharyngeal cancers

The TNM classification of nasopharyngeal cancers takes into account the presence of EBV infection, parapharyngeal structures involvement, lymphatic spread in the retropharyngeal and cervical lymph nodes, which is present from an early age and occurs in an orderly pattern, from close to close, without gaps, from the upper to the lower throat [41,42]. Metastatic lymph node hyperplasia to more than 6 cm or extension below the cricoid cartilage provides the worst prognosis. Because nasopharyngeal carcinomas are at increased risk of distant metastasis to the lung, bone, liver or distant lymph nodes, their TNM classification also includes category M, with a value of 0 for no distant metastasis and 1 for the presence of distant metastasis [38] (*Tables 8–9*).

Cancers of the nasal cavity and maxillary sinuses

Nasal cavity and maxillary sinus cancers have a differentiated course depending on the area of the maxillary sinus involved, with cancers extending into the antero-inferior portion of the maxillary sinus (infrastructure) having a favorable prognosis and those extending into the posterosuperior portion of the maxillary sinus (superstructure) having a poor prognosis, as they invade early on the critical structures at the base of the skull, including the orbit, pterygoid processes and infratemporal fossa. In terms of T staging, nasal cavity and maxillary sinus cancers are subdivided into maxillary sinus cancers and nasal cavity and ethmoid sinus cancers (*Table 10*). Nasal cavity and maxillary sinus cancers typically do not involve the regional lymph nodes, this occurs through the extension of maxillary sinus cancers, and the extra-nodal extension of metastases passes the tumour directly to stage N3 (*Table 11*). When present (M1), distant metastasis occurs in the lungs and rarely in the bones [38].

Table 10. T staging of maxillary sinus, and nasal cavity and ethmoid sinus cancers, according to AJCC Staging Manual [38]

Maxillary sinus		Nasal cavity and ethmoid sinus	
T Category	**T Criteria**	**T Category**	**T Criteria**
TX	Primary tumor cannot be assessed	TX	Primary tumor cannot be assessed
Tis	Carcinoma in situ	Tis	Carcinoma in situ
T1	Tumor limited to maxillary sinus mucosa with no erosion or destruction of bone	T1	Tumor restricted to any one subsite, with or without bony invasion
T2	Tumor causing bone erosion or destruction including extension into the hard palate and/or middle nasal meatus, except extension to posterior wall of maxillary sinus and pterygoid plates	T2	Tumor invading two subsites in a single region or extending to involve an adjacent region within the nasoethmoidal complex, with or without bony invasion
T3	Tumor invades any of the following: bone of the posterior wall of maxillary sinus, subcutaneous tissues, floor or medial wall of orbit, pterygoid fossa, ethmoid sinuses	T3	Tumor extends to invade the medial wall or floor of the orbit, maxillary sinus, palate, or cribriform plate
T4	Moderately advanced or very advanced local disease	T4	Moderately advanced or very advanced local disease
T4a	Moderately advanced local disease, primary tumor invading anterior orbital contents, skin of cheek, pterygoid plates, infratemporal fossa, cribriform plate, sphenoid or frontal sinuses	T4a	Moderately advanced local disease, primary tumor invading any of the following: anterior orbital contents, skin of nose or cheek, minimal extension to anterior cranial fossa, pterygoid plates, sphenoid or frontal sinuses
T4b	Very advanced local disease, primary tumor invading any of the following: orbital apex, dura, brain, middle cranial fossa, cranial nerves other than maxillary division of trigeminal nerve (V2), nasopharynx, or clivus	T4b	Very advanced local disease, primary tumor invading any of the following: orbital apex, dura, brain, middle cranial fossa, cranial nerves other than (V2), nasopharynx, or clivus

Table 11. N staging of maxillary sinus, and nasal cavity and ethmoid sinus cancers, according to AJCC Staging Manual [38]

N Category	N Criteria
NX	Regional lymph nodes cannot be assessed
N0	No regional lymph node metastasis
N1	Metastasis in a single ipsilateral lymph node ≤ 3 cm, and ENE(−)
N2	Metastasis in a single ipsilateral node > 3 cm and ≤ 6 cm, and ENE(−); or metastases in multiple ipsilateral lymph nodes, ≤ 6 cm, and ENE(−); or in bilateral or contralateral lymph nodes ≤ 6 cm, and ENE(−)
N2a	Metastasis in a single ipsilateral node > 3 cm and ≤ 6 cm, and ENE(−)
N2b	Metastases in multiple ipsilateral nodes ≤6 cm, and ENE(−)
N2c	Metastases in bilateral or contralateral lymph nodes ≤ 6 cm, and ENE(−)
N3	Metastasis in a lymph node > 6 cm, and ENE(−); or metastasis in any node(s) with clinically overt ENE(+)
N3a	Metastasis in a lymph node > 6 cm, and ENE(−)
N3b	Metastasis in any node(s) with clinically overt ENE (ENEc)

Laryngeal cancers

Laryngeal cancers can occur in the supraglottic region, in the glottis or under the glottis. T-staging of supraglottic carcinomas takes into account the involvement of surrounding regions and vocal cord mobility, extension into the paralaryngeal fat in the preepiglottic space or erosion of the inner cortex of the thyroid cartilage advancing tumours to stage T3, whereas erosion of the outer cortex of the thyroid cartilage classifies tumours as T4a. T-staging of glottis tumours takes into account the impairment of vocal cord mobility, and T-staging of subglottic space tumours takes into account their extension to the vocal cords with impaired mobility, or disease progression to the cricoid or thyroid cartilages, in which case the tumours are stage T4 (*Table 12*). Lymph node metastasis and hyperplasia are criteria used for N classification of laryngeal tumours. Extra-nodal extension of metastases directly moves the tumor to stage N3 [38] (*Table 13*).

Anatomical staging of head and neck cancers

Based on the association of TNM criteria, anatomical stages of head and neck tumours are defined, which indicate the size of the primary tumour and the extent of metastasis. Thus, low T parameters (Cis or T1–3) associated with N0, N1 or N2 and with M0 indicate early and middle stages in the development of neoplasia (Stage 0, I or II), and T4 generally characterises Stage IV, in which the disease is advanced. This stage is divided into stages IVA, in which the disease is moderately advanced and has local or regional spread, IVB, in which the disease is very advanced with local or regional spread, and IVC, in which the disease metastasizes to a distant site (*Tables 14–16*). Anatomical staging is a diagnostic and prognostic criterion for head and neck cancers [38].

Table 12. T staging of larynx cancers, according to AJCC Staging Manual [38]

	Supraglottis	Glottis	Subglottis
T Category	**T Criteria**	**T Criteria**	**T Criteria**
TX	Primary tumor cannot be assessed	Primary tumor cannot be assessed	Primary tumor cannot be assessed
Tis	Carcinoma in situ	Carcinoma in situ	Carcinoma in situ
T1	Tumor limited to one subsite of supraglottis with normal vocal cord mobility	Tumor limited to the vocal cord(s) (may involve anterior or posterior commissure) with normal mobility	Tumor limited to the subglottis
T1a		Tumor limited to one vocal cord	
T1b		Tumor involves both vocal cords	
T2	Tumor invades mucosa of more than one adjacent subsite of supraglottis or glottis or region outside the supraglottis (e.g., mucosa of base of tongue, vallecula, medial wall of pyriform sinus) without fixation of the larynx	Tumor extends to supraglottis and/or subglottis, and/or with impaired vocal cord mobility	Tumor extends to vocal cord(s) with normal or impaired mobility
T3	Tumor limited to larynx with vocal cord fixation and/or invades any of the following: postcricoid area, preepiglottic space, paraglottic space, and/or inner cortex of thyroid cartilage	Tumor limited to the larynx with vocal cord fixation and/or invasion of paraglottic space and/or inner cortex of the thyroid cartilage	Tumor limited to larynx with vocal cord fixation and/or invasion of paraglottic space and/or inner cortex of the thyroid cartilage
T4	Moderately advanced or very advanced	Moderately advanced or very advanced	Moderately advanced or very advanced
T4a	Moderately advanced local disease Tumor invades through the outer cortex of the thyroid cartilage and/or invades tissues beyond the larynx (e.g., trachea, soft tissues of neck including deep extrinsic muscle of the tongue, strap muscles, thyroid, or esophagus)	Moderately advanced local disease Tumor invades through the outer cortex of the thyroid cartilage and/or invades tissues beyond the larynx (e.g., trachea, cricoid cartilage, soft tissues of neck including deep extrinsic muscle of the tongue, strap muscles, thyroid, or esophagus)	Moderately advanced local disease Tumor invades cricoid or thyroid cartilage and/or invades tissues beyond the larynx (e.g., trachea, soft tissues of neck including deep extrinsic muscles of the tongue, strap muscles, thyroid, or esophagus)
T4b	Very advanced local disease Tumor invades prevertebral space, encases carotid artery, or invades mediastinal structures	Very advanced local disease Tumor invades prevertebral space, encases carotid artery, or invades mediastinal structures	Very advanced local disease Tumor invades prevertebral space, encases carotid artery, or invades mediastinal structures

Table 13. N staging of larynx cancers, according to AJCC Staging Manual [38]

N Category	N Criteria
NX	Regional lymph nodes cannot be assessed
N0	No regional lymph node metastasis
N1	Metastasis in a single ipsilateral lymph node ≤ 3 cm, and ENE(−)
N2	Metastasis in a single ipsilateral node, > 3 cm and ≤ 6 cm, and ENE(−); or metastases in multiple ipsilateral lymph nodes ≤ 6 cm, and ENE(−); or metastasis in bilateral or contralateral lymph nodes ≤ 6 cm, and ENE(−)
N2a	Metastasis in a single ipsilateral node > 3 cm and ≤ 6 cm, and ENE(−)
N2b	Metastases in multiple ipsilateral nodes < 6 cm, and ENE(−)
N2c	Metastases in bilateral or contralateral lymph nodes ≤ 6 cm, and ENE(−)
N3	Metastasis in a lymph node > 6 cm, and ENE(−); or metastasis in any lymph node(s) with clinically overt ENE(+)
N3a	Metastasis in a lymph node > 6 cm, and ENE(−)
N3b	Metastasis in any lymph node(s) with clinically overt ENE(+)

Table 14. Anatomical staging of nasopharyngeal cancers [38]

Stage 0	Cis (Tis)	N0	M0
Stage I	T1	N0	M0
Stage II	T1	N1	M0
	T2	N0	M0
	T2	N1	M0
Stage III	T1	N2	M0
	T2	N2	M0
	T3	N0	M0
	T3	N1	M0
	T3	N2	M0
Stage IVA	T4	N0	M0
	T4	N1	M0
	T4	N2	M0
Stage IVB	Any T	N3	M0
Stage IVC	Any T	Any N	M1

Table 15. Anatomical staging of oropharyngeal/ hypopharyngeal cancers [38]

Stage 0	Cis (Tis)	N0	M0
Stage I	T1	N0	M0
Stage II	T2	N0	M0
Stage III	T3	N0	M0
	T1	N1	M0
	T2	N1	M0
	T3	N1	M0
Stage IVA	T4a	N0	M0
	T4a	N1	M0
	T1	N2	M0
	T2	N2	M0
	T3	N2	M0
	T4a	N2	M0
Stage IVB	T4b	Any N	M0
	Any T	N3	M0
Stage IVC	Any T	Any N	M1

Table 16. Anatomical staging of laryngeal cancers [38]

Stage 0	Cis (Tis)	N0	M0
Stage I	T1	N0	M0
Stage II	T2	N0	M0
Stage III	T3	N0	M0
	T1	N1	M0
	T2	N0	M0
	T3	N1	M0
Stage IVA	T4a	N0	M0
	T4a	N1	M0
	T1	N2	M0
	T2	N2	M0
	T3	N2	M0
	T4a	N2	M0
Stage IVB	T4b	Any N	M0
	Any T	N3	M0
Stage IVC	Any T	Any N	M1

Conclusions

More than 90% of head and neck cancers originate from squamous cells (squamous cell cancers of the head and neck), ranking 6th among all malignancies affecting the human body (with 931931 cases estimated in 2020 worldwide, followed by breast, with 2261419 cases in 2020, lung, with 2206771 cases in 2020, colon and rectum, with 1931590 cases in 2020, prostate, with 1414259 cases in 2020, and stomach, with 1089103 cases in 2020 [43,44]), invades, to some extent, neighbouring structures (thyroid and even tracheal cartilages, internal carotid artery, thyroid gland, eyeballs and bony structures, including orbits, jaw, infratemporal fossa, pterygoid processes, base of skull, mandible and cervical spine), metastasizes in a low proportion (about 10%) and has high mortality rate. Risk factors for head and neck cancers include smoking (active and passive), alcohol consumption, especially in combination with smoking, viral infections with HPV (human papillomavirus) and EBV (Epstein-Barr virus), chewing Areca nuts (betel quid), poor oral hygiene and other dietary or behavioral habits.

Symptoms of head and neck cancers are numerous and include obstruction of the upper airways, reduced olfactory sensitivity, mucus or blood production, ulceration of the oral cavity, sore throat, especially when swallowing, or earache, hoarseness, hyperplasia of the cervical lymph nodes and others.

The occurrence of some of these symptoms may indicate the likelihood of neoplasia in the upper aerodigestive sphere, which may be refuted or confirmed by specific investigations, including direct visual assessment, endoscopy, biopsy, imaging investigations and detection of specific biomarkers. Although affecting a relatively large number of genes, head and neck cancers have a small number of specific biomarkers, candidates include *CDKN2A*, *ARF*, *TP53*, *PTEN*, *PD1*, *PDL1* or a group of three miRNAs (hsa-mir-383, hsa-mir-615 and hsa-mir-877).

For TNM staging of head and neck cancers, categories T and N are relevant, the latter also taking into account the extra-nodal extension of lymph node metastases, while category M is only relevant for staging nasopharyngeal cancers and those arising in the nasal cavity and maxillary sinuses, in which cases distant metastases mainly target the lungs and bones. These categories are used to define anatomical stages of head and neck cancers with diagnostic and prognostic value for overall survival.

Conflict of interest. The author has no conflict of interest to declare.

References

1. International Statistical Classification of Diseases and Related Health Problems 10th Revision, Version:2019 [cited 2022 Dec 30]. Available from: https://icd.who.int/browse10/2019/en#/C00-C14
2. Gormley, M., Creaney, G., Schache, A. et al. Reviewing the epidemiology of head and neck cancer: definitions, trends and risk factors. Br Dent J 233, 780–786 (2022). doi: 10.1038/s41415-022-5166-x
3. Argiris A, Karamouzis MV, Raben D, Ferris RL. Head and neck cancer. Lancet. 2008 May 17;371(9625):1695-709. doi: 10.1016/S0140-6736(08)60728-X. PMID: 18486742; PMCID: PMC7720415
4. Mehanna H, Paleri V, West CM, Nutting C. Head and neck cancer--Part 1: Epidemiology, presentation, and prevention. BMJ. 2010 Sep 20;341:c4684. doi: 10.1136/bmj.c4684. PMID: 20855405

5. Alfouzan AF. Radiation therapy in head and neck cancer. Saudi Med J. 2021 Mar;42(3):247-254. doi: 10.15537/smj.2021.42.3.20210660. PMID: 33632902; PMCID: PMC7989258
6. Szyfter K. Genetics and Molecular Biology of Head and Neck Cancer. Biomolecules. 2021 Aug 31;11(9):1293. doi: 10.3390/biom11091293. PMID: 34572506; PMCID: PMC8469154
7. Romanowska K, Rawłuszko-Wieczorek AA, Marczak Ł, Kosińska A, Suchorska WM, Golusiński W. The m6A RNA Modification Quantity and mRNA Expression Level of RNA Methylation-Related Genes in Head and Neck Squamous Cell Carcinoma Cell Lines and Patients. Biomolecules. 2021 Jun 18;11(6):908. doi: 10.3390/biom11060908. PMID: 34207099; PMCID: PMC8235215
8. Kowalski A, Malinowska K, Olszewski J, Zielińska-Bliźniewska H. Expression of Programmed Death Receptor 1 (PD-1) Gene and Its Ligand (PD-L1) in Patients with Laryngeal Cancer. Biomolecules. 2021 Jul 1;11(7):970. doi: 10.3390/biom11070970. PMID: 34356594; PMCID: PMC8301886
9. Kabzinski J, Maczynska M, Majsterek I. MicroRNA as a Novel Biomarker in the Diagnosis of Head and Neck Cancer. Biomolecules. 2021 Jun 5;11(6):844. doi: 10.3390/biom11060844. PMID: 34198889; PMCID: PMC8228566
10. Sung H, Ferlay J, Siegel RL, Laversanne M, Soerjomataram I, Jemal A, Bray F. Global Cancer Statistics 2020: GLOBOCAN Estimates of Incidence and Mortality Worldwide for 36 Cancers in 185 Countries. CA Cancer J Clin. 2021 May;71(3):209-249. doi: 10.3322/caac.21660. Epub 2021 Feb 4. PMID: 33538338
11. Gerson SJ. Oral cancer. Crit Rev Oral Biol Med. 1990;1(3):153-66. doi: 10.1177/10454411900010030101. PMID: 2129624
12. Head and Neck Cancer Diagnosis [cited 2023 Ian 20]. Available from: https://www.mskcc.org/cancer-care/types/head-neck/diagnosis
13. Overview of Head and Neck Tumors, in MSD Manual. Professional Version [cited 2023 Ian 20]. Available from: https://www.msdmanuals.com/professional/ear,-nose,-and-throat-disorders/tumors-of-the-head-and-neck/overview-of-head-and-neck-tumors
14. Head and Neck Cancer Diagnosis [cited 2023 Ian 20]. Available from: https://cancer.dartmouth.edu/head-neck/diagnosis
15. Haider SP, Burtness B, Yarbrough WG, Payabvash S. Applications of radiomics in precision diagnosis, prognostication and treatment planning of head and neck squamous cell carcinomas. Cancers Head Neck. 2020 May 4;5:6. doi: 10.1186/s41199-020-00053-7. PMID: 32391171; PMCID: PMC7197186
16. Economopoulou P, de Bree R, Kotsantis I, Psyrri A. Diagnostic Tumor Markers in Head and Neck Squamous Cell Carcinoma (HNSCC) in the Clinical Setting. Front Oncol. 2019 Aug 29;9:827. doi: 10.3389/fonc.2019.00827. PMID: 31555588; PMCID: PMC6727245
17. Ramachandran S, Ramadas K, Hariharan R, Rejnish Kumar R, Radhakrishna Pillai M. Single nucleotide polymorphisms of DNA repair genes XRCC1 and XPD and its molecular mapping in Indian oral cancer. Oral Oncol. 2006 Apr;42(4):350-62. doi: 10.1016/j.oraloncology.2005.08.010. Epub 2005 Dec 1. PMID: 16324877
18. Smeets SJ, Braakhuis BJM, Ylstra B, et al. TP53 mutations are associated with a particular pattern of genomic imbalances in head and neck squamous cell carcinoma. Cell Oncol 2007;29:160
19. Klein JD, Grandis JR. The molecular pathogenesis of head and neck cancer. Cancer Biol Ther. 2010 Jan;9(1):1-7. doi: 10.4161/cbt.9.1.10905. Epub 2010 Jan 9. PMID: 20038820; PMCID: PMC3138532
20. Leemans CR, Braakhuis BJ, Brakenhoff RH. The molecular biology of head and neck cancer. Nat Rev Cancer. 2011 Jan;11(1):9-22. doi: 10.1038/nrc2982. Epub 2010 Dec 16. PMID: 21160525
21. Stransky N, Egloff AM, Tward AD, Kostic AD, Cibulskis K, Sivachenko A, Kryukov GV, Lawrence MS, Sougnez C, McKenna A, Shefler E, Ramos AH, Stojanov P, Carter SL, Voet D, Cortés ML, Auclair D, Berger MF, Saksena G, Guiducci C, Onofrio RC, Parkin M, Romkes M, Weissfeld JL, Seethala RR, Wang L, Rangel-Escareño C, Fernandez-Lopez JC, Hidalgo-Miranda A, Melendez-Zajgla J, Winckler W, Ardlie K, Gabriel SB, Meyerson M, Lander ES, Getz G, Golub TR, Garraway LA, Grandis JR. The mutational landscape of head and neck squamous cell carcinoma. Science. 2011 Aug 26;333(6046):1157-60. doi: 10.1126/science.1208130. Epub 2011 Jul 28. PMID: 21798893; PMCID: PMC3415217
22. Loyo M, Li RJ, Bettegowda C, Pickering CR, Frederick MJ, Myers JN, Agrawal N. Lessons learned from next-generation sequencing in head and neck cancer. Head Neck. 2013 Mar;35(3):454-63. doi: 10.1002/hed.23100. Epub 2012 Aug 21. PMID: 22907887; PMCID: PMC3715072
23. Mahjabeen I, Masood N, Baig RM, Sabir M, Inayat U, Malik FA, Kayani MA. Novel mutations of OGG1

base excision repair pathway gene in laryngeal cancer patients. Fam Cancer. 2012 Dec;11(4):587-93. doi: 10.1007/s10689-012-9554-2. PMID: 22829015

24. Laborde RR, Wang VW, Smith TM, Olson NE, Olsen SM, García JJ, Olsen KD, Moore EJ, Kasperbauer JL, Tombers NM, Smith DI. Transcriptional profiling by sequencing of oropharyngeal cancer. Mayo Clin Proc. 2012 Mar;87(3):226-32. doi: 10.1016/j.mayocp.2011.10.008. PMID: 22386177; PMCID: PMC3538409
25. Scheckenbach K, Baldus SE, Balz V, Freund M, Pakropa P, Sproll C, Schäfer KL, Wagenmann M, Schipper J, Hanenberg H. RAD51C--a new human cancer susceptibility gene for sporadic squamous cell carcinoma of the head and neck (HNSCC). Oral Oncol. 2014 Mar;50(3):196-9. doi: 10.1016/j.oraloncology.2013.11.007. Epub 2013 Dec 6. PMID: 24315737; PMCID: PMC4230275
26. Su SC, Lin CW, Liu YF, Fan WL, Chen MK, Yu CP, Yang WE, Su CW, Chuang CY, Li WH, Chung WH, Yang SF. Exome Sequencing of Oral Squamous Cell Carcinoma Reveals Molecular Subgroups and Novel Therapeutic Opportunities. Theranostics. 2017 Feb 26;7(5):1088-1099. doi: 10.7150/thno.18551. PMID: 28435450; PMCID: PMC5399578
27. Farah CS. Molecular landscape of head and neck cancer and implications for therapy. Ann Transl Med. 2021 May;9(10):915. doi: 10.21037/atm-20-6264. PMID: 34164549; PMCID: PMC8184465
28. Cancer Genome Atlas Network. Comprehensive genomic characterization of head and neck squamous cell carcinomas. Nature. 2015 Jan 29;517(7536):576-82. doi: 10.1038/nature14129. PMID: 25631445; PMCID: PMC4311405
29. Cho J, Johnson DE, Grandis JR. Therapeutic Implications of the Genetic Landscape of Head and Neck Cancer. Semin Radiat Oncol. 2018 Jan;28(1):2-11. doi: 10.1016/j.semradonc.2017.08.005. PMID: 29173752; PMCID: PMC6293987
30. Rosin MP, Cheng X, Poh C, Lam WL, Huang Y, Lovas J, Berean K, Epstein JB, Priddy R, Le ND, Zhang L. Use of allelic loss to predict malignant risk for low-grade oral epithelial dysplasia. Clin Cancer Res. 2000 Feb;6(2):357-62. PMID: 10690511
31. Johnson DE, Burtness B, Leemans CR, Lui VWY, Bauman JE, Grandis JR. Head and neck squamous cell carcinoma. Nat Rev Dis Primers. 2020 Nov 26;6(1):92. doi: 10.1038/s41572-020-00224-3. PMID: 33243986; PMCID: PMC7944998
32. Liu C, Yu Z, Huang S, Zhao Q, Sun Z, Fletcher C, Jiang Y, Zhang D. Combined identification of three miRNAs in serum as effective diagnostic biomarkers for HNSCC. EBioMedicine. 2019 Dec;50:135-143. doi: 10.1016/j.ebiom.2019.11.016. Epub 2019 Nov 26. PMID: 31780396; PMCID: PMC6921333
33. Shah JP. Staging for Head and Neck Cancer: Purpose, Process and Progress. Indian J Surg Oncol. 2018 Mar;9(1):116-120. doi: 10.1007/s13193-018-0723-0. Epub 2018 Feb 5. PMID: 29563750; PMCID: PMC5856705
34. Shah JP., Montero PH. New AJCC/UICC staging system for head and neck, and thyroid cancer. Revista Médica Clínica Las Condes. 2018; 29(4):397-404.doi: 10.1016/j.rmclc.2018.07.002
35. Zanoni DK, Patel SG, Shah JP. Changes in the 8th Edition of the American Joint Committee on Cancer (AJCC) Staging of Head and Neck Cancer: Rationale and Implications. Curr Oncol Rep. 2019 Apr 17;21(6):52. doi: 10.1007/s11912-019-0799-x. PMID: 30997577; PMCID: PMC6528815
36. International Consortium for Outcome Research (ICOR) in Head and Neck Cancer; Ebrahimi A, Gil Z, Amit M, Yen TC, Liao CT, Chaturvedi P, Agarwal JP, Kowalski LP, Kreppel M, Cernea CR, Brandao J, Bachar G, Bolzoni Villaret A, Fliss D, Fridman E, Robbins KT, Shah JP, Patel SG, Clark JR. Primary tumor staging for oral cancer and a proposed modification incorporating depth of invasion: an international multicenter retrospective study. JAMA Otolaryngol Head Neck Surg. 2014 Dec;140(12):1138-48. doi: 10.1001/jamaoto.2014.1548. PMID: 25075712
37. Wreesmann VB, Katabi N, Palmer FL, Montero PH, Migliacci JC, Gönen M, Carlson D, Ganly I, Shah JP, Ghossein R, Patel SG. Influence of extracapsular nodal spread extent on prognosis of oral squamous cell carcinoma. Head Neck. 2016 Apr;38 Suppl 1(Suppl 1):E1192-9. doi: 10.1002/hed.24190. Epub 2015 Oct 30. PMID: 26514096; PMCID: PMC4996672
38. Amin MB, Greene FL, Edge SB, Compton CC, Gershenwald JE, Brookland RK, Meyer L, Gress DM, Byrd DR, Winchester DP. The Eighth Edition AJCC Cancer Staging Manual: Continuing to build a bridge from a population-based to a more "personalized" approach to cancer staging. CA Cancer J Clin. 2017 Mar;67(2):93-99. doi: 10.3322/caac.21388. Epub 2017 Jan 17. PMID: 28094848
39. Ang KK, Sturgis EM. Human papillomavirus as a marker of the natural history and response to therapy of head and neck squamous cell carcinoma. Seminars

in Radiation Oncology. 2012 Apr;22(2):128-142. DOI: 10.1016/j.semradonc.2011.12.004. PMID: 22385920

40. O'Sullivan B, Huang SH, Su J, Garden AS, Sturgis EM, Dahlstrom K, Lee N, Riaz N, Pei X, Koyfman SA, Adelstein D, Burkey BB, Friborg J, Kristensen CA, Gothelf AB, Hoebers F, Kremer B, Speel EJ, Bowles DW, Raben D, Karam SD, Yu E, Xu W. Development and validation of a staging system for HPV-related oropharyngeal cancer by the International Collaboration on Oropharyngeal cancer Network for Staging (ICON-S): a multicentre cohort study. Lancet Oncol. 2016 Apr;17(4):440-451. doi: 10.1016/S1470-2045-(15)00560-4. Epub 2016 Feb 27. PMID: 26936027
41. Ng WT, Lee AW, Kan WK, Chan J, Pang ES, Yau TK, Lau KY. N-staging by magnetic resonance imaging for patients with nasopharyngeal carcinoma: pattern of nodal involvement by radiological levels. Radiother Oncol. 2007 Jan;82(1):70-5. doi: 10.1016/j.radonc.2006.11.010. Epub 2006 Dec 12. PMID: 17166610
42. Ho FC, Tham IW, Earnest A, Lee KM, Lu JJ. Patterns of regional lymph node metastasis of nasopharyngeal carcinoma: a meta-analysis of clinical evidence. BMC Cancer. 2012 Mar 21;12:98. doi: 10.1186/1471-2407-12-98. PMID: 22433671; PMCID: PMC3353248
43. International Agency for Research on Cancer, Cancer today – Data visualization tools for exploring the global cancer burden in 2020, Copyright 2022, available at http://gco.iarc.fr/today, and accessed in January 2023
44. Hotnog CM, Mihaila M, Puiu L, Botezatu A, Roman V, Popescu ID, Bostan M, Brasoveanu LI. Modulation of the interplay between p53, ICAM-1 and VEGF in drug-treated LoVo colon cancer cells. Rom Biotechnol Lett. 2019;24(2): 261-270. doi: 10.25083/rbl/24.2/261.270

ISSN print: 1224-5984
ISSN online: 2248-3942

Rom Biotechnol Lett. 2022; 27(5): 3713-3721
doi: 10.25083/rbl/27.5/3713.3721

Received for publication, November, 12, 2022
Accepted, February, 16, 2023

Original article

Streptomyces lasiicapitis KSA18 isolated from Saharan soil in Algeria effective against most bacteria and fungi

MOKHTAR BENREGUIEG [1,2], DJALLAL EDDINE HOUARI ADLI [1,2], TAHA AHMED BENABBOU [1,2], KADDOUR ZIANI [1,2], MOSTAPHA BRAHMI [2,6], AYSE OZDEMIR [3], KERIMAN GUNAYDIN [4] AND JOACHIM WINK [5]

[1]Department of Biology, Faculty of ciences, University of Saida-Dr. Moulay Tahar, 20000 Saida, Algeria.

[2]Laboratory of biotoxicology, pharmacognosy and biological recovery of plants, University of Saida-Dr. Moulay Tahar, 20000 Saida, Algeria.

[3]Department of Chemistry, Istanbul Technical University, Istanbul, Turkey.

[4]Department of biology, Istanbul university, Turkey.

[5]Microbial Strain Collection, Helmholtz Centre for Infection Research, Inhoffenstrasse 7, Braunschweig D-38124, Germany.

[6]Department of Biology, Faculty of Science and Technology, Ahmed ZABANA University of Relizane

Abstract

Saharan soil still represents a formidable source of microorganisms that produce bioactive substances. Twenty-three Actinobacteria strains were isolated from sand samples collected from saharian field in Algeria. Isolates were evaluated for antimicrobial activity. After primary screening, 79% of the isolates showed antimicrobial activity. KSA18 strains were selected for their intense activity. Bioactive metabolite was extracted with ethyl acetate and tested against pathogens microorganisms using the disk diffusion method. The crude extract was partially purified by column chromatography and evaluated for antimicrobial activity. Fraction A1 showed good activity against Staphylococcus aureus (3.25 mg/mL) and Listeria monocytogenes (4 mg/mL). This strain has been identified as Streptomyces lasiicapitis by 16S rRNA sequencing. GC-MS analysis of crude extract showed the presence of about 17 different volatile compounds). Some of them could be directly responsible for antibacterial or antifungal activity. The most important compounds are Phenol, 2,4-Bis(1,1-Dimethylethyl), 3-Isobutylhexahydropyrrolo[1,2-A] Pyrazine-1,4-Dione, 2-methyloctacosane and dibutyl phthalate.

However, this study requires other approaches to identify the bioactive molecules present in the extract.

Keywords Saharian soil, Actinobacteria, Algeria, antimicrobial activity, *Streptomyces lasiicapitis*, GC-MS

To cite this article: MOKHTAR BENREGUIEG. *Streptomyces lasiicapitis* KSA18 isolated from Saharan soil in Algeria effective against most bacteria and fungi. *Rom Biotechnol Lett.* 2022; 27(5): 3713-3721 DOI: 10.25083/rbl/27.5/3713.3721

*Corresponding author: Mokhtar Benreguieg. E-mail : mokhtar_benreguieg@yahoo.com; mokhtar.benreguieg@univ-saida.dz. Phone: +213557143424

Introduction

Abraham and Chain described in 1945 a substance produced by a Colibacillus which completely inhibited penicillin and called it penicillinase. In 1945 Fleming warned the population, in a New York Times article dated June 26, 1945, that abusive use of penicillin could lead to the emergence and spread of resistant bacteria. Five years later, in Paris and London, half of the strains of Staphylococcus were resistant to penicillin (Briand, 2009). From then on, the problem of antibiotic resistance spread to the world and became a global problem. Indeed, the WHO declared through its director-general "Margaret Chan" during the World Health Day organized on April 7, 2011: "... if we do not take urgent measures to correct this situation and protect its achievements, we are moving towards a post-antibiotic era in which many common infections can no longer be treated and will begin to kill again." Considering the above, the long-term solution to counter microbial resistances is to develop or research new molecules with antimicrobial activity, whether by synthesis of new molecules and/or hemi-synthesis from known structures; Exploit non-culturable microbial populations by the concept of metagenomics (PERIC & LONG, 2003), which consists in the extraction of DNA from a sample of the environment, the metagenome, which will be cloned into vectors Which are transformed into substitution hosts. These environmental DNA libraries are then screened for their biological activities (Zhang & Demain, 2005), or isolation of new bacterial or fungal species from less or less explored ecosystems, and analysis of their fermentation products.

Good fellow and Haynes (1984) reviewed the literature on actinomycete isolation and suggested that only 10% of actinomycetes are naturally isolated. The majority of antibiotics currently in use are derived from natural products of actinomycetes and fungi (BUTLER & BUSS, 2006; NEWMAN & CRAGG, 2007). Actinomycetes are isolated from marine sediments and soil. While the pharmaceutical industry has been analyzing soils for about 50 years, only a tiny fraction of the world's surface has been sampled. A tiny fraction of actinomycete taxa has been discovered (BALTZ, 2005; 2007). Our work is registered in the research of actinomycetes, the most promising actors for producing metabolites with antimicrobial activity.

Materials and methods

Isolation of Actinobacteria

In Kasdir, Naâma, Algeria (33° 42′ 35″, 1° 21′ 32″), poor soil samples were taken. A sterile spatula was used to remove the top 5 cm of dirt. Then, 100-150 g of dirt from 5 to 15 cm deep is gathered with a sterile spatula and placed on a sterile aluminium paper. 50 g were transported to the lab as soon as feasible (POCHON & TARDIEUX, 1962). Soil samples were room-temperature air-dried for a week. 9 ml of double-distilled sterile water contained 1 g of dirt. Diluted 10^{-1}. 10^{-2}, 10^{-3}, 10^{-4}, and 10^{-5} were dispersed over starch-casein agar. Nalidixic acid and Actidione were supplemented to inhibit bacterial and fungal growth. 10-day incubation at 28 to 30°C. Based on morphological characters, Actinobacterial colony were purified on ISP2 medium. Our pilot-scale screening isolated 23 actinomycetes, KSA 1–23.

Microbial organisms

Pasteur Institute of Algiers provided the Gram- negative, Gram- positive, and fungal strains used in this study: *Escherichia coli* (ATCC 25922), *Salmonella Typhimurium* (ATCC13311), *Pseudomonas aeruginosa* (ATCC 27853), *Staphylococcus aureus* (ATCC 25923), *Listeria monocytogenes* (ATCC 19115), *Bacillus subtilis* (ATCC 10876), *Enterococcus faecalis* (ATCC 29212), methicillin-resistant S. aureus (MRSA) (ATCC 43300), *Candida albicans* (ATCC 2019) and *Aspergillus flavus* (ATCC 9643). Growing bacteria and fungi in Mueller Hinton and Saboraud broth at 37°C and 25 °C for 24 and 72 hours repectively.

Antibacterial activity

Actinomycetes were cultivated for 7 days on Bennett's sand GLM agar (LEE & HWANG, 2002). With a hollow punch, 3 mm cylinders of agar were placed on Mueller–Hinton media (Merck) seeded with each test bacteria. After 4 hours at 4 °C, Petri dishes were placed at 37°C for 24 hours. Measured inhibition diameters (LEMRISS et al., 2003).

Antifungal activity

Actinomycetals isolates were tested against filamentous fungi from the Pasteur Institute's Mycology Unit. Activity was tested using 9 g l^{-1} Bactocasitone, 5 g.l^{-1} yeast extract, 10 g.l^{-1} sodium citrate, 20 g l^{-1} glucose, 3.34 g l^{-1} disodium hydrogen phosphate, 0.54 g l-1 potassium di-hydrogen phosphate, and 18 g l^{-1} agar (KITOUNI et al, 2005). After 24–48 hours at 28°C, yeast and filamentous fungus inhibition zones were measured.

DNA extraction, PCR and 16S rRNA sequencing

A DNA extraction kit was used on 0.5 ml of KSA18 liquid culture (Stratec Molecular Invisorb Spin Plant kit, Berlin, Germany). DNA extraction efficiency was tested with agarose gel electrophoresis. Using two primers (27F: 5′-AGTTTGATCCTGGCTCAG-3′ and 1492R: 5′-ACGGCTACCTTGTTAGGACTT-3′), 16S rRNA was amplified in a thermocycler. The DSMZ sequencing of the PCR products was performed at DSMZ center (Brauchweig, Germany). BLAST was used to match the nucleotide sequence to GENBANK database at NCBI.

Fermentation

Primary screening showed that the isolate (called KSA18) has a zone of inhibition, indicating antibacterial activity. ISP-2 broth produced bioactive substances. 125 milliliters In a 250 ml Erlenmeyer flask, the soup was sterilized. The sterile broth included 4% two-day-old mother inoculum was placed at 28°C for 7 days and 150 rpm. Broth was filtered with Whatman N°1 after incubation. Centrifuged for 15 min to separate the filtrate.

Extraction and purification

The culture filtrate (800 ml) was extracted twice with ethyl acetate, and the pooled extracts were evaporated to dryness under reduced pressure. The antibacterial ingredient was purified using silica gel column (2.5 25) chromatography. 100-200 mm silica gel was utilized to stuff the column. Methanol and ethyl acetate (6-4 v/v) eluted. 5 g of this crude extract was diluted in 50 ml of methanol and passed through a silica gel column at 0.2 ml/min; 25 fractions (5 ml each) were collected and evaluated for antibacterial activity (AOUICHE, 2012).

Thin-layer chromatography combined with bioautography

Bio-autography and TLC were used to detect anti-S. aureus molecules. Samples were spotted on 20 cm 20 cm silica gel plates (Si60, Merck Art. 5735, Kiessel gel 60F254), washed with methanol and acetate ethyl (6:4, v/v), and air-dried overnight at 37°C. Fractionation experiments used two plates. First, bioactive chemicals were localized using retention factor (Rf) (MENDHAM, 2006). Spraying sulfuric vanillin (vanillin/H2SO4/ethanol 3:3:100, w/v/v) visualized these molecules. The second plate was placed over S. aureus-seeded Mueller–Hinton media (Merck) at 37°C for 24 hours. Antifungal compounds were discovered by matching their Rf on reference TLC plates to S. aureus-free regions.

Identification of bioactive metabolites using GC-MS analysis

The chemical composition of the TLC active eluent molecule was discovered by GC-MS (PARTHASARATHI, 2012). The program ranged from 40–280 °C, and 250 °C was chosen for injection. The GC had a capillary column and a 1 l injection volume. The sample flowed at 1 ml/s and 36.5 cm/s (BARTON, 2006). The results were compared to NIST 11.

Determination of minimum inhibitory concentrations

Minimum inhibitory concentrations (MICs) of pure bioactive substances were determined using agar dilution. Inoculated on Mueller Hinton medium for bacteria and Sabouraud medium for yeasts and filamentous fungi with 10, 20, 30, 50, 75, and 100 g/mL active chemicals. After 24–48 h at 37°C for bacteria and 48–72 h at 28°C for fungi, growth plates were inspected to find the lowest antibiotic concentration that inhibited each organism's growth. Mueller-Hinton and Sabouraud medium lacking active chemicals and target microorganisms were employed as controls.

Results

Isolation and Preliminary screening

Kasdir and Naâma, Algeria, soil samples were taken. 1g of soil was dried for actinomycetes isolation. The 23 probable actinomycetes were isolated and purified in ISP-2. The pure colonies were kept at 4°C on ISP-2 slant. The isolated cultures were KSA 1, 2, 3,... and 23. 23 cultures were tested for bacteria and fungus. Antibacterial and antifungal activity was screened by diffusion on Mueller–Hinton for bacteria and YMA and casitone for fungi. In the initial screening, 34% of the strains had weak action, 22% had moderate activity, 25% had promising activity, and 19% had no hostile activity (Table1). 8 strains with good activity were also investigated for cultural features (Table 2). The KSA18 antibacterial chemical suppressed bacteria and fungus development. KSA18 was chosen based on early screening findings to explore its extraction and antibacterial property. KSA18 methanol extract evaluated against bacteria and fungus.

Genetic Identification of KSA18 strain, Phylogenetic Analysis and Clustering

The sequencing results of the 16S rRNA gene of KSA18 straine was compared using BLAST (ZOETENDAL, 2008). Clustal W was used to align these homologous sequences with KSA18's 16S rRNA gene sequence. Figure 1 shows the phylogenetic tree based on 16S rRNA gene sequences using MEGA X (Thompson et al, 1994). illustrating the links between the KSA18 strain and the Streptomyces genus. The 16S rRNA sequence of bacterium KSA18 is 99.17% similar to *Streptomyces lasiicapitis'* sequence (accession number SUB11207111).

Extraction and purification of fermentation products

The KSA18 fermentation took 120 hours at 28 C. The culture supernatant was collected and centrifuged. Ethyl acetate (1:2, v/v) was used for the extraction and afterwards was evaporated until dry to get a yellow staining precipitate. In 50 ml of methanol, 5 g of the precipitate was separated on column chromatography using methanol and acetate ethyl (6:4,v/v). 25 5-ml portions were taken. Active portions ranged from N° 14 to N° 27. Using sil-

Table 1: Primary screening of actinomycetal isolates using agar cylinder method

	Test microorganisms									
	B. subtilis	*S. aureus*	*L. monocytogenes*	*MRSA*	*E. coli*	*P. aeruginosa*	*E. faecalis*	*S. tyfimirium*	*C.albicans*	*A. flavus*
KSA 1	–	–	–	–	–	–	–	–	–	–
KSA 2	–	+	+	–	–	–	+	–	–	–
KSA 3	–	–	–	–	–	–	–	–	–	–
KSA 4	+	+	–	–	+	–	+	–	–	–
KSA 5	–	+	–	–	+	–	+	–	–	–
KSA 6	+	+	+	+	+	–	–	+	–	+
KSA 7	–	–	+	–	+	+	+	–	–	–
KSA 8	+	+	–	–	+	–	–	–	–	+
KSA 9	–	–	–	–	–	–	–	–	–	–
KSA10	+	+	–	–	–	+	–	–	–	–
KSA11	–	+	–	–	–	–	–	+	–	–
KSA12	+	+	+	–	+	–	+	–	–	–
KSA13	–	+	+	–	+	–	–	+	–	+
KSA14	+	–	+	–	–	–	+	–	–	–
KSA15	–	–	–	–	–	–	–	–	–	–
KSA16	+	+	+	–	–	–	+	–	–	–
KSA17	–	+	+	–	–	–	–	+	–	–
KSA18	+	+	+	+	–	+	+	+	–	+
KSA19	+	+	+	+	+	+	+	+	–	+
KSA20	+	+	+	+	–	–	+	+	-	–
KSA21	+	–	–	–	–	+	–	–	+	–
KSA22	–	+	–	–	+	–	–	–	-	–
KSA23	+	+	–	–	–	–	+	+	–	–

– no inhibition; + inhibition

Table 2: Colony characteristics of most actives isolates cultivated on Isp2

Culture code	Colour	Mycelium type	Pigment production	Gram'sreaction
KSA6	White	Substrate	Orange	+
KSA7	White	Aerial	-	+
KSA8	Yellow	Aerial	Red	+
KSA13	Grey	Substrate	Yellow	+
KSA14	White	Aerial	Yellow	+
KSA16	Green	Aerial	-	+
KSA18	White	Substrate	Yellow	+
KSA19	Yellow	Substrate	Yellow	+

Table 3:.Minimum inhibitory concentrations (MIC) of the purified bioactive metabolite isolated from Streptomyces KSA18.

Test organisms	MIC (µg/ml)
Aspergillus flavus	92
Bacillus subtilis	22
Candida albicans	71
Escherichia coli	55
Enterococcus faecalis	26
Listeria monocytogenes	24
MRSA	37
Pseudomonas aeruginosa	62
Staphylococcus aureus	36
Salmonella Tyfimirium	53

ica gel column chromatography, unwanted contaminants and metabolites were removed. Obtained fractions were analyzed by TLC. Ays1 (122 mg) and Ays2 (21 mg) got substantial fractions. Fraction Ays 1 was the most antimicrobial.

Growth and antimicrobial production

The KSA18's synthesis of active metabolites was measured for 120 hours. Antibiotic production was dependent on the growth phase, with the best efficiency of the product in the end of the exponential phase and stationary periods. The highest yield was obtained after 72 hours of incubation with an inhibition zone of 22 mm (Fig. 2).

UV-visible analysis

The Uv-visible spectrum of the crude extract methanol showed distinctive absorption at 205, 210, and 240 nm. UV absorption maxima was detected at 205 nm with another peak at 240 nm, confirming a non-polyenic nature of the molecule (Fig. 3).

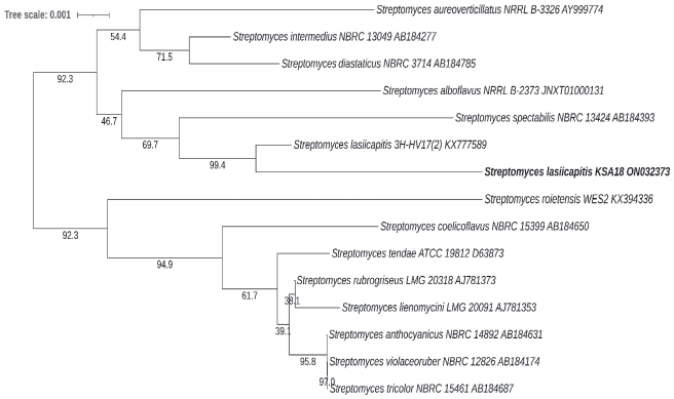

Fig. 1: A Cladogram, using neighbour-joining method of selected 16S rRNA gene sequences of the genus Streptomyses, obtained from BLAST hits, showing relationships between strains KSA18 and some closely related representative members.

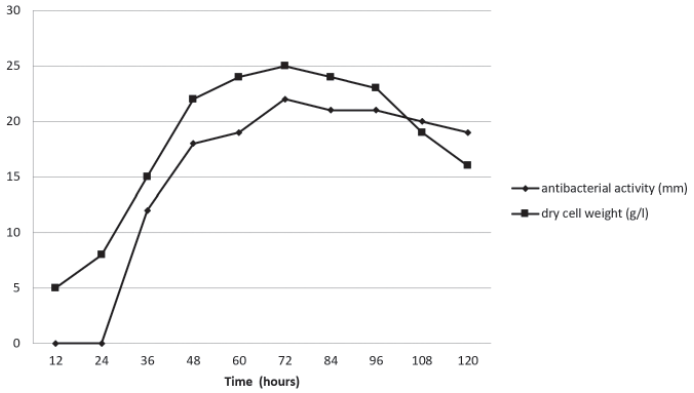

Fig. 2: Time course of growth and antimicrobial metabolites production by Streptomyces KSA18 in ISP2.

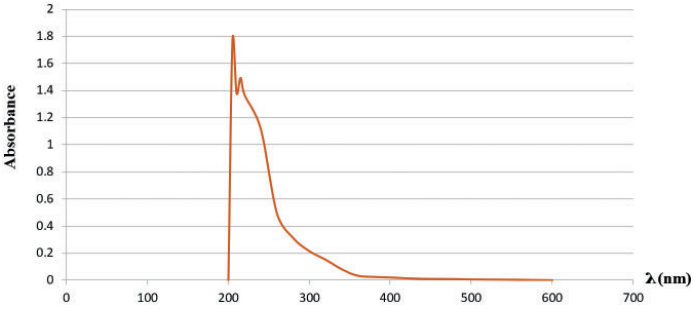

Fig. 3: UV-Visible spectrum of the crude extract of Streptomyces KSA18.

Minimal Inhibitory Concentration

The purified chemical compound showed antibacterial and antifungical activity on a wide spectrum of tested micro-organisms. The MIC for Bacillus subtilis and Listeria monocytogenes was 22 and 24 mg/ml, respectively. The MIC for Gram-negative bacteria was 53–62 mg/ml. The minimal inhibitory concentration of fungus was greatest compared to bacteria (71mg/ml for Candida albicans and 92mg/ml for A. flavus) (Table 3).

GC-MS spectrum

Analysis by GC-MS detected different chemicals (Figs. 4 and 5). 2,4-Bis (1,1-Dimethylethyl) and O-D-glucopyranoside, ß-D-fruc are important chemicals. Other compounds are in table 4.

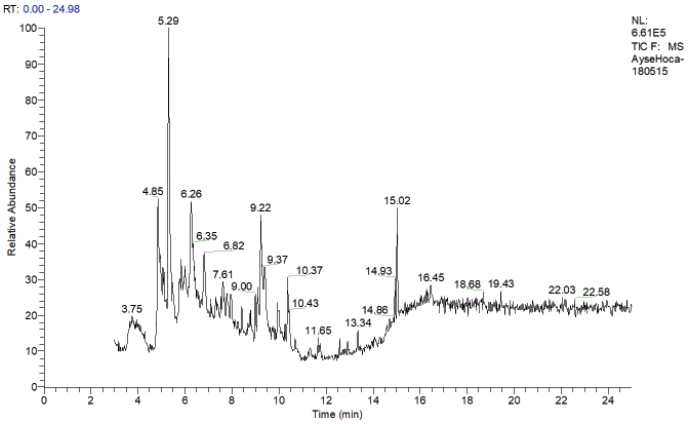

Fig. 4: GC-MS spectrum of the active compound of the crude extract of KSA18.

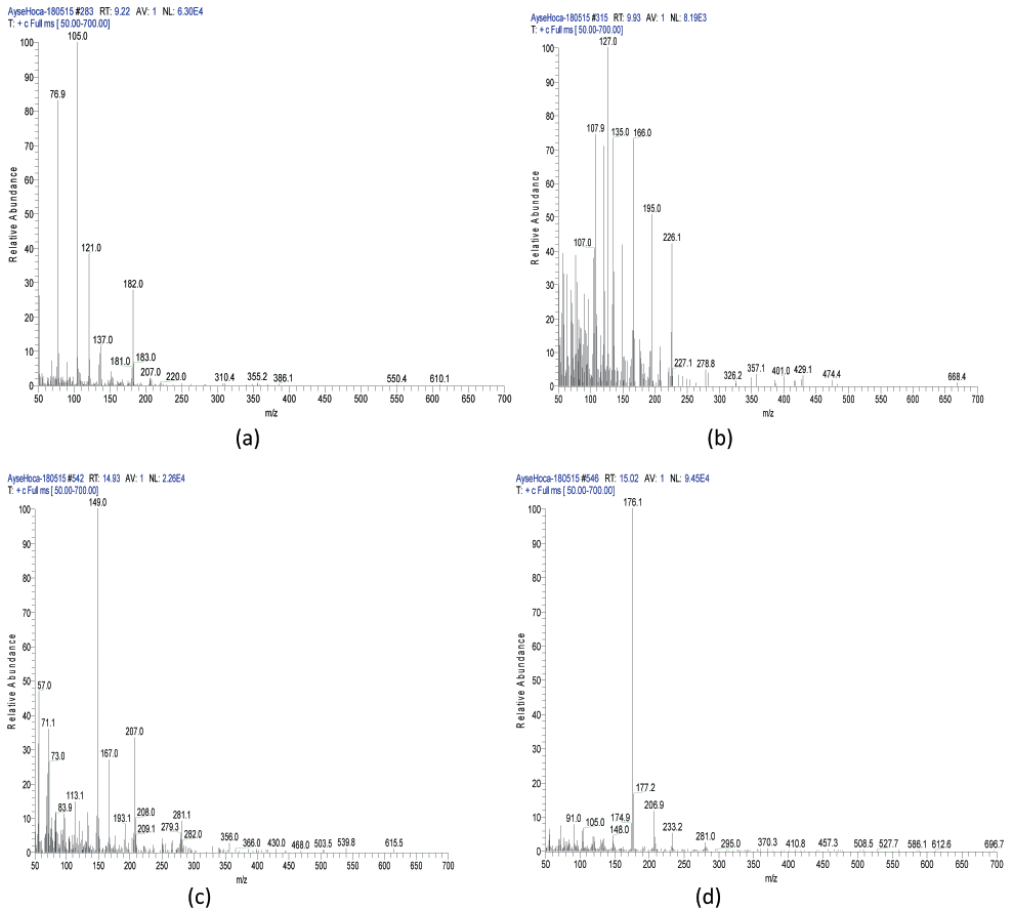

Fig. 5: MS Spectrum of Most important compounds : (a) Benzofuran, 2,3-dihydro, (b) Phenol, 2,4-Bis(1,1-Dimethylethyl) , (c) 3-Isobutylhexahydropyrrolo[1,2-A]Pyrazine-1,4-Dione, (d) 2-methyloctacosane

Table 4: GC-MS identification of bioactive compounds

Peak N°	R. Time	Name	Chemical formula	Molecular weight	Activity
1	4.85	DL-Arabinose	$C_5H_{10}O_5$	150.05	Antivirus activity
2	5.29	Xylitol	$C_5H_{12}O_5$	152.15	Antimicrobial
3	5.82	Glucitol, 6-O-nonyl	$C_{15}H_{32}O_6$	308.41	No activity reported
4	6.26	α- DGlucopyranoside,O-αD-glucopyranosyl-(1.fwdarw.3)-ß-D-fruc	$C_{18}H_{32}O_{16}$	504.40	Anticarcinogenic antimutagenic
5	6.82	N, N-Dimethylglycine	$C_4H_9NO_2$	103.12	Antioxydant
6	7.61	Glycerin	$C_3H_8O_3$		Emulsifiant
7	9.22	Benzofuran, 2,3-dihydro-	C_8H_8O	120.10	anti-inflammatory activity
8	9.29	Maltol	$C_6H_{12}O_3$	126.11	Antioxydant
9	9.37	Phenol, 2,4-Bis(1,1-Dimethylethyl)	$C_{17}H_{30}OSi$	278.50	Anti-inflammatory, antioxydant, antimicrobial
10	10.37	Levomernthol	$C_{10}H_{20}O$	156.26	Antimicrobial
11	14.93	3-Isobutylhexahydropyrrolo[1,2-A]Pyrazine-1,4-Dione	$C_{11}H_{18}N_2O_2$	210.27	Antibacterial
12	15.02	2-methyloctacosane	$C_{29}H_{60}$	408.80	Antimicrobial, antioxydant
13	16.45	Benzenepropanoic acid, 3,5-bis(1,1-dimethylethyl)-4-hydroxy-, methyl ester	$C_{18}H_{28}O$	292.40	Antioxydant
14	18.68	Propanoic acid	$C_3H_6O_2$	74.07	antibacterial
15	19.43	Thieno[3,2-e] benzofuran	$C_{10}H_7NOS$	189.24	Antimicrobial
16	22.03	Pyrrolo[1,2-a] pyrazine-1,4-dione, hexahydro-3-(phenylmethyl)	$C_{14}H_{16}N_2O_2$	244.29	Antioxydant
17	22.58	Bis (2-ethyl hexyl) phthalate	C24H38O4	390.6	Antibacterial

Discussion

23 actinomycetes were isolated from a poor Algerian field. Isolation of actinomycetes has been difficult compared to bacteria and fungi (KUMAR et al, 2018). It may be attributed to lengthy incubation. Strach casein agar medium with nalidixic acid 100 mgl.l-1 and actidione 20 mg.l-1 inhibited contaminating bacteria and fungi.

The isolation and morphological identification showed that 79% of identified isolates are antibacterial. This study only kept the KSA18 strain because it inhibited most examined bacteria. Morphological, physiological, and biochemical traits matched Streptomyces. KSA18 isolate generated secondary metabolites and gave antimicrobial activity against a wide range of bacteria. VALAN ARASU et al, (2008) found similar results, who recovered Streptomyces spp. (ERI-3) from Western Ghats rock soil. Actinomycete microflora from Saharian soils in southeast Algeria were identified using molecular methods. Then they checked if they killed fungus. Extract of KSA18 Streptomyces showed antibacterial and antifungal activity.

Secondary metabolite production obtained in the end of the exponential phase and continued during the stationary periods. We noticed that the production of antimicrobial compounds was significantly related to the development of the KSA18 strain.

When the crude extract's UV-VIS spectrum was checked against the maximum molecular absorption of polyenes, it was evident that the KSA18 extract's absorption peaks lacked a non polyenic structure. Since polyenes are notorious for being poisonous and difficult to dissolve, this is bad for the screening of novel antifungal compounds (KANDULA & TERLI, 2013).

The TLC results showed that the best composition of solvent used for crude extract is ethyl acetate/methanol. BOUGHACHICHE (2012), found that ethyl acetate-Methanol gives fast migration of actives compounds. Therefore, it gives good split and a suitable purification for the crude extract obtained with methanol.

The GC-MS analysis has shown a great diversity with about 17 different volatile compounds in the active fraction of the methanolic extract. Most between them could be responsible for biological activity. Devi et al. showed antifungal activity of Phenol, 2,4-Bis(1,1-Dimethylethyl) produced by Actinomycete applicable as Growth-promoting for Mangrove (BADJI et al, 2005). 3-Isobutylhexahydropyrrolo[1,2-A] Pyrazine-1,4-Dione have antimicrobial activity (DEVI et al, 2021). 2-methyloctacosane also showed antimicrobial and antioxidant activity in the work of Pelo et al, (2021). Streptomyces albidoflavus produce Dibutyl phthalate which has antimicrobial activity (ABOOBAKER et al, 2009). But this study needs to use different methods to find the structures of different molecules of technological and biological interest found in our extract.

The different MICs obtained for our extract show its effectiveness against most pathogenic microorganisms, which reveals the presence of several interesting molecules

Conclusion

Standard therapies for infections due to multiresistant strains have no longer become sufficient, even 2nd and 3rd line drugs are not active enough against them. It then becomes crucial to seek new bioactive compounds of natural origin in order to continuously stimulate the discovery and development of new drugs. This is why the main goal of this work is the isolation of Actinobacterial strains and the demonstration of their antimicrobial activity. A total of 23 actinomycetes are isolated from Saharan soil. Most of them showed microbial activity. The KSA 18 strain is retained because of their effectiveness to the majority of the pathogens tested. The molecular identification of the strain a makes it possible to classify it in the species Streptomyces lasiicapitis. A submerged fermentation of the selected bacteria allows the production and extraction of metabolites. The GC-MS technique showed a richness of the extract in various bioactive substances. This work deserves to be continued to identify the different chemical structures of the active molecules.

Author Contributions Material preparation, data collection and analysis were performed by MB, DEA and TAB. and MB. KZ and M.B. writing original draft; AO, KG. supervision, review and editing; JW. co-supervised the work; M.B., KZ. conceptualized, revised and corrected the paper. All authors listed have made a substantial, direct and intellectual contribu-tion to the work and approved the work for publication. All authors have read and agreed to the published version of the manuscript.

Funding This research received no external funding

Data Availability The datasets generated and/or analysed during the current study are not publicly available for ethical reasons, as well as privacy reasons, but are available from the author on reasonable request

Code Availability Not applicable.

Declarations

Conflicts of Interest The authors declare no conflict of interest.

Acknowledgment

The authors are grateful to the Departments of Molecular Biology and Genetics, Istanbul University, Turkey, for all their contributions to the realization of this work.

References

1. ABOOBAKER Z., VILJOEN A., CHEN W., CROUS P., MAHARAJ V., VAN VUUREN S. (2019). Endophytic fungi isolated from Pelargonium sidoides DC: antimicrobial interaction and isolation of a bioactive compound. S Afr J Bot 122:535–42.
2. AOUICHE A., SABAOU N., MEKLAT A., ZITOUNI A., MATHIEU F., LEBRIHI A. (2012). Activité antimicrobienne de Streptomyces sp. PAL111 d'origine saharienne contre divers microorganismes cliniques et toxino-gènes résistants aux antibiotiques. J Mycol Med 22 :42-51.
3. BADJI B., RIBA A., MATHIEU F., LEBRIHI A., SABAOU N. (2005). Antifungal activity of a Saharan Actinomadura strain against various pathogenic and toxinogenic fungi. J Mycol Med 15 :211-219.
4. BALTZ R.H. (2005). Antibiotic discovery from actinomycetes: Will a renaissance follow the decline and fall? SIM News 55:186-196.
5. BALTZ R.H. (2007). Antimicrobials from actinomycetes: Back to the future. Microbe 2:125-131.
6. BARTON H.A. (2006). Introduction to cave microbiology: a review for the non-specialist. J Caves Karst Stud 68(2):43–54.
7. BOUGHACHICHE F. (2012). Study of antibiotic molecules secreted by strains belonging to the genus Streptomyces, isolated from Sebkha," Ph.D. thesis, University Mentouri-Constantine. faculty of Natural and Life Sciences, Algeria.
8. BRIAND Y.M. (2009). A history of antibiotic resistance in six bacteria, Edition L'harmattan. Paris.

9. BUTLER M.S., BUSS A.D. (2006). Natural products: The future scaffolds for novel antibiotics. Biochem Pharmacol 71: 919-929.
10. CAVALLA M., EBERLIN T. (1994). Isolation of soil streptomycetes, The operon 19 :13–17.
11. DEVI T.S., VIJAY K., VIDYAVATHI R.M., KUMAR P., GOVARTHANAN M., KAVITHA T. (2021). Antifungal Activity and Molecular Docking of Phenol, 2, 4-Bis (1, 1-Dimethylethyl)-Produced By Plant Growth-Promoting Mangrove Actinobacteria; Kutzneria Sp. Strain TSII.
12. GOODFELLOW M., HAYNES J.A. (1984). Actinomycetes in marine sediments. Biological, biochemical and biomedical aspects of actinomycetes, 453-472.
13. KANDULA S.K., TERLI R. (2013). Production, purification and characterization of an antimicrobial compound from marine Streptomyces coeruleorubidus BTSS-301. J. Pharm. Res 7:397-403.
14. KITOUNI M., BOUDEMAGH A., OULMI L., REGHIOUA S., BOUGHACHICHE F., ZERIZER H., HAMDIKEN H., COUBLE A., MOUNIEE D., BOULAHROUF A., BOIRON P. (2005). Isolation of actinomycetes producing bioactive substances from water, soil and tree bark samples of the north–east of Algeria. Journal de Mycologie Médicale 15:45–51.
15. KUMAR S., STECHER G., LI M., KNYAZ C., TAMURA K. (2018) MEGA X: molecular evolutionary genetics analysis across computing platforms. Molecular biology and evolution 35(6):1547.
16. LEE D.S. (2000). Dibutyl phthalate, an -glucosidase inhibitor from Streptomyces melanosporofaciens. J Biosci Bioeng 89(3):271–3.
17. LEE J.Y., HWANG B.K. (2002). Diversity of antifungal actinomycetes in various vegetative soils of Korea. Can J. Microbiol 48:40.-417.
18. LEMRISS S., LAURENT F., COUPLE A., CASOLI E., LANCELIN J.M., SAINTPIERRE B.D. (2003). screening of nonpolymeric antifungal metabolites produced by clinical isolates of actinomycetes. Can J Microbiol 49:669-674.
19. MANGAMURI U., MUVVA V., PODA S., NARAGANI K., MUNAGANTI R.K., CHITTURI B. (2016). Bioactive metabolites produced by Streptomyces cheonanensis VUK-A from Coringa mangrove sediments: isolation, structure elucidation and bioactivity. 3 Biotech 6(1):63.
20. MENDHAM J., DENNEY R.C., BARNES J.D., THOMAS M. (2006.) Vogel's quantitative chemical analysis, De Boeck Ed, Brussels.
21. NEWMAN D.J., CRAGG G.M. (2007). Natural products as sources of new drugs over the last 25 years. J Nat Prod 70:461-477. https://doi.org/10.1021/np068054v
22. PARTHASARATHI S., SATHYA S., BUPESH G., SAMY R.D., MOHAN M.R., KUMAR G.S. (2012). Isolation and characterization of antimicrobial compound from marine Streptomyces hygroscopicus BDUS 49. World J Fish Mar Sci 4(3):268-77.
23. PELO S.P., OLUWAFEMI A.A., EZEKIEL G. (2021) Chemotaxonomic profiling of fungal endophytes of Solanum mauritianum (alien weed) using gas chromatography high resolution time-of-flight mass spectrometry (GC-HRTOF-MS)." Metabolomics 17.5: 1-13.
24. PERIC C.N., LONG P.F. (2003). Mining the microbial metabolism: a new frontier for natural product lead discovery. Drug Discov Today 8:1078-1084.
25. POCHON J., TARDIEUX P. (1962). Analytical techniques in soil microbiology. Saint Mandé: Edition de la tourtourelle.
26. RABEK J.F. (1995). Polymer photodegradation: mechanisms and experimental methods, 1st Ed., Chapman & Hall, London.
27. SHIRLING E.B., GOTTLIEB D. (1966). Methods for characterization of Streptomyces species. Int J Syst Bacteriol 16 :313-340.
28. SUN S., TIAN L., WANG Y., WU H., LU X., PEI Y. (2009). A novel natural product from the fermentation liquid of marine fungus Trichoderma atroviride G20-12. Asian J. Trad. Med 4: 123-127.
29. THOMPSON J.D., HIGGINS D.G., GIBSON T.J., CLUSTAL W. (1994). Improving the sensitivity of progressive multiple sequence alignment through sequence weighting, position-specific gap penalties and weight matrix choice. Nucleic acids research 22(22): 4673-4680.
30. ZHANG L., DEMAIN A.L. (2005). Integrated approaches for discovering novel drugs from natural microbial products. Natural product, drug discovery and therapeutic medicine. Totowa, New Jersey 4:375-382.
31. ZOETENDAL E.G., RAJILIĆ S.M., DE VOS W.M. (2008). High-throughput diversity and functionality analysis of the gastrointestinal tract microbiota. Gut 57(11):1605-1615.

ISSN print: 1224-5984
ISSN online: 2248-3942

Rom Biotechnol Lett. 2022; 27(5): 3722-3729
doi: 10.25083/rbl/27.5/3722.3729

Received for publication, December, 21, 2022
Accepted, February, 16, 2023

Review

Antibiotics and antibiotic resitant bacteria: from hotspots into the aquatic environment

ECATERINA SARBU[1], LUMINITA MARUTESCU[2], IRINA GHEORGHE BARBU[2], CARMEN POSTOLACHE[2], ILDA CZOBOR BARBU[2,3], MARCELA POPA[2], GRATIELA GRADISTEANU PIRCALABIORU[1,3], MARIANA-CARMEN CHIFIRIUC[1,2,3,4]

[1] Research Institute of University of Bucharest, Bucharest, Romania
[2] Faculty of Biology, University of Buchrest, Bucharest, Romania
[3] Academy of Romanian Scientists, Bucharest, Romania
[4] Romanian Academy, Bucharest, Romania

Abstract

There is a vast literature on the occurrence of antibiotics and antibiotic resistant bacteria (ARB) of human or animal origin in natural aquatic ecosystems as result of anthropogenic activities. Although hotspots for AR discharge in the environment were identified, that include: sewage and wastewater treatment plants (WWTP), industrial drug manufacurers, food and animal production, agriculture and aquaculture, and clinical settings such as hospitals, effcient current regulations to mitigate this pollution are lacking. The aim of this review is to provide insights regarding the spread of antibiotics and ARB from hotspots into aquatic environment and also an overview of current EU and UN regulations for combating AR pollution of our natural ecosystems.

Keywords antibiotic resistant bacteria, wastewater treatment plant, antibiotic resistance

To cite this article: ECATERINA SARBU. Antibiotics and antibiotic resitant bacteria: from hotspots into the aquatic environment. *Rom Biotechnol Lett.* 2022; 27(5): 3722-3729 DOI: 10.25083/rbl/27.5/3722.3729

*Corresponding author: *Corresponding author: Ţogoe Dorin, University of Agronomic Science and Veterinary Medicine of Bucharest, Splaiul Independenței nr 105.
E-mail: dtogoe@yahoo.com

Introduction

Infections due to antibiotic resistant-bacteria (ARB) are jeopardizing modern health care. Experts and world leaders of Global Research on Antimicrobial Resistance (GRAM) Project call for action against antibiotic resistance (AR) (Lancet 2022; 399: 629–55). It has estimated that more than 1.2 million people—died in 2019 as a direct result of ARB infections. Nowadays, AR is responsible for more deaths than HIV/AIDS or malaria and the strongest approach in our hands to control AR is the correct and judicious use of the available antibiotics in order to preserve their effectiveness, including the unnecessary use of antimicrobials in humans and animals (Giurazza et al., 2021). As highlighted by an ad hoc World Health Organization panel, very few antimicrobials that are in clinical development are exhibiting a novel mechanism of action (WHO, 2021). A secondary approach for controlling the AR is to limit the release of the antibiotics and ARB into environment (Bengtsson-Palme et al., 2018).

Several reports are indicating that wastewater systems are continuously discharging high amounts of ARB and ARG in surface waters, worldwide (Gao et al., 2012; Huijbers et al., 2015; Bougnom et al., 2018; Pärnänen et al, 2019; Adelowo et al., 2018;), suggesting that AR pollution is enriching the environmental resistance pool. As a result of the anthropogenic contamination, the levels of ARBs is extremely high in most of the river systems (up to 98% of the total detected bacteria), and lakes (up to 77% of the total detected bacteria) (Nnadozie and Odume, 2019). Understanding the role of AR pollution in the emergence and evolution of resistance is particularly important, as this could represent an important driver with major health consequences (Bengtsson-Palme et al., 2018). The aim of this review is to provide insights regarding the spread of antibiotics and ARB from hotspots into environment and also an overview of current public regulations for combating AR pollution of the natural ecosystems.

Hotspots for AR spread into environment

Until recently, the prevention and control of AR has been largely focused on improving the rational use of antibiotics in the hospital and community and surveillance programs for the emergence and spread of resistance in clinical settings. It was reported that effective stewardship programs can reduce antibiotic use by 20–40%, frequency of healthcare associated infections (MRSA, Clostridium difficile), hospitalization, and bacterial resistance rates (Charani et al., 2019). Stewardship efforts are important; however they cannot win the war (Laxminarayan et al., 2013). The challenges of AR emergence and dissemination have advanced a One Health Approach that is recognizing that the health of people is connected to the health of animals and the environment (Kraemer et al., 2019).

The main anthropogenic sources of antibiotic residues and ARB are the human, animal and agricultural waste. It was estimated that a high amount of antibiotics and/or its metabolites (between 20 and 97%) are excreted through urine and feces (Jelic et al., 2015). The hospitals, urban, industrial, sewer systems are transporting these chemical pollutants and ARB of human and animal origin to the treatment facilities. However, the treatment technologies of these plants were reported to be unable to completely eliminate these pollutants, antibiotics ARB of human and animal origin being detected in the treated released water into the environment and in the animal sludge applied to fields with cultivated crops (Auguet et al., 2017). For example, the analysis of wastewater samples from a German urban wastewater treatment plants (WWTP) did not show differences in resistance between E. coli isolates taken from the inflow and from the outflow . Also, an integrated surveillance of European wastewaters that analyzed the influent and final effluent of 12 urban WWTPs located in seven countries (Portugal, Spain, Ireland, Cyprus, Germany, Finland, and Norway) has highlighted the strong relationship between clinical and environmental AR (Pärnänen et al, 2019).

Agriculture run-off, and process waters and wastewater from slaughterhouses are also considered hot spots for AR (Figure 1). The increased usage of antibiotics in livestock animals has led to the selection of ARB that can be transmitted directly from animal to human or indirectly via the food chain and eventually causing difficult-to-treat diseases in humans (Binsker et al., 2022). The direct entry of antibiotics, ARB and ARG in the environment takes place when cattle are out door or manure is used as fertilizer on nearby crop lands, where ARGs and surviving ARBs come into contact with the soil microbiome and could modify the profiles of ARB, ARGs and bacterial communities in receiving soils (Chen et al., 2018). Once in the soil, ARB and ARG may enter aquatic systems indirectly via surface runoff to surface water and/or by leaching to groundwater.

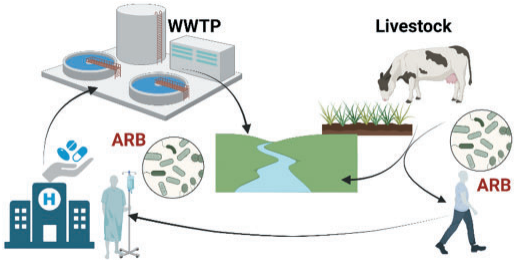

Figure 1. Hotspots for selection of ARB

The ARB discharged by the WWTP effluents and agriculture run-off into water bodies may be particularly prone to transfer AR genes to environmental bacteria via different horizontal gene transfer (HGT) mechanisms: conjugation, transformation, and transduction. Several researchers showed that conjugation take place in aquatic environments (Kimihiro et al., 2020). It has been showed that the incidence of the HGT is enhanced by low concentrations of antibiotics that are released into receiving water bodies (Aminov 2011). The possibility for HGT using MGEs (plasmids, transposons, insertion sequences, integrons, and integrative-conjugative elements) between ARB of human or animal origin and environmental bacteria is huge and it seems that it doesn't take bacteria much time to acquire the resistances markers (Sultan et al., 2018). Furthermore, the frequency of HGT is increased in biofilms due to the proximity of the cells, making biofilms in hot spots of antibiotic resistance (Aminov, 2011; Balcázar et al., 2015). However, despite the wealth of information about medical biofilms, the potential contribution of the environmental biofilms to the acquisition and spread of antibiotic resistance has not been fully investigated in aquatic systems (Balcázar et al., 2015). Environmental biofilms are a key component of ecosystem functioning, playing an essential role in the biogeochemical cycling of nutrients. Taken into consideration that biofilms are exposed to antibiotics used in veterinary and human medicine released into these waterbodies mainly through WWTP effluents and agricultural run-off, research is needed to investigate how such hot spots of AR may represent a concern for human health (Balcázar et al., 2015).

The dissemination of antibiotics ARB and ARG into environment

Antibiotics are considered the main driver of AR. Several researches have indicated a direct correlation between AR and the use of antibiotics (Olesen et al., 2018). Global estimates have indicated that similar amounts are used in humans and animals (118 mg/PCU and 133 mg/kg respectively) (Pokharel et al., 2020). Moreover, antibiotics used as plant protection products in some regions of the world (Pokharel et al., 2020). Residual antibiotics from agriculture run-off, poorly metabolized antibiotics from animal and human waste as well as antibiotics from drug manufacturer effluents are discharged in the environment. These antibiotic pollutants were already found in waterways and sediments worldwide (Table 1). They can accumulate in the environment and exert selective pressure on the soil and water microorganisms, enriching the environment AR pool.

Several reports have indicated connections between the enteric pathogens isolated from surface waters, impacted by human activity and active disease in the community (Yan et al., 2018; Yang et al., 2014). Bacterial isolates resistant to different antibiotic classes, were detected in surface water samples collected from lakes, rivers and sea (Lepuschitz et al. 2019, Zurfluh et al., 2013). As, lake and river waters is used for drinking water production, recreational activities and irrigation of crops, humans and animals are exposed to these ARB and could get colonized with such bacteria (Blaak et al., 2015). The antimicrobial susceptibility tests are showing that rivers and lakes are containing bacteria with high resistance rates to several classes of

Table 1. Antibiotics found in aquatic environments.

Antibiotic	Class	Max concentration ng/L	Type of environment	Location	References
Acetylsulfamethoxazole	Sulfonamid es	70	River water	United Kingdom	Ashton et al., 2004
Sulfadiazine	Sulfonamid es	209	River water	Pearl River, Guangzhou, China	Xu et al., 2007
Sulfamethoxazole	Sulfonamid es	259.6	River water	Huangpu River, Shanghai,China	Chen and Zhou, 2014
Amoxicillin	Penicillins	5,70	River water	River Arno, Italy	Zuccato et al., 2010
Cefalexin	B-lactams	12,60	Sediment	Dongjiang River, China	Chen et al., 2018
Chlortetracycline	Tetracyclin es	353400	Lagoon water	Iowa and Ohio, USA	Campagnolo et al., 2002
Oxytetracycline	Tetracyclin es	52.8	Sediment	Taihu Lake, China	Xu et al., 2014
Tetracycline	Tetracyclin es	107400	Lagoon water	Iowa and Ohio, USA	Campagnolo et al., 2002
Doxycycline	Tetracyclin es	11,30	River water	Huangpu River, Shanghai,China	Chen and Zhou, 2014
Azithromycin	Macrolides	72,1	Sediment	Mar Menor lagoon, Spain	Moreno-González et al., 2015
Clarithromycin	Macrolides	25,40	River water	River Arno, Italy	Zuccato et al., 2010
Erythromycin	Macrolidea	62.1	River water	Laizhou Bay, China	Zhang et al., 2012
Nalidixic acid	Quinolones	77	Sediment	Charmoise River, France	Dinh et al., 2017
Norfloxacin	Fluoroquinolones	267	Sediment	Baiyangdian Lake, China	Li et al., 2012
Ciprofloxacin	Fluoroquinolones	569	Sediment	Charmoise River, France	Dinh et al., 2017
Chloramphenicol	Chloramphenicol	127	River water	Pearl River, Guangzhou	Xu et al., 2007

antibiotics (Table 2). For example, in a study performed by Zurfluh et al. (2013), the enterobacteria collected from rivers and lakes in Switzerland were resistant to cefotaxime (77%), gentamicin (36.5%) kanamycin (28.4%), streptomycin 44.6%, nalidixic acid (59.5%) ciprofloxacin (44.6%), tetracycline (67.6%) chloramphenicol (23%), sulfamethoxazole (85.1%) and trimethoprim (74.3%) (Zurfluh, 2013). Through continously release of ARB into waterbodies, the environment could become a pool of AR at which human population, but also animals (livestock, wild life) may be exposed, therefore increasing the colonization rate.

The AR increase to fluoroquinolones and extended-spectrum cephalosporins due to the production of the ESBL CTX-M-15, was suggested to be responsible for the worldwide spread, on three continents, of Escherichia coli ST131, which is an extraintestinal pathogenic clone. Currently, this clone has been identified as the predominant E. coli in the gut of human healthy population. A public health problem of global dimension is the possibility of this clone to acquire MGE encoding carbapenemases. The colonization of human or animal gut with such bacteria could hamper medical treatment-options of severe infections caused by ESBL producing Enterobacteriaceae, consequently resulting in higher morbidity and mortality rates (Oteo et al., 2016; Yang et al., 2018). E. coli ST131 was found in various freshwaters ((Jiquiriçá and Brejões rivers (Brazil) (Bartley et al., 2019) (Furlan et al., 2020); Orontes River (Lebanon) (Moussa et al., 2021), rivers of Guadeloupe (France), (Guyomard-Rabenirina, 2017), River Thames, UK (Dhanji et al., 2011), river water in Spain (Colomer-Lluch et al., 2013); rivers and lakes, in Switzerland (Zurfluh et al., 2013.), river Ouche (France) (Bollache et al., 2019), river Inn (Austria), and marine environments (Adriatic Sea, Italy (Vignaroli et al., 2013), Salish Sea (Vingino et al., 2021)) i.e. rising questions about the health risks.

An important threat to public health of international concern are carbapenemase-producing Enterobacteriaceae, which are producing difficult to treat infections, being associated with high level of mortality. These bacteria have the potential for widespread transmission of resistance via MGEs. The current WHO guidelines are aiming to effectively prevent their occurrence and control their spread in acute health care facilities. In Europe, a total of 23 European countries reported a an increased prevalence of epidemiological situation of carbapenemase-producing Enterobacteriaceae between the years 2010 and 2018 (Brolund et al. 2019). These bacteria have been found to have a widespread distribution in waterways (Table 3) and sediments (Piedra-Carrasco et al., 2017), rising questions about the health risks. Their dissemination into surface water will increase the colonization level of human population with carbapenemase-producing Enterobacteriaceae, threatening our ablity to treat infections. Therefore, the prevalence carbapenemase-producing Enterobacteriaceae, especially those resistant to colistin is important to monitor in all the interconnected compartments: humans, animals and enviroment.

The worlwide rise in carbapenemase-producing Enterobacteriaceae has led to the reintroduction of colistion

Table 2. ARB detected in the environment.

Bacterial species	Class of antibiotics resistant to	Surface water, Country	References
Escherichia coli	β-lactams (cefotaxime) Lipopetides (Aminoglycosides (kanamycin, streptomycin, gentamicin) Nalidixic acid Quinolones Tetracyclines Phenicols (chloramphenicol) Folate pathway antagonists (sulfamethoxazole and trimethoprim)	Rivers and lakes, Switzerland	Zurfluh et al., 2013
Escherichia coli	β-lactams Aminoglycosides Quinolones	Rhine and New Meuse rivers	Blaak, H. et al, 2011

Table 3. Water bodies in which carbapenemase-producing *Enterobacteriaceae* were detected.

Water bodies	References
West Coast (California, USA)	Harmon et al., 2019
Midwest (California, USA)	Aubron et al., 2005
Vouga river basin (Portugal)	Tacão et al., 2015
River in Santo Tirso (Portugal)	Kieffer et al., 2016; Poirel et al., 2012
Lis river (Portugal)	Teixeira et al., 2020
River Rhine (Switzerland)	Zurfluh et al., 2013
River Mur (Austria)	Zarfel et al., 2017
River Danube (Germany)	Kittinger et al., 2016
River in Guangzhou (China)	Ye et al., 2017

in the therapy, as last line antibiotic for the medical care of infections in which these pathogens are implicated. However, data reports from EU/EEA countries, China and Japan are indicating an alarming increase of colistin resistance. An important contribution to the increase of bacteria resistant to colistin is represented by the use of this antibiotic in the livestock production. These selected ARB can be directly or indirectly spread from animals to humans though food chain. This health problem is reflected by the results of the environmental studies. Two reports, from South Africa and Tunisia have found Enterbacteriales resistant to colistin in wastewater (Ovejero et al., 2017; Adegoke et al. 2020; Hassen et al. 2020). The highest amount of ARB has been reported in the hospital effluents (Bardhan, Chakraborty and Bhattacharjee 2020). These findings are highlighting the importance of monitoring the colistin resistance in bacteria of animal and human origin, and the need for environmental studies for the elucidation of occurrence and distribution of these bacteria resistance to colistin in water bodies. These data will provide scientific evidence for the assessment of AR burden in clinical sector, community and environment and therefore the development of effective strategic interventions.

The impact of human activities on aquatic ecosystems is also highlighted by the occurrence and widespread distribution of AR genes of human or animal origins (Yang et al., 2017). Several ARGs have been identified in the freshwater biofilms receiving fecal contamination (Proia et al. 2013). Research studies have demonstrated significant correlations between several ARGs and corresponding antibiotics in water samples. Thus, low concentrations of antibiotics in freshwater play an important role in the maintenance and enrichment of AR pool (Xiong et al., 2015). Additional studies are necessary for a more complete understanding of human-based environmental reservoirs of ARB and ARGs. In particular, upstream and downstream urban WWTP sites would be useful for assessing and quantifying the influence of human contamination of freshwaters.

Current EU and UN regulations for combating AR pollution of the environment

Studies on environmental AR are growing and as emphasized in this paper, current research is aimed at investigating the health risks associated with the exposure of natural environments (soil and water) to ARB, AR genes and antibiotics. In recognition of the importance of tackling the AR, several international and national polices and regulations were developed. The United Nations Environment Program (Gaze and Depledge, 2017) emphasized that the spread of AR in the environmental is representing one of the most important environmental pollution problems of our time. The New EU One Health Action Plan against Antimicrobial Resistance (http://ec.europa.eu/health/amr/sites/amr/files/amr_summary_action_plan_2017_en.pdf) provides the framework for actions needed to decrease the emergence and dissemination of AR. National bodies of the EU need to elaborate and implement surveillance plans of AR in the environment and also to advance innovative and green technologies for waste removal containing AR from pharmaceutical companies, health care units, livestock and crop production sites, wastewater plants (https://www.who.int/news/item/02-03-2022-world-leaders-and-experts-call-for-action-to-protect-the-environment-from-antimicrobial-pollution). Standards and regulations are urgently required to monitor and control of AR release in the environment and countries of the EU should prioritize their development.

Conclusions

The extensive use of antibiotics had contributed to the exposure of natural environments (soil and water) to the detection of worrisome high levels of ARB and ARG of animal and human origin in different types of environmental samples collected from various ecosystems. These findings are of public health concern because the natural ecosystems are providing important services to the communities. Therefore there is of crucial importance to assess the baseline levels of AR in such environments in order to adequately address the health concerns. Additionally, the environmental microbial populations with essential roles in Earth ecosystems and knowledge about the way that are responding to the bacterial diversity and community to anthropogenic disturbances, in particular pathogenic ARBs, ARGs and antibiotics is of great significance. ARB from human sources have been found in sewage, in treated effluent and in sludge applied to farmland, these pollutants are discharged into the environment. Therefore, to stop the spread and enrichment of our environment with AR, innovative technologies for the treatment of sewage and agricultural waste are needed. The UN Environment Program and The New EU One Health Action Plan against Antimicrobial Resistance are providing the needed actions for combat AR. The EU countries should prioritize the elaboration and implementation of national standards for controlling the discharge of AR in the environment.

Acknowledgements. The support of projects PN-III-P1-1.1-TE-2021-1515 (TE 112/2022) and AOSR Teams/2022 is gratefully acknowledged.

References

1. Antimicrobial Resistance Collaborators. Global burden of bacterial antimicrobial resistance in 2019: a systematic analysis. Lancet. 2022 Feb 12;399(10325):629-655.
2. Giurazza R, Mazza MC, Andini R, Sansone P, Pace MC, Durante-Mangoni E. Emerging Treatment Options for Multi-Drug-Resistant Bacterial Infections. Life (Basel). 2021 Jun 3;11(6):519. doi: 10.3390/life11060519.
3. WHO WHO—Global Shortage of Innovative Antibiotics Fuels Emergence and Spread of Drug-Resistance. Departmental News. Apr 15, 2021. Available online: https://www.who.int/news/item/15-04-2021-global-shortage-of-innovative-antibiotics-fuels-emergence-and-spread-of-drug-resistance.
4. Bengtsson-Palme J, Larsson DGJ. Antibiotic resistance genes in the environment: prioritizing risks. Nature Review Microbiology, 2015, 13:396.
5. Munir M,Wong K, Xagoraraki I. Release of antibiotic resistant bacteria and genes in the effluent and biosolids of five wastewater utilities in Michigan. Water Res. 2011, 45, 681–693.
6. Huijbers PM, Blaak H, de Jong MC, Graat EA, Vandenbroucke-Grauls CM, de Roda Husman AM. Role of the Environment in the Transmission of Antimicrobial Resistance to Humans: A Review. Environ Sci Technol. 2015, 49(20):11993-2004.
7. Pärnänen KMM, Narciso-da-Rocha C, Kneis D, Berendonk TU, Cacace D, Do TT, Elpers C, Fatta-Kassinos D, Henriques I, Jaeger T, Karkman A, Martinez JL, Michael SG, Michael-Kordatou I, O'Sullivan K, Rodriguez-Mozaz S, Schwartz T, Sheng H, Sørum H, Stedtfeld RD, Tiedje JM, Varela Della Giustina S, Walsh F, Vaz-Moreira I, Virta M, Manaia CM. Antibiotic resistance in European wastewater treatment plants mirrors the pattern of clinical antibiotic resistance prevalence. Sci. Adv., 2019; 5 : eaau9124
8. Adelowo OO, Caucci S, Banjo OA, Nnanna OC, Awotipe EO, Peters FB, Fagade OE, Berendonk TU. Extended Spectrum Beta-Lactamase (ESBL)-producing bacteria isolated from hospital wastewaters, rivers and aquaculture sources in Nigeria. Environ Sci Pollut Res Int. 2018; 25(3):2744-2755.
9. Nnadozie CF, Odume ON. Freshwater environments as reservoirs of antibiotic resistant bacteria and their role in the dissemination of antibiotic resistance genes. Environ Pollut, 2019, 254(Pt B):113067.
10. Charani E, Smith I, Skodvin B, Perozziello A, Lucet J-C, Lescure F-X, et al. (2019) Investigating the cultural and contextual determinants of antimicrobial stewardship programmes across low-, middle- and high-income countries—A qualitative study. PLoS ONE 14(1): e0209847. doi:10.1371/journal.pone.0209847
11. Larsson DGJ, Flach CF. Antibiotic resistance in the environment. Nat Rev Microbiol. 2022 May;20(5):257-269. doi: 10.1038/s41579-021-00649-x.
12. Kraemer SA, Ramachandran A, Perron GG. Antibiotic Pollution in the Environment: From Microbial Ecology to Public Policy. Microorganisms. 2019 Jun 22;7(6):180. doi: 10.3390/microorganisms7060180.
13. Laxminarayan R, Duse A, Wattal C, Zaidi AKM, Wertheim HFL, Sumpradit N, et al. Antibiotic resistance—the need for global solutions. Lancet Infect Dis. 2013;3099(13):1057–1098.
14. Jelic A., Rodriguez-Mozaz S., Barceló D., Gutierrez O. Impact of in-sewer transformation on pharmaceuticals in a pressurized sewer under anaerobic conditions. Water Res., 68 (2015), pp. 98-108, 10.1016/j.watres.2014.09.033.
15. Auguet O., Pijuan M., Borrego C.M., Rodriguez-Mozaz S., Triadó-Margarit X., Varela Della Giustina S., Gutierrez O.. Sewers as potential reservoirs of antibiotic resistance. Science of The Total Environment, 605–606, (2017), 1047-1054, doi:10.1016/j.scitotenv.2017.06.153.
16. Yang, P., Chen, Y., Jiang, S. et al. Association between antibiotic consumption and the rate of carbapenem-resistant Gram-negative bacteria from China based on 153 tertiary hospitals data in 2014. Antimicrob Resist Infect Control 7, 137 (2018). doi:10.1186/s13756-018-0430-1
17. Bartley PS, Domitrovic TN, Moretto VT, Santos CS, Ponce-Terashima R, Reis MG, Barbosa LM, Blanton RE, Bonomo RA, Perez F. Antibiotic Resistance in Enterobacteriaceae from Surface Waters in Urban Brazil Highlights the Risks of Poor Sanitation. Am J Trop Med Hyg. 2019 Jun;100(6):1369-1377. doi: 10.4269/ajtmh.18-0726.
18. Jennifer Moussa, Edmond Abboud, Sima Tokajian, The dissemination of antimicrobial resistance determinants in surface water sources in Lebanon, FEMS Microbiology Ecology, Volume 97, Issue 9, September 2021, fiab113, doi:10.1093/femsec/fiab113
19. Guyomard-Rabenirina S, Dartron C, Falord M, Sadikalay S, Ducat C, Richard V, et al. (2017) Resistance to antimicrobial drugs in different surface waters and wastewaters of Guadeloupe. PLoS ONE 12(3): e0173155. doi: 10.1371/journal.pone.0173155
20. Vingino, A.; Roberts, M.C.; Wainstein, M.; West, J.; Norman, S.A.; Lambourn, D.; Lahti, J.; Ruiz, R.; D'Angeli, M.; Weissman, S.J.; Rabinowitz, P. Surveil-

lance for Antibiotic-Resistant E. coli in the Salish Sea Ecosystem. Antibiotics 2021, 10, 1201. doi:10.3390/antibiotics10101201

21. Bollache L, Bardet E, Depret G, Motreuil S, Neuwirth C, Moreau J, Hartmann A. Dissemination of CTX-M-Producing Escherichia coli in Freshwater Fishes From a French Watershed (Burgundy). Front Microbiol. 2019 Jan 8;9:3239. doi: 10.3389/fmicb.2018.03239.
22. Furlan JPR, Savazzi EA, Stehling EG. Widespread high-risk clones of multidrug-resistant extended-spectrum β-lactamase-producing Escherichia coli B2-ST131 and F-ST648 in public aquatic environments. Int J Antimicrob Agents. 2020 Jul;56(1):106040. doi: 10.1016/j.ijantimicag.2020.106040. Epub 2020 May 29.
23. Aminov RI. Horizontal gene exchange in environmental microbiota. Front Microbiol. 2011 Jul 26;2:158. doi: 10.3389/fmicb.2011.00158
24. Sultan I, Rahman S, Jan AT, Siddiqui MT, Mondal AH, Haq QMR. Antibiotics, Resistome and Resistance Mechanisms: A Bacterial Perspective. Front Microbiol. 2018 Sep 21;9:2066. doi: 10.3389/fmicb.2018.02066.
25. Kimihiro Abe, Nobuhiko Nomura, Satoru Suzuki, Biofilms: hot spots of horizontal gene transfer (HGT) in aquatic environments, with a focus on a new HGT mechanism, FEMS Microbiology Ecology, Volume 96, Issue 5, May 2020, fiaa031, doi:10.1093/femsec/fiaa
26. Balcázar JL, Subirats J and Borrego CM (2015) The role of biofilms as environmental reservoirs of antibiotic resistance. Front. Microbiol. 6:1216. doi: 10.3389/fmicb.2015.01216
27. Binsker U, KäsbohrerA, Hammerl JA, Global colistin use: a review of the emergence of resistant Enterobacterales and the impact on their genetic basis, FEMS Microbiology Reviews, 2022, 46:1, fuab049, doi:10.1093/femsre/fuab049
28. Chen J, Quiles-Puchalt N, Chiang YN, Bacigalupe R, Fillol-Salom A, Chee MSJ, Fitzgerald JR, Penadés JR. Genome hypermobility by lateral transduction. Science, 2018, 362(6411):207-212.
29. Pokharel, S., Shrestha, P. & Adhikari, B. Antimicrobial use in food animals and human health: time to implement 'One Health' approach. Antimicrob Resist Infect Control 9, 181 (2020). doi:10.1186/s13756-020-00847-x
30. Gaze WH, Depledge M. Antimicrobial resistance: investigating the environmental dimension. Frontiers 2017: Emerging Issues of Environmental Concern. 2017: p. 12–22.
31. Olesen SW, Barnett ML, MacFadden DR, Brownstein JS, Hernández-Díaz S, Lipsitch M, Grad YH. The distribution of antibiotic use and its association with antibiotic resistance. Elife. 2018 Dec 18;7:e39435. doi: 10.7554/eLife.39435.
32. Ashton D, Hilton M, Thomas KV. Investigating the environmental transport of human pharmaceuticals to streams in the United Kingdom. Sci Total Environ. 2004 Oct 15;333(1-3):167-84. doi: 10.1016/j.scitotenv.
33. Xu W, Zhang G, Li X, Zou S, Li P, Hu Z, Li J. Occurrence and elimination of antibiotics at four sewage treatment plants in the Pearl River Delta (PRD), South China. Water Res. 2007 Nov;41(19):4526-34. doi: 10.1016/j.watres.2007.06.023.
34. Chen K, Zhou JL. Occurrence and behavior of antibiotics in water and sediments from the Huangpu River, Shanghai, China. Chemosphere. 2014 Jan;95:604-12. doi: 10.1016/j.chemosphere.2013.09.119.
35. Zuccato E, Castiglioni S, Bagnati R, Chiabrando C, Grassi P, Fanelli R. Illicit drugs, a novel group of environmental contaminants. Water Res. 2008;42:961–968. doi: 10.1016/j.watres.2007.09.010.
36. Campagnolo, E.R, Johnson, K.R, Karpati, A, Rubin, C.S, Kolpin, D.W, Meyer, M.T, Esteban, J.E, Currier, R.W, Smith, K, Thu, K.M, and McGeehin, M. Antimicrobial residues in animal waste and water resources proximal to large-scale swine and poultry feeding operations. The Science of the Total Environment, 299, 89-95, 2002.
37. Xu, J.; Zhang, Y.; Zhou, C.; Guo, C.; Wang, D.; Du, P.; Luo, Y.; Wan, J.; Meng, W. Distribution, sources and composition of antibiotics in sediment, overlying water and pore water from Taihu Lake, China. Sci. Total Environ. 2014, 497–498, 267–273.
38. Zhang R, Zhang G, Zheng Q, Tang J, Chen Y, Xu W, Zou Y, Chen X. Occurrence and risks of antibiotics in the Laizhou Bay, China: Impacts of river discharge, Ecotoxicology and Environmental Safety, 2012: 80: 208-215, doi:10.1016/j.ecoenv.2012.03.002.
39. Moreno-González R., Rodriguez-Mozaz S., Gros M., Barceló D., and Leon V.M. 2015. Seasonal distribution of pharmaceuticals in marine water and sediment from a mediterranean coastal lagoon (SE Spain). Environ. Res. 138: 326–344.
40. Dinh, Q.T.; Moreau-Guigon, E.; Labadie, P.; Alliot, F.; Teil, M.J.; Blanchard, M.; Chevreuil, M. Occurrence of antibiotics in rural catchments. Chemosphere 2017, 168, 483–490.
41. Li W, Shi Y, Gao L, Liu J, Cai Y. Occurrence of antibiotics in water, sediments, aquatic plants, and animals from Baiyangdian Lake in North China. Chemosphere. 2012 Nov;89(11):1307-15. doi: 10.1016/j.chemosphere.2012.05.079. Epub 2012 Jun 12. PMID: 22698376.

42. Chen M, Lu G, Wu J et al (2018) Migration and fate of metallic elements in a waste mud impoundment and affected river downstream: a case study in Dabaoshan Mine, South China. Ecotoxicol Environ Saf 164:474–483.
43. Chen, Y.; Chen, H.; Zhang, L.; Jiang, Y.; Gin, K.Y.-H.; He, Y. Occurrence, Distribution, and Risk Assessment of Antibiotics in a Subtropical River-Reservoir System. *Water* 2018, *10*, 104. doi:10.3390/w10020104
44. Blaak, H. et al. RIVM report 703719071/2011. Prevalence of antibiotic resistant bacteria in the rivers Meuse, Rhine, and New Meuse. (2011).
45. Harmon, D.E., Miranda, O.A., McCarley, A., et al., 2019. Prevalence and characterization of carbapenem-resistant bacteria in water bodies in the Los Angeles-Southern California area. Microbiologyopen 8, e00692. doi:10.1002/mbo3.692.
46. Aubron, C., Poirel, L., Ash, R. J., & Nordmann, P. (2005). Carbapenemase-producing Enterobacteriaceae, U.S. rivers. Emerging Infectious Diseases, 11(2), 260–264. doi:10.3201/eid1102.030684.
47. Tacão, M.; Correia, A.; Henriques, I.S. Low prevalence of carbapenem-resistant bacteria in river water: Resistance is mostly related to intrinsic mechanisms. Microb. Drug Resist. 2015, 21, 497–506.
48. Poirel, L., Barbosa-Vasconcelos, A., Simões, R.R., Da Costa, P.M., Liu, W., Nordmann, P., 2012. Environmental KPC-producing Escherichia coli isolates in Portugal. Antimicrob Agents Chemother. 56, 1662–1663. https://doi.org/10.1128/718 AAC.05850-11
49. Kieffer, N., Poirel, L., Bessa, L.J., Barbosa-vasconcelos, A., 2016. VIM-1, VIM-34, and IMP-8 carbapenemase-producing Escherichia coli strains recovered from a Portuguese river. Antimicrob. Agents Chemother. 60, 2585–2586. doi:10.1128/AAC.02632-15.Address
50. Teixeira, P., Tacão, M., Pureza, L., Gonçalves, J., Silva, A., Cruz-Schneider, M. P., & Henriques, I. (2020). Occurrence of carbapenemase-producing Enterobacteriaceae in a Portuguese river: blaNDM, blaKPC and blaGES among the detected genes. Environmental Pollution, 113913. doi:10.1016/j.envpol.2020.113913.
51. Zurfluh K, Hächler H, Nüesch-Inderbinen M, Stephan R. Characteristics of extended-spectrum β-lactamase- and carbapenemase-producing Enterobacteriaceae Isolates from rivers and lakes in Switzerland. Appl Environ Microbiol. 2013 May;79(9):3021-6. doi: 10.1128/AEM.00054-13.
52. Zarfel G , Lipp M, Gurtl Eet al. Troubled water under the bridge: screening of River Mur water reveals dominance of CTX-M harboring Escherichia coli and for the first time an environmental VIM-1 producer in Austria. Sci Total Environ. 2017;593–594:399–405.
53. Kittinger C , Lipp M, Baumert Ret al. Antibiotic resistance patterns of Pseudomonas spp. isolated from the river Danube. Front Microbiol. 2016;7:586.
54. Ye, Q., Wu, Q., Zhang, S., et al., 2017. Antibiotic-resistant extended spectrum ß-lactamase- and plasmid-mediated AmpC-producing enterobacteriaceae isolated from retail food products and the pearl River in Guangzhou, China. Front. Microbiol. 8, 96. doi:10.3389/fmicb.2017.00096.
55. Lepuschitz S, Schill S, Stoeger A, Pekard-Amenitsch S, Huhulescu S, Inreiter N, Hartl R, Kerschner H, Sorschag S, Springer B, Brisse S, Allerberger F, Mach RL, Ruppitsch W. Whole genome sequencing reveals resemblance between ESBL-producing and carbapenem resistant Klebsiella pneumoniae isolates from Austrian rivers and clinical isolates from hospitals. Sci Total Environ., 2019, 662:227-235.
56. Zurfluh K, Bagutti C, Brodmann P, Alt M, Schulze J, Fanning S, et al. Wastewater is a reservoir for clinically relevant carbapenemase- and 16s rRNA methylase-producing Enterobacteriaceae. Int. J. Antimicrob. Agents, 2017, 50, 3, 436-440.
57. Adegoke AA, Madu CE, Aiyegoro OA et al. Antibiogram and beta-lactamase genes among cefotaxime resistant E. coli from wastewater treatment plant. Antimicrob Resist Infect Cont 2020;9:46
58. Piedra-Carrasco N, Fàbrega A, Calero-Cáceres W, Cornejo-Sánchez T, Brown-Jaque M, Mir-Cros A, Muniesa M, González-López JJ. Carbapenemase-producing enterobacteriaceae recovered from a Spanish river ecosystem. PLoS One. 2017 Apr 5;12(4):e0175246. doi: 10.1371/journal.pone.0175246
59. Bardhan T, Chakraborty M, Bhattacharjee B. Prevalence of Colistin-Resistant, Carbapenem-Hydrolyzing Proteobacteria in Hospital Water Bodies and Out-Falls of West Bengal, India. Int J Environ Res Public Health. 2020 Feb 5;17(3):1007. doi: 10.3390/ijerph17031007.
60. Yang K, Pagaling E, Yan T. Estimating the prevalence of potential enteropathogenic Escherichia coli and intimin gene diversity in a human community by monitoring sanitary sewage. Appl Environ Microbiol. 2014 Jan;80(1):119-27. doi: 10.1128/AEM.02747-13.
61. Proia L, Von Schiller D, Sànchez-Melsió et al. Occurrence and persistence of antibiotic resistance genes in river biofilms after wastewater inputs in small rivers. Environmental Pollution, 2016, 210, 121–128.
62. Xiong W, Sun Y, Zhang T, Ding X, Li Y, Wang M, Zeng Z. Antibiotics, Antibiotic Resistance Genes, and Bacterial Community Composition in Fresh Water Aquaculture Environment in China. Microb Ecol. 2015 Aug;70(2):425-32. doi: 10.1007/s00248-015-0583-x.

ISSN print: 1224-5984
ISSN online: 2248-3942

Rom Biotechnol Lett. 2022; 27(5): 3730-3745
doi: 10.25083/rbl/27.5/3730.3745

Received for publication, March, 07, 2022
Accepted, March, 08, 2023

Review

SARS CoV-2 virus and the COVID-19 pandemic worldwide and in Romania. An updated data review

MARIAN CONSTANTIN[1,2]

[1]Institute of Biology Bucharest of Romanian Academy, 296 Splaiul Independenţei, 060031 Bucharest, Romania

[2]Fellow of the Research Institute of the University of Bucharest, ICUB, Bucharest, Romania

Abstract

SARS CoV-2 is a coronavirus first identified in November-December 2019 in Wuhan, China that causes respiratory infections of varying severity. Spreading rapidly in human populations, SARS CoV-2 has caused concern worldwide, and on 11 March 2020 the World Health Organization declared a pandemic with the virus for two months, with most countries entering a lockdown period between March and May 2020 in the hope of stopping the spread of the virus. The main symptoms of SARS CoV-2 infection include fever, cough, shortness of breath and fatigue, but less common symptoms such as loss of smell and taste and gastrointestinal disturbances including vomiting, lack of appetite, diarrhoea, etc. are also reported. From March 2020 to March 2023, there were eight waves of increasing numbers of infections, the largest being the sixth wave between January and April 2022. The total number of deaths also followed roughly the same trends with the increase in newly confirmed cases. As an RNA virus with RNA-dependent RNA polymerase, SARS CoV-2 mutates frequently, leading to the stabilisation of several variants: B.1.1.7 (Alpha), B.1.351 (Beta), P.1 (Gamma), B.1.614.2 (Delta), B.1.427 and B.1.429 (Epsilon), P.2 (Zeta), B1.525 (Eta), P.3 (Theta), B.1.617.1 (Kappa) and C.37 (Lambda). The severity of some cases and the intense spread in human populations around the world has led the scientific community to focus its efforts on developing effective vaccines against SARS CoV-2, with nine approved vaccines being developed, BNT162b/2, mRNA-1273, AZD1222 Covishield, Sputnik V rAd26 rAd5, Ad26. CoV.S JNJ-78436735, COVAXIN BBVI52, Corona Vac, NVX-CoV2373 Covavax and BBIBP-CoV vaccines, with which a large part of the global population has been immunised.

Keywords SARS CoV-2, pandemics, COVID-19, virus, viral infection

To cite this article: MARIAN CONSTANTIN. SARS CoV-2 virus and the COVID-19 pandemic worldwide and in Romania. An updated data review. *Rom Biotechnol Lett.* 2022; 27(5): 3730-3745 DOI: 10.25083/rbl/27.5/3730.3745

*Corresponding author: Marian Constantin, Institute of Biology Bucharest of Romanian Academy, 296 Splaiul Independenţei, 060031 Bucharest, Romania; Fellow of the Research Institute of the University of Bucharest, ICUB, Bucharest, Romania. E-mail: cvgmarian@gmail.com

Introduction

SARS CoV-2 viruses. SARS CoV-2 (*Severe Acute Respiratory Syndrome Coronavirus-2*) viruses are members of the family Coronaviridae, order Nidovirales, genus Coronavirus, with numerous members, which cause respiratory and gastrointestinal infections. Coronaviruses are enveloped viruses and infect a wide variety of wild and domestic animal hosts and humans [1] (*Fig. 1*). They are classified into four major genera, *Alphacoronavirus*, *Betacoronavirus*, *Gammacoronavirus*, and *Deltacoronavirus* [2, 3], have a pleiomorphic appearance, ranging in size from 80 to 160 nm [4].The name coronavirus comes from the protein projections on the surface of the virions, which are shaped like a brood and, under the electron microscope, give them the appearance of a crown (in Latin, corona means crown) [5].

Coronavirus genome

Coronaviruses have a large, unsegmented, positive-sense, single-stranded RNA genome ranging in size from 27 to 32 kb (kilobases) [4], capped at the 5' end, with a poly-A sequence at the 3' end and 6-11 open reading frames (ORFs). Thus, ORF 1 covers approximately 67% of the viral genome and comprises two overlapping coding regions encoding 16 non-structural proteins. The remaining 33% of the genome comprises the remaining ORFs, which encode structural proteins and accessory proteins [6].

SARS Cov-2 virus genome

The SARS CoV-2 genome (*Fig. 2*) is almost 30 kb long and encodes 29 proteins, four of which are structural and 25 putative non-structural and accessory proteins. The four structural proteins are used during virion assembly and enter into the composition of mature viral particles, the non-structural proteins have an enzymatic role and are involved in viral RNA replication and immune evasion, and the accessory proteins are involved in viral infectivity, virion survival and cell propagation. At the 5' end, the SARS CoV-2 genome includes the replicase gene, with two non-overlapping ORFs, ORF1a and ORF1b, covering about two-thirds of the genome, followed by several ORFs towards the 3' end, including spicular glycoprotein (S), membrane glycoprotein (M), envelope glycoprotein or hemagglutinin esterase (E) and nucleocapsid protein (N). Of these, the S, E

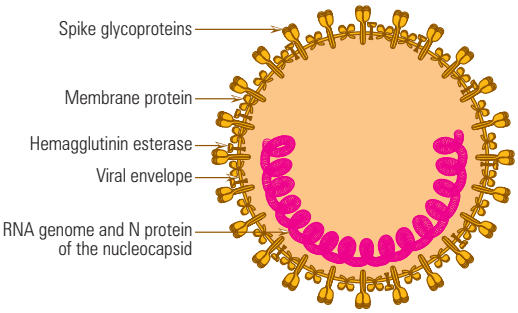

Fig. 1. The structure of the SARS CoV-2 virion

and M glycoproteins protrude into the virion membrane, the spicular glycoprotein forms those strands that give virions their crown-like appearance under the electron microscope, and the nucleocapsid protein is embedded in the envelope and packages the RNA genome. Other ORFs, 3a, 3b, 6, 7a, 7b, 9a, 9c, 10 and others up to 29 encode accessory and non-structural proteins [7]. Translation of ORF1 results in the replicase polyprotein 1a, pp1a, and the -1 shift of the ribosomal frame at the 3' end of ORF1a contributes to translation of ORF1b and synthesis of the replicase polyprotein pp1ab. Proteolytic cleavage of pp1a gives rise to 11 functional non-structural proteins, whereas pp1ab cleavage gives rise to 15 non-structural proteins. Thus, nonstructural protein 1 interacts with ribosomes in infected cells and inhibits the production of host proteins, nonstructural protein 2 can interfere with viral transcription and translation by interacting with ribosomes and replication-transcription complexes [8]. Non-structural protein 3 includes several domains, ubiquitin-like, nucleic acid-binding macrodomain (found only in SARS), transmembrane (with a role in the rearrangement of endoplasmic reticulum membranes, for the formation of the vesicle double membrane and for promoting viral replication), Y1-3 and a papain-like proteolytic sequence (PLpro) and, by cleavage into three sites, forms nonstructural proteins 1, 2 and 3, while nonstructural protein 5 or major protease (Mpro) and, by cleavage pp1a and pp1ab into 11 sites, gives rise to nonstructural proteins 4–16 [9, 10]. Nonstructural proteins 7 and 8 interact with nonstructural protein 12 and stimulate RNA polymerase activity. Non-structural proteins 7–16 contribute to SARS CoV-2 transcription and replication by forming the replication and transcription complex, nonstructural protein 9 inhibits the nucleotidyl-

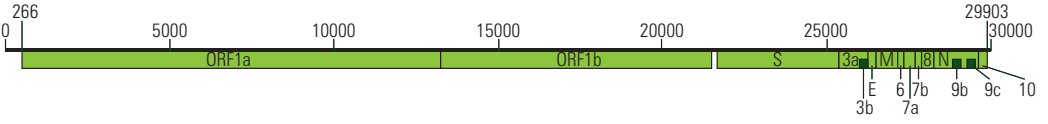

Fig. 2. The structure of the SARS CoV-2 genome

transferase activity of the nonstructural protein, nonstructural protein 10 is a cofactor for nonstructural proteins 14 and 16, non-structural protein 12 is RNA-dependent RNAse and nucleotidyltransferase, non-structural protein 13 is helicase, non-structural protein 14 is exoribonuclease and N7-guanine methyltransferase, non-structural protein 15 has uridine-specific endoribonuclease activity, and non-structural protein 16 is 2'-O-methyltransferase, which is involved in the mRNA cap process. Structural protein N serves to package the viral genome, and the structural proteins on the viral envelope have the following functions: protein S is involved in the binding of receptors such as the angiotensin-converting enzyme or angiotensin-converting enzyme II (ACE2) on host cells and in the fusion of the envelope to the cell membrane; proteins M and N promote viral assembly, and protein E forms an ion channel with a function in pathogenesis and viral assembly. The remaining ORFs have an accessory role. Thus, ORF3a forms a homodimer and forms an ion channel in the host cell membrane; ORF7a participates in the evasion of host immune effectors and is involved in inflammation; ORF7b promotes increased virulence of SARS-CoV-2; ORF8 interacts with HLA-A/CMH I molecules, degrading them; ORF9b is involved in suppressing the interferon response, and ORF3b, ORF6, ORF9c and ORF10 have unknown functions [11].

SARS CoV-2 multiplication cycle

The multiplication cycle of SARS CoV-2 (*Fig. 3*) begins with the triggering of mucopolysaccharidase activity of the viral spicules on the glycocalyx layer, which covers and protects the apical pole of the epithelial cells, exposing the cell receptors, to which it becomes bound. SARS CoV-2 spicular glycoprotein S has 71% amino acid sequence homology to SARS-CoV glycoprotein S and 97% homology to RaTG13 virus isolated from bats, explaining the cross-species spread of these viruses. After binding of the spicular protein S on the virion surface to cell receptors and fusion of the envelope to the cytoplasmic membrane, the viral nucleocapsid is endocytosed in the cytosol [1]. Under the action of proton pumps, the environment in the endocytosis vesicle (endosome) becomes acidic, favouring the cleavage of spikelets into S1/S2 and S20 sites by furin, present in the lungs, liver and small intestine, for which the virus shows tropism [12, 13].

The viral genome is associated with the replication and transcription complex and is transcribed into negative (antigenomic)mRNA in a set of seven subgenomic-length variants, each with the same 5′ leader sequence of 75-78 nucleotides derived from the 5′ end of the genomic RNA and the 3′ terminal sequence, with the 5′ leader sequence remaining

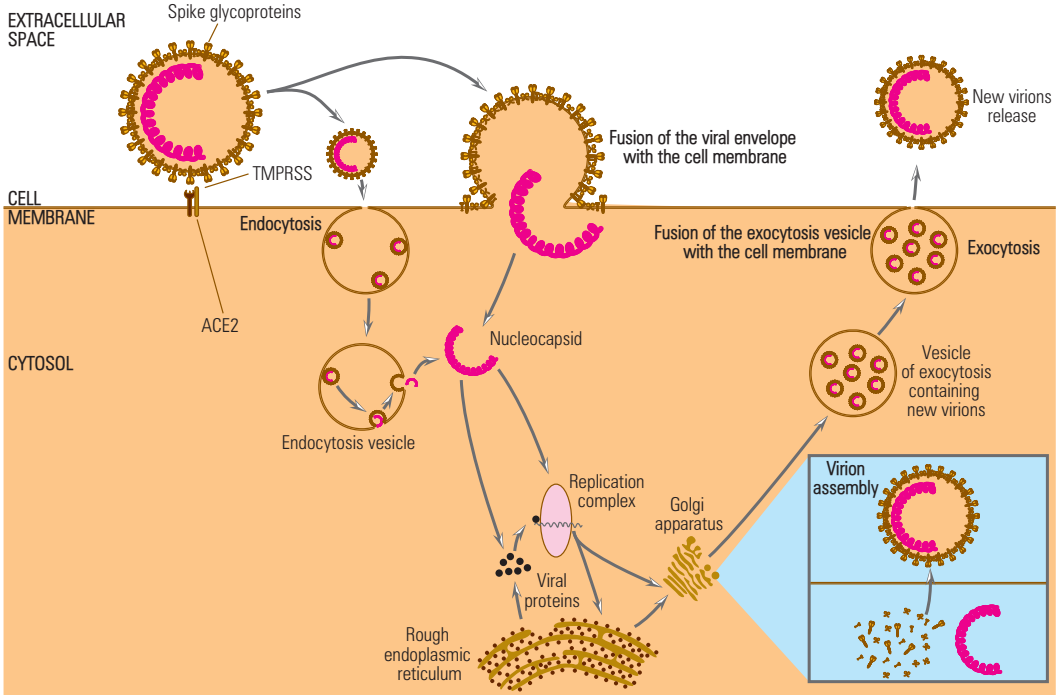

Fig. 3. Multiplication cycle of SARS CoV-2.

associated with RNA polymerase and being transcribed into all mRNA types. Structural proteins S, M and E are synthesized and inserted into endoplasmic reticulum membranes, passing to the Golgi complex, and protein N, synthesized by free polyribosomes, becomes associated with genomic RNA and forms the nucleocapsid [14].

By budding from the endoplasmic reticulum and cisternae of the Golgi apparatus, this assembly is covered with envelopes, becoming virions, in which form they are transported in exocytosis vesicles to the cell surface, where they are released [15].

SARS CoV-2 pandemic

Origin of SARS CoV-2

SARS CoV-2 is the ninth coronavirus to infect humans and the seventh identified in the last 20 years. Since all previous human coronaviruses are of zoonotic origin and the penetration of SARS CoV-2 into the human population does not appear to differ from their penetration (SARS-CoV spread in November 2002 in Foshan, Guangdong Province, China, and in 2003 in Guangzhou, Guangdong Province, China), the transmission of SARS CoV-2 to humans is regarded as a natural interspecific transmission event. The source of SARS CoV has been identified as the cages and raccoon dogs sold in live animal markets in these cities, whereas the source of SARS CoV-2 appears to be bats (based on the 97% homology of SARS CoV-2 spicular proteins with those of bat RaTG13) sold in the Wuhan market. The hypothesis of zoonotic transmission is also supported by similarities between SARS CoV-2 and four endemic human coronaviruses, human coronavirus-OC43 (HCoV-OC43), human coronavirus-HKU1 (HCoV-HKU1), human coronavirus-229E (HCoV-229E), and human coronavirus NL63 (HCoV-NL63), transmitted from animals but with no known circumstances of transmission. The hypothesis of SARS CoV-2 escape from the laboratory has been considered, but its low pathogenicity in commonly used laboratory animals and the absence of genomic markers associated with virus adaptation to them indicate that this event is unlikely [16].

SARS CoV-2 pandemic in the world

On 17 November 2019, China reported the first confirmed case of infection from an unknown virus [17, 18], with a 95% confidence interval, dropping to no earlier than 4 October [18]. Initially, this was named 2019-nCoV, and later SARS CoV-2 (Severe Acute Respiratory Syndrome Coronavirus-2). The first confirmed case was a woman who, according to the epidemiological pathway, contracted it in a market in Wuhan city (Hubei province) where live animals were sold. On the other hand, a retrospective study reports the onset of the first known case of 2019-nCoV infection on 8 December 2019 [7], with the first cases positioned in the second part of November 2019 and the first part of December 2019. By the end of 2019, the virus had already spread to some extent in the human population, and in December 2019, several health facilities in Wuhan reported the diagnosis of pneumonia of unknown etiology in several people, but which, similar to patients with SARS-CoV (*Severe Acute Respiratory Syndrome Coronavirus*) and MERS-CoV (*Middle East Respiratory Syndrome Coronavirus*), the coronaviruses that had produced small-scale outbreaks in 2002–2003 and 2012, had symptoms of viral pneumonia, including fever, coughing and chest discomfort [19], and severe cases, dyspnea and bilateral pulmonary infiltration. Although unconfirmed, 2019-nCoV has been predicted to represent the causative agent of this pneumonia [20]. Genome sequencing of the novel viral agent was performed soon after its identification, and the first sequence was published a day after confirmation, on 10 January, by Yong-Zhen Zhang [21–23] and researchers at Fudan University in Shanghai, with five more sequences published on 11 January. The publication of the sequences has enabled the beginning of the search and identification of the SARS CoV-2 genome worldwide. The first hospitalized cases of 2019-nCoV infection in China were identified in people frequenting the Huanan Seafood Wholesale Market in downtown Wuhan, where seafood, poultry and several wildlife species were sold. As of 17 January 2020, 62 cases had been confirmed in China, two cases in Thailand and one in Japan, but in reality the number of existing cases may have been higher, a situation proven by the identification on 19 January of a batch of 136 cases in Wuhan, 126 with mild symptoms, 35 in serious condition and 9 in critical condition, bringing the total number of cases in China to 198 [24], following the development of diagnostic tests for infection with the new coronavirus. Symptomatology was complemented by fever, dry cough, shortness of breath and leukopenia, and severe cases required extracorporeal membrane oxygenation. At that time, 26 deaths had been recorded, many with comorbidities and aged over 50 years. Compared to SARS-CoV, in which mortality had been 10%, and MERS-CoV, in which mortality had been 35%, 2019-nCoV appeared, at the start of the pandemic, to be less virulent, affecting mainly older people and those with pre-existing conditions [20]. Soon, several cases unrelated to Huanan Seafood Wholesale Market were identified, with some contracting the infection in health care facilities, proving human-to-human transmission [7, 23], especially favored by New Year's travel, contributing to the spread of the infection to other areas in China [23]. As new cases were continuously identified, on 30 Janu-

ary, the World Health Organization declared a global public health emergency and the new virus was recognized as having epidemic potential [25, 26], on 11 February 2020, the name of the virus was changed to SARS CoV-2, and the disease caused by it was named COVID-19 [27].

The spread of SARS CoV-2 infection has continued apace, and in mid-February it reached pandemic levels in China, with more than 3,000 cases a day, after the city of Wuhan was shut down on 23 January. In the following weeks, outdoor activities, gatherings and travel were restricted, in many localities in China, leading to a reduction in the number of cases in the country [28, 29]. However, the frequency of international travel has allowed the spread and spread of SARS CoV-2 infection to many countries around the world, prompting the World Health Organization to declare a COVID-19 pandemic. The next outbreaks where the rapid expansion of the virus occurred were in Europe, particularly Italy (as of 11 March 2020, there were 10 149 confirmed cases and 631 deaths in infected persons), Iran (as of 11 March 2020, there were 8 042 confirmed cases and 291 deaths in infected persons) and South Korea (as of 11 March 2020, there were 7 755 confirmed cases and 60 deaths in infected persons), with 696 cases of infection and 7 deaths confirmed on the International conveyance (Diamond Princess). Globally, 37 364 confirmed cases of infection and 1 130 deaths were reported, of which 4589 cases of infection and 258 deaths were reported on 11 March 2020 alone [25].

As of the second half of February 2020, the measures taken in China have been successful, with the country managing the SARS CoV-2 infection well, and in the following months, other countries have followed suit and closed down, limiting contact between residents to a minimum. Although in February-March 2020, Europe was the leader in terms of the number of confirmed cases of SARS CoV-2 infection, since April 2020, it has been overtaken by North America, with the United States of America as the main exponent, where the number of SARS CoV-2 cases has exploded, and since June 2020, also by Asia. Thus, at the end of June 2020, globally, there were a total of 10 112 754 confirmed cases of coronavirus infection (with 159 964 new cases), of which 501 562 deaths (3 043 deaths were new). Five months later, on 11 August 2020, a total of 20 274 865 COVID-19 cases and 807 530 deaths were reported globally, with 222 318 cases and 5701 new deaths recorded on 11 August 2020. The end of 2020 found humanity in the midst of the SARS CoV-2 pandemic, which had already seen three waves of increasing numbers of cases of infection in February–March, June–August and October 2020–January 2021. As of 31 December, a total of 82,626,055 cases of COVID-19 (including 681 694 new cases) and 1 804 223 deaths (including 15 283 new deaths) were reported worldwide.

The first six months of 2021 were marked by the end of the third pandemic wave, towards the end of February, which mainly affected Europe and the Americas, and the transition to the fourth wave, between April and May, with a peak of 997 105 cases on 24 April, which mainly affected Asia. In the second half of 2021, the evolution of the SARS CoV-2 pandemic crossed the fifth pandemic wave, between July and October, predominantly affecting Europe and the Americas, with a new phase of increase in the number of new confirmed cases in November. On 31 December 2021, the total number of confirmed SARS CoV-2 cases was 286 826 415, of which 1 889 175 on 31 December alone, and the number of deaths was 5 445 957, with 7 058 deaths on 31 December.

The year 2022 began with a sharp increase in the number of SARS CoV-2 infections in what was to become the sixth pandemic wave and the one with the most cases. Between January and April 2022, more than one million new confirmed cases were reported almost daily worldwide, with up to 3 652 595 new cases, including 9 063 deaths on 22 January. This surge led to an increase in statistics and by the end of June 2022, globally, a total of 551 746 601 cases were reported (865 480 cases on 30 June alone), of which 6 356 176 deaths, with 1 608 reported on 30 June, and after a reduction in the number of reported cases in May and June, from July onwards, a new small pandemic surge was recorded. Thus, the sixth pandemic wave almost doubled the number of confirmed cases of SARS CoV-2 infection worldwide, with the European population predominantly affected, followed by the Asian population and the Americas. In July and August, the number of SARS Cov-2 infections worldwide increased again, but much less than in wave 6 and compared to wave 4 from April to May 2021. This seventh wave mainly affected Asia and, less so, the Americas and Europe, and was followed by a small increase in the number of cases in October 2022 in Europe. After China dropped the zero COVID policy towards the end of 2022, a new pandemic wave affected mainly East Asia and was extended until mid-January 2023. According to the World Health Organization, the eighth wave is the most active, with more than 6 000 000 daily cases from 21–25 December globally and peaking at 7 946 896 cases on 23 December 2022 (Fig. 4–5). On the other hand, the www.worldometers.info website and Johns Hopkins University of Medicine describe it as modest, with magnitude at most at the level of the fifth pandemic wave. According to the latter, cited by the Romanian Ministry of Health, at the end of 2022, there were 664 480 798 confirmed cases of SARS CoV-2 infection worldwide (with 443 500 new cases as of

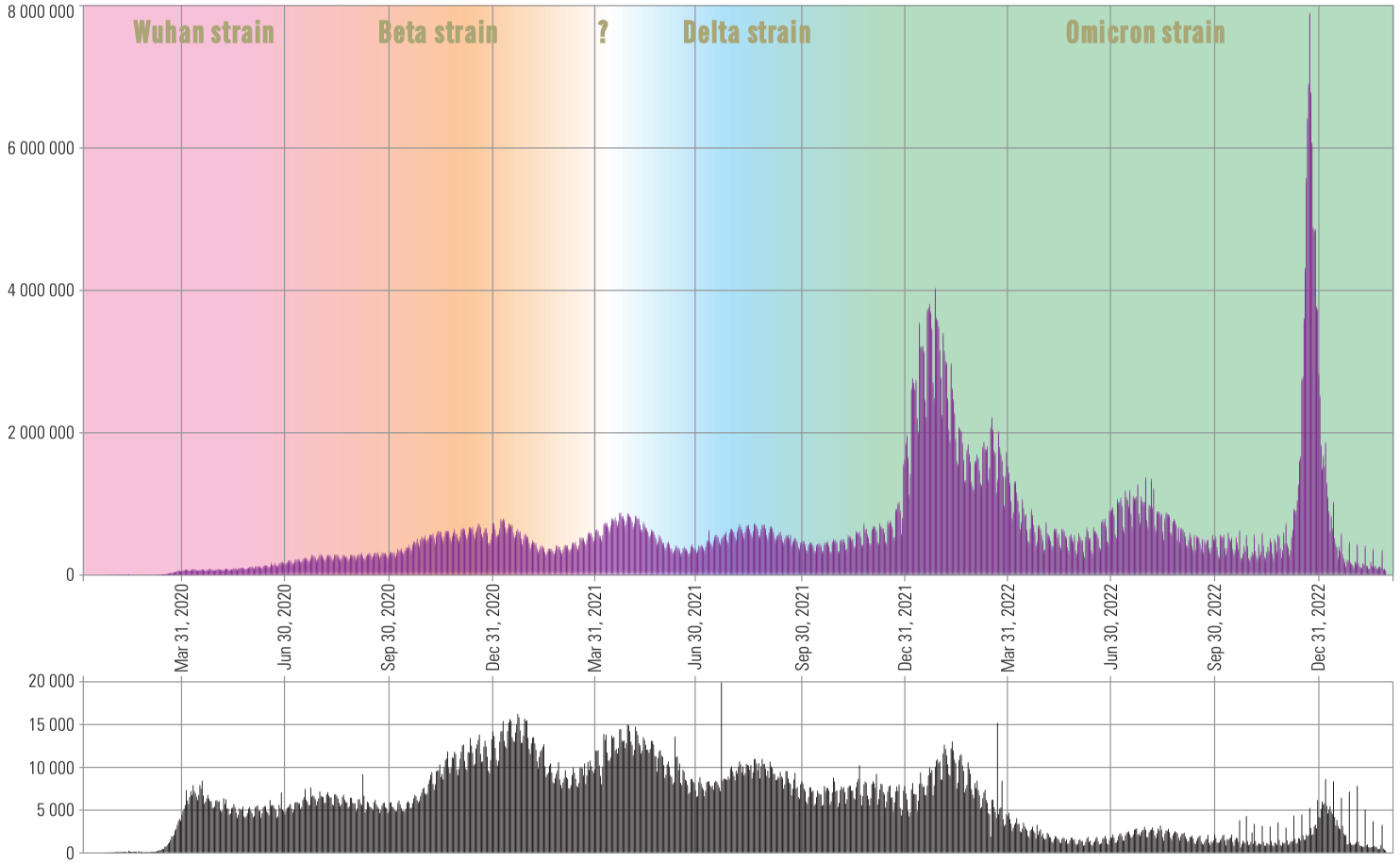

Fig. 4. SARS CoV-2 infection (puple bars, top) and the number of deaths (black bars, bottom) in people infected with SARS CoV-2, worldwide, between December, 31,2019–February, 28,2023. Source: WHO COVID-19 Dashboard. Geneva: World Health Organization, 2020. Available online: https://covid19.who.int/ (last cited: [07.03.2023]).

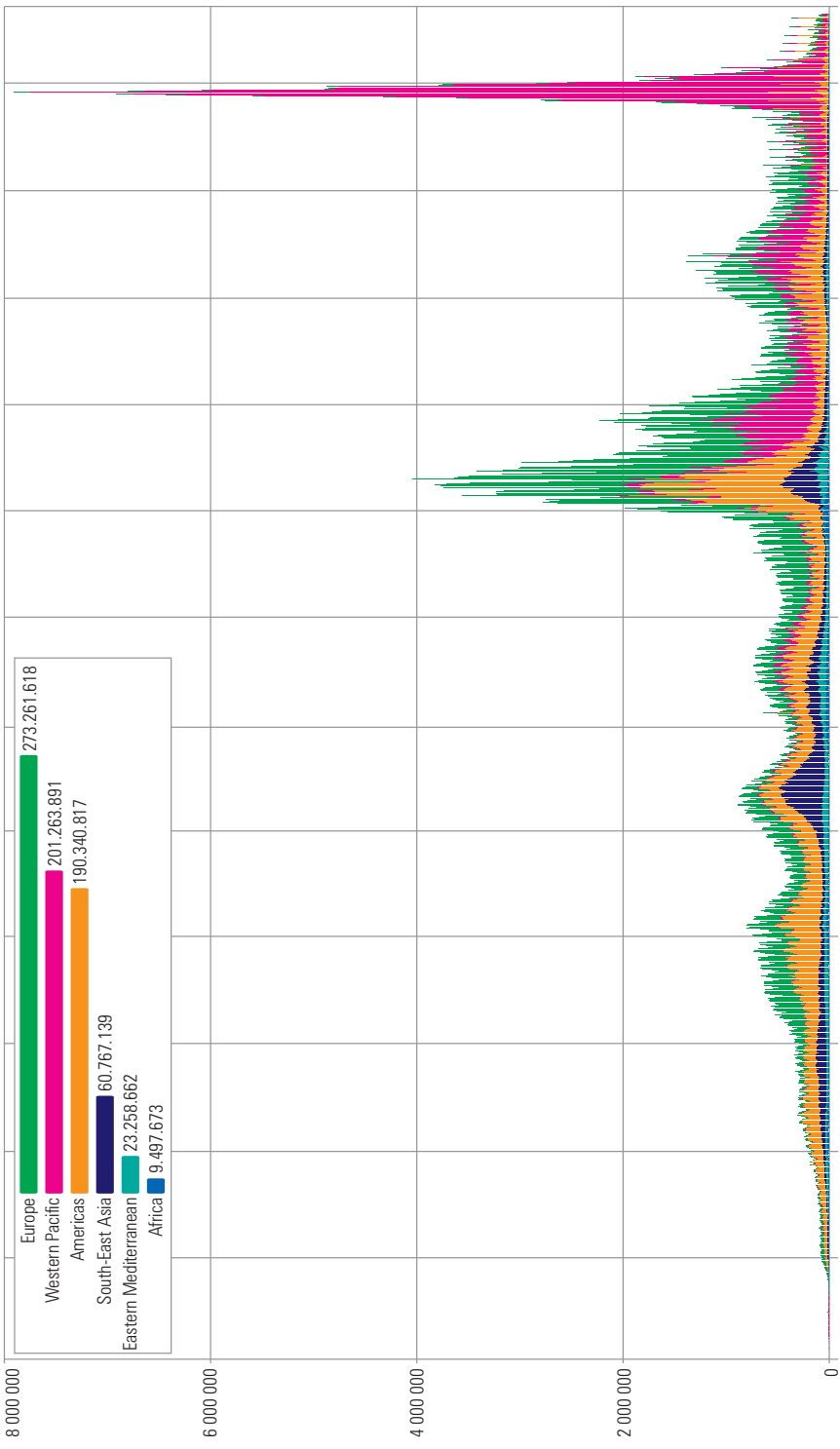

Fig. 5. Share of each WHO region in the total number of SARS CoV-2 confirmed cases, worldwide, between December, 31,2019–February, 28,2023. Source: WHO COVID-19 Dashboard. Geneva: World Health Organization, 2020. Available online: https://covid19.who.int/ (last cited: [07.03.2023]).

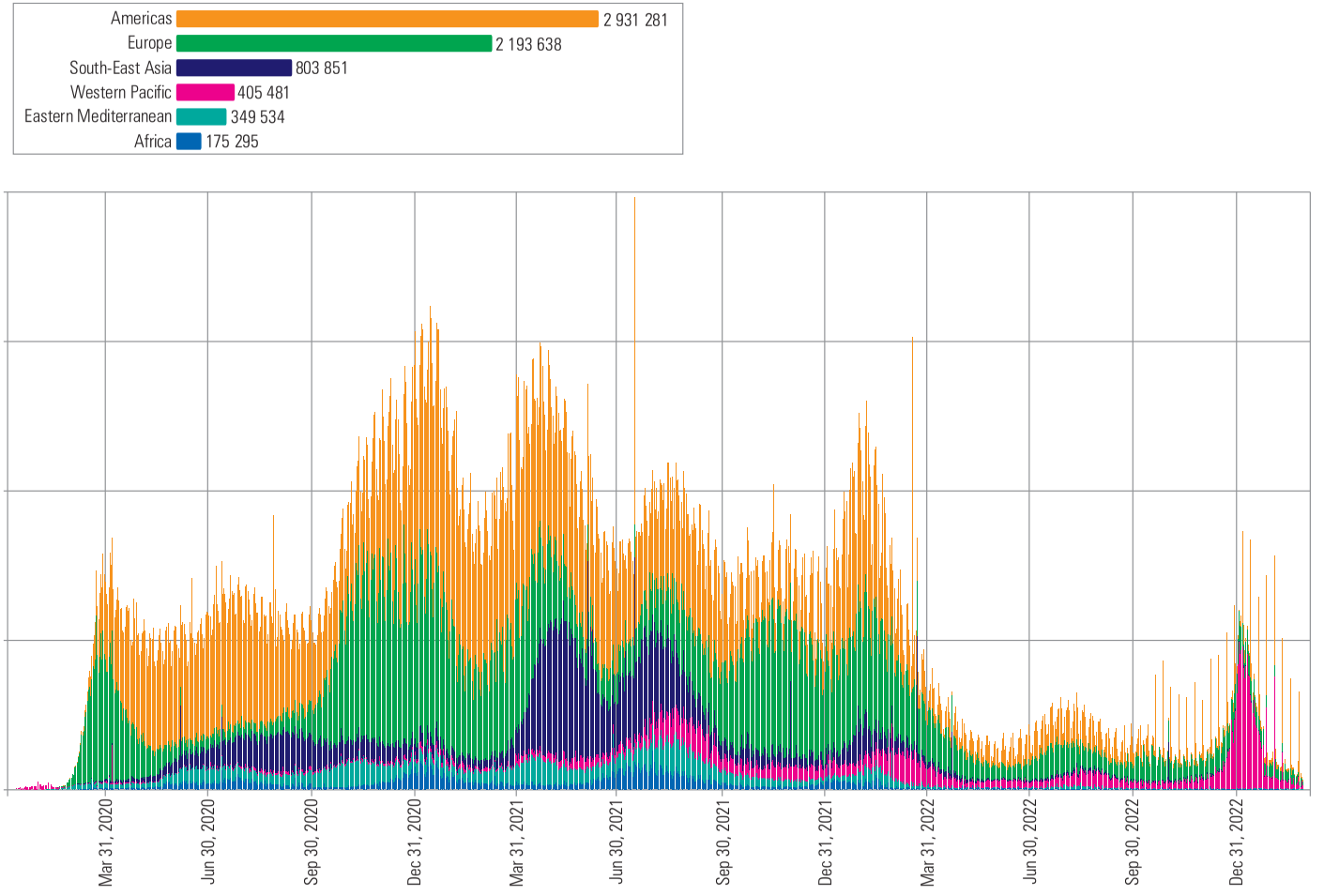

Fig. 6. Share of each WHO region in the total number of SARS CoV-2 deaths, worldwide, between December, 31,2019–February, 28,2023. Source: WHO COVID-19 Dashboard. Geneva: World Health Organization, 2020. Available online: https://covid19.who.int/ (last cited: [07.03.2023]).

31 December), including 6 696 132 deaths (with 1 399 new deaths as of 31 December).

The year 2023 marks a reduction in the number of SARS CoV-2 cases to less than 200 000 new confirmed cases every day, with the majority of cases reported in Asia. The most recent World Health Organization report on 28 February indicates 758 390 564 confirmed cases of SARS CoV-2 infection and 6 859 093 deaths, and the most recent report from Johns Hopkins University of Medicine indicates, as of 7 March 2023, a total of 676 125 671 confirmed cases worldwide, including 638 000 cases in the period 26 February to 5 March, and 6 877 999 deaths, with 4,750 deaths recorded in the period 26 February to 5 March [30–35] (Fig. 4–6).

SARS CoV-2 pandemic in Romania

In Romania, the first SARS CoV-2 infection was reported in a 25-year-old man from Gorj county on 26 February 2020, after testing all persons with whom a 71-year-old Italian man had come into contact in Romania and who had been confirmed on 25 February 2020. He had recently arrived from Italy, travelling in a coach, and had come into contact with the 25-year-old man on 19 February. The second case was that of a 38-year-old woman from Timişoara who had travelled by plane from Italy and infected a 47-year-old man from Timişoara en route. The fourth case involved a man from Maramureş. The fifth case was that of a man from Timiş, a direct contact of the 47-year-old man. The sixth confirmed case was a 16-year-old boy from Timişoara, who infected a classmate and was registered as the seventh case. Travelling in a coach with the 71-year-old Italian man, a 51-year-old man was infected by him and is the eighth case. A 49-year-old man arriving from Italy is the ninth case. He has infected a 42-year-old woman and others, both of whom have been confirmed in Bucharest and indicate the start of intra-Community transmission of SARS CoV-2 infection. On 26 February, a 60-year-old former MAI officer arrived from Israel and, on 2 March, handed out marzipan at the ADP headquarters in Bucharest's 4th sector, in a building with 120 people, the next day he showed symptoms, was admitted and, on 9 March, was confirmed with SARS CoV-2 infection. This is the 17th case and he has transmitted the virus intra-communitarily to several people. Intra-community transmission became more pronounced after a state of epidemiological emergency was instituted in Romania on 15 March 2020 at 22:00 Romania time, with the population having movement restrictions, except in special cases, aimed at exercising, going out with pets, obtaining food and medicines and travelling for work purposes, for areas with continuous professional activity. As of 0900 on 16 March 2020, 139 confirmed cases of SARS CoV2 infection had been recorded, including 16 in the last 24 hours. The first psychological threshold of 25 confirmed cases in Romania was recorded on 10 March 2020. The second psychological threshold of 50 cases was exceeded on 12 March (64 cases, with 19 new cases) and the third psychological threshold of 100 cases was exceeded on 14 March (113 cases, with 24 new cases). On 26 March 2020, the total number of 1000 newly confirmed cases was exceeded (1029, with 123 in the last 24 hours alone), and on 23 April the number exceeded 10 000 (10 096, with 386 new cases). After two months of restrictions, on 15 May 2020, Romania came out of the epidemiological emergency, with 16 437 confirmed cases of SARS CoV-2, surpassing the first wave of infection (*Fig. 4*). This peaked at 523 daily infections on 11 April 2020. On 18 May 2020, Romania entered a state of alert, which was extended until 8 March 2022. With the onset of the second wave of the pandemic at the beginning of June 2020, the number of confirmed infections started to increase again, more sharply in June, leading to a total of 26 970 cases (with 388 cases recorded in the last 24 hours) on 30 June 2020, of which 19 050 people were cured (70.634%), and 1 651 deaths (with 17 in the last 24 hours). According to official estimates, 6 269 people were still active but under observation and quarantine. In July-August 2020, the number of newly confirmed daily cases remained at a standstill, after which it began to rise more sharply, reaching a peak of 10 269 cases on 18 November, with more than 10 000 cases being recorded daily on 6, 12, 18 and 19 November. Towards the end of 2020, the number of confirmed cases per day began to fall to below 5–6 000, marking the end of the second wave. As of 31 December 2020, Romania reported a total of 632,263 confirmed cases, up from 4,322 on 31 December, and 15,767 deaths, including 171 in the last 24 hours. Of the total reported cases, 560 793 people were cured (88.696%), with 6 737 cases reported cured in the last 24 hours, 55 703 cases still active but quarantined.

The steep rise in the number of newly confirmed cases of SARS CoV-2 infection since the early days of 2022 characterised the onset of the fifth pandemic wave, which had three peaks, on 26 January with 34 255 newly confirmed cases, on 1 February with 40 018 cases, and on 8 February with 36 269 cases. The fifth wave was characterised by the greatest amplitude in the evolution of the daily number of newly-confirmed SARS CoV-2 cases, which dropped sharply in the second part of February to 7 191 cases on 26 February. The drop in the number of newly confirmed daily cases and public pressure led the Romanian authorities to completely lift the restrictions as of 8 March 2022. At that time, Romania came out of the alert status and the request for a green

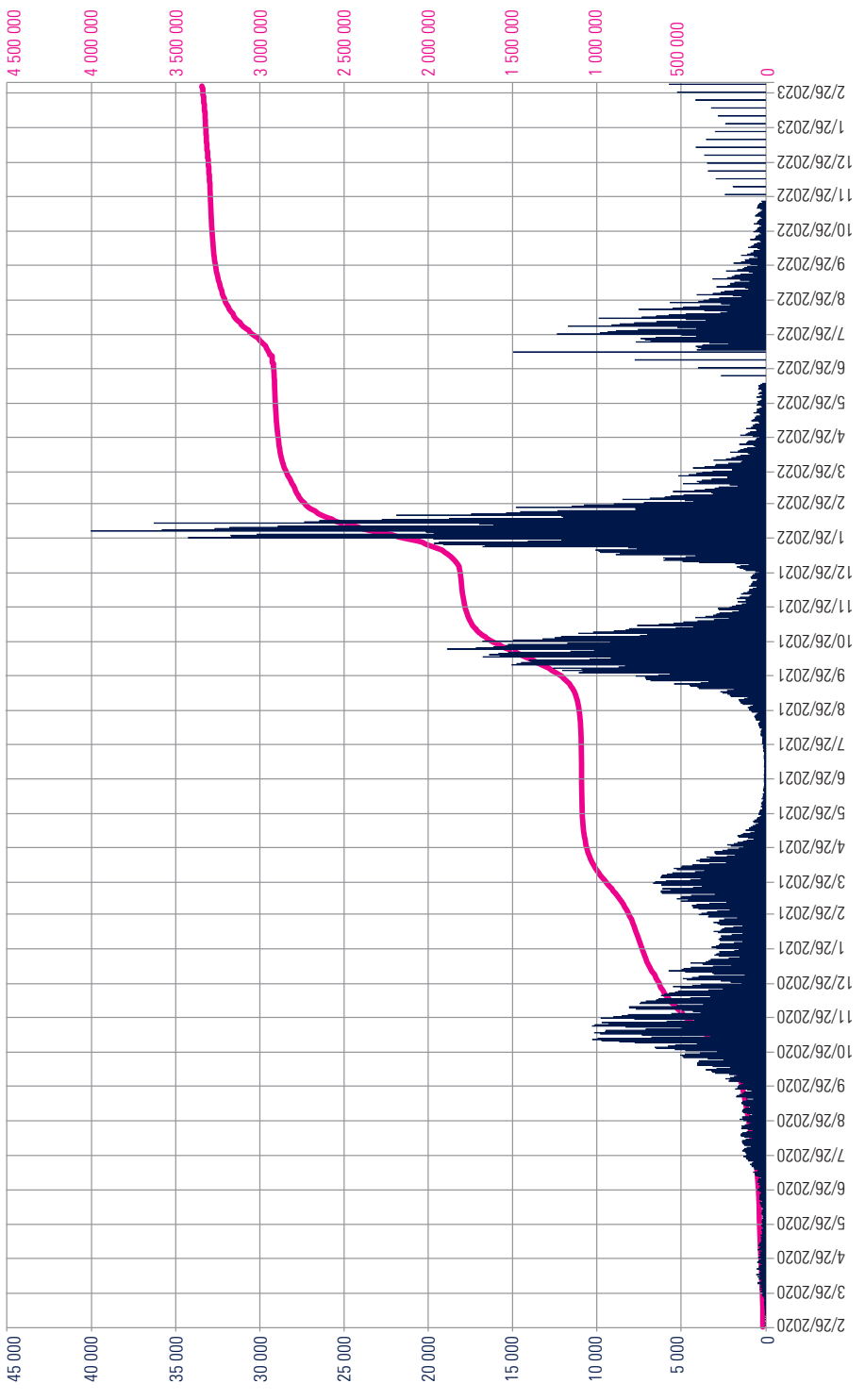

Fig. 7. Combined graph illustrating the daily/weekly number of newly confirmed SARS CoV-2 cases in Romania between 26 February 2020 and 5 March 2023 (with blue bars and baseline values on the left side of the graph) and their cumulative curve (with magenta and baseline values on the right side of the graph).
Source: https://www.ms.ro/buletine-de-presa-covid/.

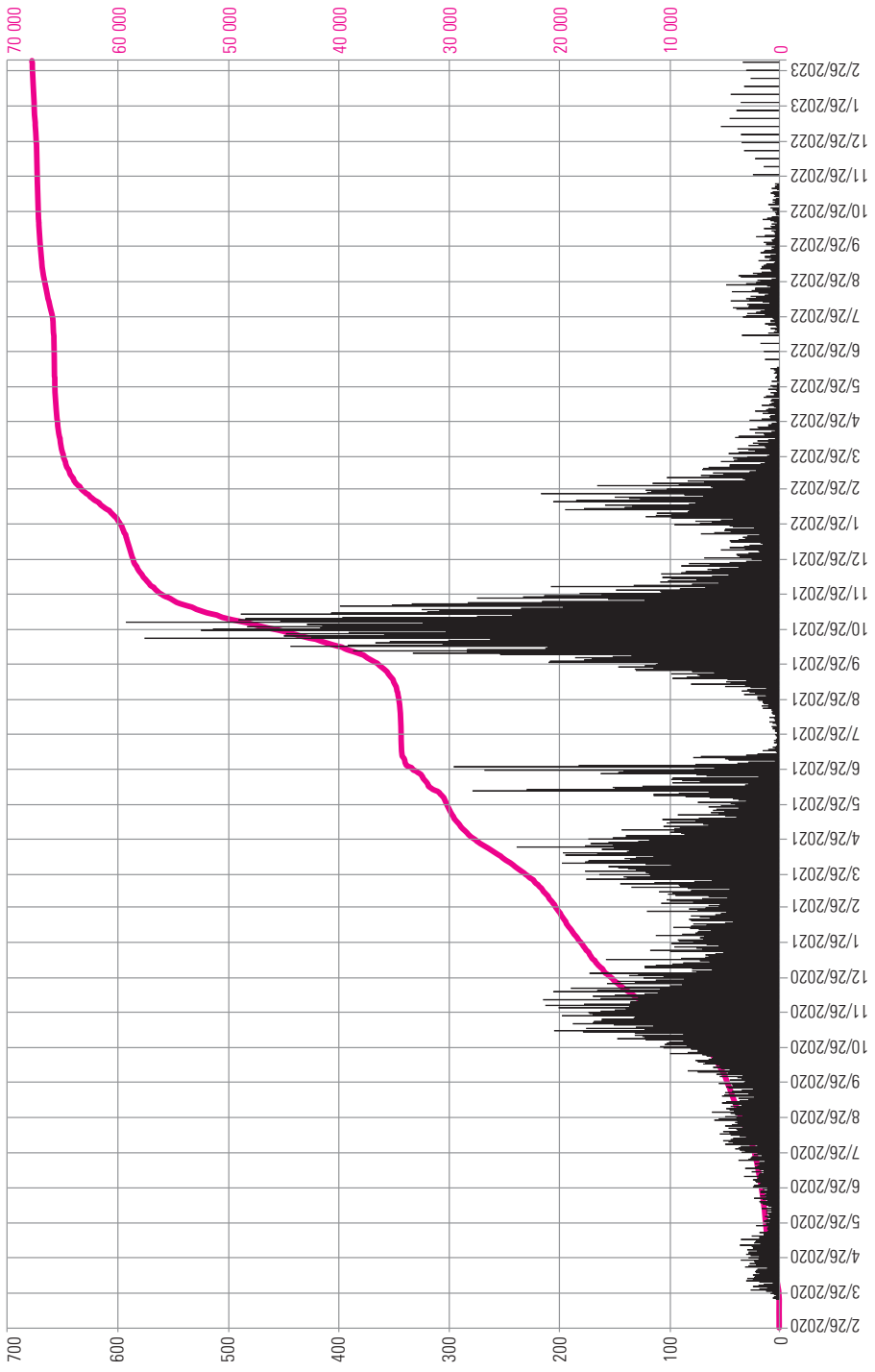

Fig. 8. Combined graph illustrating the daily/weekly number of deaths in persons confirmed with SARS CoV-2 infection in Romania between 26 February 2020 and 5 March 2023 (with black bars and baseline values on the left side of the graph) and their cumulative curve (with magenta and baseline values on the right side of the graph). Source: https://www.ms.ro/buletine-de-presa-covid/.

certificate for access to non-food and food shops or some public institutions was stopped. The low number of cases during the spring of 2022 led the Romanian authorities to stop reporting the number of cases on a daily basis, starting on 12 June, when 168 cases were recorded. For 12 June, the press release (official communiqué) of the Romanian Ministry of Health indicated a cumulative total of 2 912 705 cases of SARS CoV-2 infections at national level, and on the same day a press release (official communiqué) of the Romanian Ministry of Health was issued for 6–12 June, which reports a cumulative national total of 2 912 878 cases of SARS CoV-2 infections, resulting in a difference of 173 cases, which is maintained in subsequent releases, without resulting from daily or weekly reporting of the number of cases of SARS CoV-2 infection. On 1 October 2022, this difference increased to 174 cases and is maintained to date. It may be generated by an error in daily reporting or by an error in the accumulation of the total number of cases. All official bulletins issued by the Romanian Ministry of Health are available at: https://www.ms.ro/buletine-de-presa-covid/.

Towards the end of June and beginning of July, the number of SARS CoV-2 cases started to rise again, and from 12 July, the authorities reverted to daily reporting. As of 3 July 2022, a total of 2 927 014/2 927 187 cases of SARS CoV-2 infection had been confirmed, including 7 726 in the last 7 days, and 65 755 deaths, with 16 deaths in the last 7 days.

On 12 July, 4 044 new cases were confirmed, rising to over 5 000 cases after 17 July, reaching a peak of 12 353 cases on 26 July, the peak of the sixth wave. Less intense than the previous one, it began to decrease in intensity and by autumn 2022 the number of newly confirmed daily cases had fallen to below 500. For this reason, since 22 November, the Romanian authorities have resorted to weekly reporting of cases of SARS CoV-2 infection. On 1 January 2023, Romania totalled 3 311 911/3 312 085 cases of COVID-19, with 3 615 in the last 7 days, and 67 408 deaths, including 34 deaths recorded in the last 7 days.

The latest report, dated 6 March 2023, which totals cases from 27 February to 5 March 2023, shows 5 704 new cases and 32 deaths. In total, as of 5 March, Romania had 3 345 872/3 346 046 cases of SARS CoV-2 infection and 67 736 deaths (Fig. 7, 8).

In terms of the number of people infected with SARS CoV-2 who died (Figure 5), the first two deaths were recorded on 22 March 2020 and the first wave of deaths in spring 2020, with three peaks: 34 deaths on 25 April and 13 May, and 35 deaths on 8 May. After a relative decrease in the number of deaths in the second part of May, the second wave of deaths began in June and lasted until the end of January 2021, with the daily maximum of SARS CoV-2 deaths recorded on 8 December 2020 (213 people). February and the first part of March 2021 saw a reduction in the number of deaths, with a low of 41 people recorded on 14 February, after which the third wave of deaths began, extending into early May. During this, the daily peak of 237 deaths was recorded on 20 April. After a short period of decline, the number of cases increased again in June 2021, with daily highs of 277 deaths on 8 June, 266 deaths on 26 June and 294 deaths on 29 June 2021, with the lowest number of deaths of SARS CoV-2-infected persons recorded on 3 and 4 July, followed by steep positive and negative variations, considered the fourth wave or the end of the third wave of deaths. On 11 July, there was a low of one death, then between 12 July and 18 August, the number of deaths was reduced. From the second part of August, the fifth and largest wave of deaths associated with SARS CoV-2 infection began, with two days when more than 550 deaths were recorded, on 19 October (574 cases) and 2 November (591 cases), as many as the population of small towns in Romania. Towards the end of November, the number of deaths went into a steep downward slope, so that at the halfway point between 2021 and 2022, there would be a clear gap between the fifth and sixth waves, stretching from the end of January to the beginning of March 2022. The highest number of deaths recorded daily was on 22 February (215). Since March, the number of deaths of people infected with SARS CoV-2 has been kept low, with zero reported on 16 and 30 May 2022. On 27 July, the seventh wave of deaths associated with SARS CoV-2 infection began, peaking on 23 August (47). After the Romanian authorities stopped daily reporting of the number of cases and deaths, it is difficult to follow the evolution of these from official data [30–33] (Fig. 8).

SARS CoV-2 variants

Being propagated in a very large number of human individuals (hosts) in a relatively short and sustained time, SARS CoV2 is an RNA virus susceptible to a high mutation rate and the evolution of several variants. The main reasons for their occurrence are related to strand switching, RNA-dependent RNA polymerase activity, an enzyme lacking corrective mechanisms, and frequent recombination events of different strains of SARS CoV-2. Point mutations cause the replacement of one nitrogenous base by another and of one amino acid by another, altering cell tropism, transmissibility and pathogenicity of viruses [3]. Thus, between February and June 2020, the D614G mutation in the C-terminal region of the S1 domain of the spicular protein predominated in 74% of published sequences.

Table 1. SARS CoV-2 variants and their characteristic mutations

Pango lineage	WHO label	Isolated from	Mutations in eceptor-binding domain	Mutations in S-glycoprotein
B.1.1.7	Alpha	UK (November, 2020)	E484K, S494P, N501Y	69/70del, 144del, A570D, D614G, P681H, T716I, S982A, D1118H, K1191N
B.1.351	Beta	South Africa (October, 2020)	K417N, E484K, N501Y	D80A, D215G, 241/243del, D614G, A701V
P.1	Gamma	Japan/Brazil (December, 2020)	K417T, E484K, N501Y	L18F, T20N, P26S, D138Y, R190S, D614G, H655Y, T1027I
B.1.614.2	Delta	India (December, 2020)	L452R, T478K	T19R, G142D, D614G, P681R, R158G, 156/157del, D950N
B.1.427	Epsilon	USA (July, 2020)	L452R	D614G
B.1.429	Epsilon	USA (July, 2020)	L452R	S13I, W152C, D614G
P.2	Zeta	Brazil (April, 2020)	E484K	F565L, D614G, V1176F
B1.525	Eta	USA (December, 2020)	E484K	A67V, 69/70del, 144del, D614G, Q677H, F888L
P.3	Theta	Japan/Philippines (February, 2021)	E484K, N50	141/143del, D614G, P681H, E1092K, H1101Y, V1176F
B.1.617.1	Kappa	India (December, 2020)	E484Q, L452R	T95I, D614G, E154K, P681R, G142D, Q1071H
C.37	Lambda	Peru (November 2020)	L452Q, F490S	G75V, T76I, D614G, T859
B.1.1.529	Omicron	South Africa/Botswana (May, 2020)	?	A67V, 69–70del, 142–144del, T95I, Z145D, 211del, L212I, 214epe, G339D, R346K, S371L, S373P, S375F, K417N, N440K, G446S, L452X, S477N, T478K, E484A, F486V, Q493R, G496S, Q498R, N501Y, Y505H, T547K, D614G, H655Y, K679K, P681H, N764K, D796Y, N856K, Q954H, N969K, L981F

This mutation provides more efficient virus functionality, is associated with higher nasopharyngeal viral load and is the only mutation present in all six variants of interest (Epsilon, Eta, Iota, Kappa, Zeta and Lambda) and five variants of concern (Alpha, Beta, Gamma, Delta, and Omicron) circulating worldwide (*Table 1*) [36, 37].

Worldwide, in the first wave (February–March 2020) and the second wave (June–August 2020) the Wuhan strain (Wuhan waves) predominated, in the third wave (October 2020–January 2021) the Beta strain (Beta wave) predominated, in the fifth wave (July–October 2021) the Delta variant (Delta wave) predominated, and in the following waves (sixth, between January and April 2022, seventh, between July and August 2022, and eighth, between mid-December 2022 and mid-January 2023), the Omicron variant became dominant [36, 38, 39].

In Romania, the Wuhan strain was dominant at the end of 2020, but from the second half of February 2021 it was overtaken by the Alpha variant. In spring 2021, a few cases of Beta and Gamma variant infections were identified, but they never became dominant. From late April, the Delta variant emerged and became prevalent from July 2021. Towards the end of 2021, the Omicron variant emerged and dominated almost all of 2022, towards the end of the year sharing cases with variants other than Omicron [40] (Fig. 9).

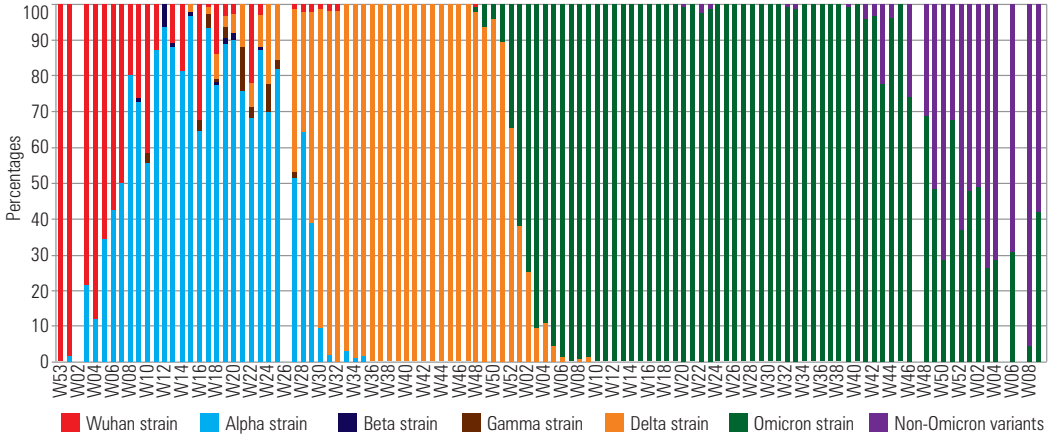

Fig.9. The proportion of variants in SARS CoV-2 samples collected from Romania and sequenced between weeks 53/2020 and 9/2023. Source: https://insp.gov.ro/centrul-national-de-supraveghere-si-control-al-bolilor-transmisibile-cnscbt/infectia-cu-noul-coronavirus-sars-cov-2/analiza-cazuri-confirmate-covid19/

Table 2. Anti-SARS CoV-2 vaccines and their main characteristics

Vaccine name	Vaccine type	Producer	Origin country	Administration	Efficiency (%)
BNT162b/2	Nucleoside-modified mRNA-based vaccine	Pfizer-BioNTech	USA	2 doses 3 weeks apart	91.3
mRNA-1273	mRNA-based vaccine encapsulated in lipid nanoparticle	Moderna	USA	2 Doses 4 weeks apart 94.5	
AZD1222 Covishield	Recombinant ChAdOx1 adenovirus vector encoding spike protein Ag of the SARS-CoV-2	AstraZeneca-Oxford	UK, USA	2 doses between 4 and 12 weeks apart	90.0
Sputnik V rAd26 rAd5	Recombinant adenovirus vector-based COVID-19 vaccine	Gamaleya Research Institute	Russia	2 different doses 3 weeks apart	92.0
Ad26.CoV.S JNJ-78436735	Recombinant, non-replicating adenovirus type 26 vectored vaccine encoding SARSCoV-2 spike protein	Johnson & Johnson, Janssen vaccines	Netherland, USA	Single dose	72.0
COVAXIN BBVI52	The whole SARSCoV-2 virus inactivated (Vero cell)	Bharat Biotech	India	2 doses 4 weeks apart	81.0
Corona Vac	Inactivated vaccine (Vero cell, formalin with alum)	Sinovac	China	2 doses	50.0–84.0
NVX-CoV2373 Covavax	Recombinant NP profusion spike protein formulated with matrix-M adjuvant	NovaVax	USA	2 doses	89.3
BBIBP-CoV vaccine	Inactivated SARSCoV-2 vaccine produced in Vero cell	Sinopharm	China	2 doses	78.0

Anti-SARS CoV-2 vaccines

During the pandemic, 9 vaccines targeted against SARS CoV-2 were developed (*Table 2*). Two of these, BNT162b/2, produced by Pfizer-BioNTech of the US, and mRNA-1273, produced by Moderna of the US, are based on mRNA platforms, AZD1222 Covishield vaccines, produced by Astra-Zeneca-Oxford, a UK-US collaboration, Sputnik V rAd26 rAd5, produced by Gamaleya Research Institute of Russia, and Ad26.CoV. S JNJ-78436735, produced by the Americans from Johnson & Johnson and the Dutch from Janssen vaccines, are based on recombinant adenoviral vectors, COVAXIN BBVI52 vaccines, produced by Bharat Biotech of India, and BBIBP-CoV vaccine, produced by the Chinese from Sinopharm, use inactivated SARSCoV-2 vaccine produced in Vero cell, Corona Vac vaccine, produced by the Chinese of Sinovac, is an inactivated vaccine, in Vero cell and formalin with alum, and NVX-CoV2373 Covavax, produced by the Americans of NovaVax, uses Recombinant NP profusion spike protein. These are capable of inducing the synthesis of specific anti-SARS CoV-2 antibodies with variable efficiency. Thus, BNT162b/2 and mRNA-1273 vaccines are more than 90% effective against Alpha variant infections, but less effective against Gamma variant. Most CoV-2 SARS vaccines are less effective against the Beta variant [Thakur, 2022].

Globally, by the end of February 2023, 13228728467 doses of SARS CoV-2 vaccine had been administered, immunising 5 512 995 309 people who had received at least one dose of vaccine, of which 5 073 870 238 people were fully immunised against SARS CoV-2 [32]. In Romania, the administration of SARS CoV-2 vaccines began on 27 December 2020, and by 5 March 2023, 16 919 549 doses of vaccine had been administered, immunising 8 141 569 people with the first dose, of whom 8 130 345 people received the full vaccination schedule and 2 666 628 people with the last booster dose [40].

Bibliografie

1. Mihaescu G, Chifiriuc MC, Iliescu C, Vrancianu CO, Ditu LM, Marutescu LG, Grigore R, Berteșteanu Ș, Constantin M, Gradisteanu Pircalabioru G. SARS-CoV-2: From Structure to Pathology, Host Immune Response and Therapeutic Management. Microorganisms. 2020 Sep 24;8(10):1468. doi: 10.3390/microorganisms8101468. PMID: 32987852; PMCID: PMC7600570
2. Pal M, Berhanu G, Desalegn C, Kandi V. Severe Acute Respiratory Syndrome Coronavirus-2 (SARS-CoV-2): An Update. Cureus. 2020 Mar 26;12(3):e7423. doi: 10.7759/cureus.7423. PMID: 32337143; PMCID: PMC7182166
3. Parczewski M, Ciechanowicz A. Molecular epidemiology of SARS-CoV-2: a review of current data on genetic variability of the virus. Pol Arch Intern Med. 2020 Jan 29;131(1):63-69. doi: 10.20452/pamw.15550. Epub 2020 Aug 11. PMID: 32785209
4. Sahin A, Erdogan A, Mutlu Agaoglu P, Dineri Y, Cakirci A, Senel M, et al. 2019 Novel Coronavirus (COVID-19) Outbreak: A Review of the Current Literature. EJMO. 2020; 4(1): 1-7
5. Ksiazek TG, Erdman D, Goldsmith CS, Zaki SR, Peret T, Emery S, Tong S, Urbani C, Comer JA, Lim W, Rollin PE, Dowell SF, Ling AE, Humphrey CD, Shieh WJ, Guarner J, Paddock CD, Rota P, Fields B, DeRisi J, Yang JY, Cox N, Hughes JM, LeDuc JW, Bellini WJ, Anderson LJ. SARS Working Group. A novel coronavirus associated with severe acute respiratory syndrome.

N Engl J Med. 2003 May 15;348(20):1953-66. doi: 10.1056/NEJMoa030781. Epub 2003 Apr 10. PMID: 12690092

6. Norouzi M, Miles MA, Norouzi S. Genetics and Biological Characteristics of SARS-CoV-2. In: Adibi S, Griffin P, Sanicas M, Rashidi M, Lanfranchi F. (eds). Frontiers of COVID-19. Springer Cham. 2022. https://doi.org/10.1007/978-3-031-08045-6_4
7. Wu CR, Yin WC, Jiang Y, Xu HE. Structure genomics of SARS-CoV-2 and its Omicron variant: drug design templates for COVID-19. Acta Pharmacol Sin. 2022 Dec;43(12):3021-3033. doi: 10.1038/s41401-021--00851-w. Epub 2022 Jan 20. PMID: 35058587; PMCID: PMC8771608
8. Gupta M, Azumaya CM, Moritz M, Pourmal S, Diallo A, Merz GE, Jang G, Bouhaddou M, Fossati A, Brilot AF, Diwanji D, Hernandez E, Herrera N, Kratochvil HT, Lam VL, Li F, Li Y, Nguyen HC, Nowotny C, Owens TW, Peters JK, Rizo AN, Schulze-Gahmen U, Smith AM, Young ID, Yu Z, Asarnow D, Billesbølle C, Campbell MG, Chen J, Chen KH, Chio US, Dickinson MS, Doan L, Jin M, Kim K, Li J, Li YL, Linossi E, Liu Y, Lo M, Lopez J, Lopez KE, Mancino A, Moss FR, Paul MD, Pawar KI, Pelin A, Pospiech TH, Puchades C, Remesh SG, Safari M, Schaefer K, Sun M, Tabios MC, Thwin AC, Titus EW, Trenker R, Tse E, Tsui TKM, Wang F, Zhang K, Zhang Y, Zhao J, Zhou F, Zhou Y, Zuliani-Alvarez L; QCRG Structural Biology Consortium; Agard DA, Cheng Y, Fraser JS, Jura N, Kortemme T, Manglik A, Southworth DR, Stroud RM, Swaney DL, Krogan NJ, Frost A, Rosenberg OS, Verba KA. CryoEM and AI reveal a structure of SARS-CoV-2 Nsp2, a multifunctional protein involved in key host processes. bioRxiv [Preprint]. 2021 May 11:2021.05.10.443524. doi: 10.1101/2021.05.10.443524. PMID: 34013269; PMCID: PMC8132225
9. Lei J, Kusov Y, Hilgenfeld R. Nsp3 of coronaviruses: Structures and functions of a large multi-domain protein. Antiviral Res. 2018 Jan;149:58-74. doi: 10.1016/j.antiviral.2017.11.001. Epub 2017 Nov 8. PMID: 29128390; PMCID: PMC7113668
10. Shin D, Mukherjee R, Grewe D, Bojkova D, Baek K, Bhattacharya A, Schulz L, Widera M, Mehdipour AR, Tascher G, Geurink PP, Wilhelm A, van der Heden van Noort GJ, Ovaa H, Müller S, Knobeloch KP, Rajalingam K, Schulman BA, Cinatl J, Hummer G, Ciesek S, Dikic I. Papain-like protease regulates SARS-CoV-2 viral spread and innate immunity. Nature. 2020 Nov;587(7835):657-662. doi: 10.1038/s41586-020-2601-5. Epub 2020 Jul 29. PMID: 32726803; PMCID: PMC7116779
11. Wu Z, McGoogan JM. Characteristics of and Important Lessons From the Coronavirus Disease 2019 (COVID-19) Outbreak in China: Summary of a Report of 72 314 Cases From the Chinese Center for Disease Control and Prevention. JAMA. 2020 Apr 7;323(13):1239-1242. doi: 10.1001/jama.2020.2648. PMID: 32091533
12. Xia S, Lan Q, Su S, Wang X, Xu W, Liu Z, Zhu Y, Wang Q, Lu L, Jiang S. The role of furin cleavage site in SARS-CoV-2 spike protein-mediated membrane fusion in the presence or absence of trypsin. Signal Transduct Target Ther. 2020 Jun 12;5(1):92. doi: 10.1038/s41392-020-0184-0. PMID: 32532959; PMCID: PMC7289711
13. Li G, Fan Y, Lai Y, Han T, Li Z, Zhou P, Pan P, Wang W, Hu D, Liu X, Zhang Q, Wu J. Coronavirus infections and immune responses. J Med Virol. 2020 Apr;92(4):424-432. doi: 10.1002/jmv.25685. Epub 2020 Feb 7. PMID: 31981224; PMCID: PMC7166547
14. Masters PS. The molecular biology of coronaviruses. Adv Virus Res. 2006;66:193-292. doi: 10.1016/S0065-3527(06)66005-3. PMID: 16877062; PMCID: PMC7112330
15. McBride R, van Zyl M, Fielding BC. The coronavirus nucleocapsid is a multifunctional protein. Viruses. 2014 Aug 7;6(8):2991-3018. doi: 10.3390/v6082991. PMID: 25105276; PMCID: PMC4147684
16. Holmes EC, Goldstein SA, Rasmussen AL, Robertson DL, Crits-Christoph A, Wertheim JO, Anthony SJ, Barclay WS, Boni MF, Doherty PC, Farrar J, Geoghegan JL, Jiang X, Leibowitz JL, Neil SJD, Skern T, Weiss SR, Worobey M, Andersen KG, Garry RF, Rambaut A. The origins of SARS-CoV-2: A critical review. Cell. 2021 Sep 16;184(19):4848-4856. doi: 10.1016/j.cell.2021.08.017. Epub 2021 Aug 19. PMID: 34480864; PMCID: PMC8373617
17. Bryner J. 1st known case of coronavirus traced back to November in China. 2020 March 14. [cited 2023 March 06]. Available from: https://www.livescience.com/first-case-coronavirus-found.html
18. Roberts DL, Rossman JS, Jarić I. Dating first cases of COVID-19. PLoS Pathog. 2021 Jun 24;17(6):e1009620. doi: 10.1371/journal.ppat.1009620. PMID: 34166465; PMCID: PMC8224943
19. Zhu N, Zhang D, Wang W, Li X, Yang B, Song J, Zhao X, Huang B, Shi W, Lu R, Niu P, Zhan F, Ma X, Wang D, Xu W, Wu G, Gao GF, Tan W; China Novel Coronavirus Investigating and Research Team. A Novel Coronavirus from Patients with Pneumonia in China,

2019. N Engl J Med. 2020 Feb 20;382(8):727-733. doi: 10.1056/NEJMoa2001017. Epub 2020 Jan 24. PMID: 31978945; PMCID: PMC7092803
20. Gralinski LE, Menachery VD. Return of the Coronavirus: 2019-nCoV. Viruses. 2020 Jan 24;12(2):135. doi: 10.3390/v12020135. PMID: 31991541; PMCID: PMC7077245
21. Virological.org; 10th January 2020 [cited 2023 March 06]. Available from: https://virological.org/t/novel-2019-coronavirus-genome/319
22. Severe acute respiratory syndrome coronavirus 2 isolate Wuhan-Hu-1, complete genome; 2020 [cited 2023 March 06]. Available from: https://www.ncbi.nlm.nih.gov/nuccore/MN908947
23. Hu B, Guo H, Zhou P, Shi ZL. Characteristics of SARS-CoV-2 and COVID-19. Nat Rev Microbiol. 2021 Mar;19(3):141-154. doi: 10.1038/s41579-020-00459-7. Epub 2020 Oct 6. Erratum in: Nat Rev Microbiol. 2022 May;20(5):315. PMID: 33024307; PMCID: PMC7537588
24. Jiang S, Du L, Shi Z. An emerging coronavirus causing pneumonia outbreak in Wuhan, China: calling for developing therapeutic and prophylactic strategies. Emerg Microbes Infect. 2020 Jan 31;9(1):275-277. doi: 10.1080/22221751.2020.1723441. Erratum in: Emerg Microbes Infect. 2020 Dec;9(1):539. PMID: 32005086; PMCID: PMC7033706
25. World Health Organization. Coronavirus disease 2019 (COVID-19). Situation report – 51. 2020 [cited 2023 March06].Availablefrom:https://www.who.int/docs/default-source/coronaviruse/situation-reports/20200311-sitrep-51-covid-19.pdf?sfvrsn=1ba62e57_10
26. Eurosurveillance editorial team. Note from the editors: World Health Organization declares novel coronavirus (2019-nCoV) sixth public health emergency of international concern. Euro Surveill. 2020 Feb;25(5):200131e. doi: 10.2807/1560-7917.ES.2020.25.5.200131e. Epub 2020 Jan 31. PMID: 32019636; PMCID: PMC7014669
27. Coronaviridae Study Group of the International Committee on Taxonomy of Viruses. The species Severe acute respiratory syndrome-related coronavirus: classifying 2019-nCoV and naming it SARS-CoV-2. Nat Microbiol. 2020 Apr;5(4):536-544. doi: 10.1038/s41564-020-0695-z. Epub 2020 Mar 2. PMID: 32123347; PMCID: PMC7095448
28. Fisher D, Heymann D. Q&A: The novel coronavirus outbreak causing COVID-19. BMC Med. 2020 Feb 28;18(1):57. doi: 10.1186/s12916-020-01533-w. PMID: 32106852; PMCID: PMC7047369
29. Lai CC, Shih TP, Ko WC, Tang HJ, Hsueh PR. Severe acute respiratory syndrome coronavirus 2 (SARS-CoV-2) and coronavirus disease-2019 (COVID-19): The epidemic and the challenges. Int J Antimicrob Agents. 2020 Mar;55(3):105924. doi: 10.1016/j.ijantimicag.2020.105924. Epub 2020 Feb 17. PMID: 32081636; PMCID: PMC7127800
30. https://www.ms.ro/buletine-de-presa-covid/
31. https://covid19.stirioficiale.ro/informatii
32. WHO COVID-19 Dashboard. Geneva: World Health Organization, 2020. Available online: https://covid19.who.int/ (last cited: [07.03.2023])
33. Situația la nivel global, actualizată zilnic. Infecția cu noul coronavirus (SARS-CoV-2). 2020 [cited 2023 March 06]. Available from: https://insp.gov.ro/centrul-national-de-supraveghere-si-control-al-bolilor-transmisibile-cnscbt/infectia-cu-noul-coronavirus-sars-cov-2/situatia-la-nivel-global-actualizata-zilnic/
34. https://www.worldometers.info/coronavirus/
35. https://coronavirus.jhu.edu/map.html
36. He X, Hong W, Pan X, Lu G, Wei X. SARS-CoV-2 Omicron variant: Characteristics and prevention. MedComm (2020). 2021 Dec 16;2(4):838-845. doi: 10.1002/mco2.110. PMID: 34957469; PMCID: PMC8693031
37. Thakur V, Bhola S, Thakur P, Patel SKS, Kulshrestha S, Ratho RK, Kumar P. Waves and variants of SARS-CoV-2: understanding the causes and effect of the COVID-19 catastrophe. Infection. 2022 Apr;50(2):309-325. doi: 10.1007/s15010-021-01734-2. Epub 2021 Dec 16. Erratum in: Infection. 2022 Jan 14;: PMID: 34914036; PMCID: PMC8675301
38. Wassenaar TM, Wanchai V, Buzard G, Ussery DW. The first three waves of the Covid-19 pandemic hint at a limited genetic repertoire for SARS-CoV-2. FEMS Microbiol Rev. 2022 May 6;46(3):fuac003. doi: 10.1093/femsre/fuac003. PMID: 35076068; PMCID: PMC9075578
39. Koné A, Diallo D, Kané F, Diarra B, Coulibaly TA, Sameroff SC, Diarra HB, Diakité MT, Camara F, Maiga O, Keita D, Dolo O, Somboro A, Coulibaly Y, Bane S, Togo ACG, Somboro AM, Togo J, Coulibaly M, Coulibaly G, Kone M, Degoga B, Dramé HB, Traoré FG, Diallo F, Sanogo F, Kone K, Diallo IB, Sanogo M, Diakité M, Mishra N, Neal A, Saliba-Shaw K, Sow Y, Hensley L, Lane HC, Briese T, Lipkin WI, Doumbia S. Dynamics of SARS-CoV-2 variants characterized during different COVID-19 waves in Mali. IJID Reg. 2023 Mar;6:24-28. doi: 10.1016/j.ijregi.2022.11.009. Epub 2022 Nov 25. PMID: 36448028; PMCID: PMC9691504
40. https://insp.gov.ro/